

**STUDY OF IMPACT IONIZATION AND TRANSPORT PHENOMENA
IN SOME SEMICONDUCTOR MATERIALS**

A Thesis
Submitted in Partial fulfilment
of the Requirements
for
**DOCTOR OF PHILOSOPHY
IN THE FACULTY OF SCIENCE**

by
CHANDRA SHEKHAR

**DEPARTMENT OF PHYSICS
BIRIA INSTITUTE OF TECHNOLOGY & SCIENCE
PILANI (RAJASTHAN) INDIA
MARCH, 1975**

TO SWAMI SHRI
PARAMANAND JI MAHARAJ
MY REVERED GURUDEV.

BIRLA INSTITUTE OF TECHNOLOGY & SCIENCE
PILANI (RAJASTHAN)

C E R T I F I C A T E

The work on "STUDY OF IMPACT IONIZATION AND TRANSPORT PHENOMENA IN SOME SEMICONDUCTOR MATERIALS" carried out and presented herein by Mr. Chandra Shekhar embodies original investigations and was carried out under my supervision and guidance during the period from August 1971 to March 1975. It is recommended that the thesis be accepted for the award of the degree of Doctor of Philosophy in the Department of Physics, Birla Institute of Technology & Science, Pilani (Rajasthan).

S.K. Sharma

(S. K. Sharma)
Asstt. Prof. of Physics.

A C K N O W L E D G E M E N T S

It gives me a great pleasure to place on record my deep sense of gratitude towards Dr. S. K. Sharma, Asst. Prof. of Physics, B.I.T.S., Pilani (Raj.), who so ably and inspiringly guided and encouraged me during the entire course of this work.

Thanks are due to Dr. H. M. Ghule, Dr. V. Subrahmaniam, Dr. S. Ahmad and Dr. P. Singh for providing valuable help in my doctoral programme at various stages.

I wish to express my heartfelt thanks to Dr. M. L. Joshi, Dr. B. K. Kaushik, Dr. P. K. Banerjee, Dr. G. P. Srivastava, Mrs. G. P. Srivastava, Dr. B. C. Kashyap, Dr. C. S. G. Prasad, Dr. A. N. Pant, Dr. A. D. Taneja, Dr. S. C. Taneja, Dr. P. Dhyani, Dr. V. Sharma, Dr. D. R. Sharma, Messers G. R. Rao, M. C. Gupta, D. C. Tiwari, A. K. Jain, S. K. Jain, V. S. Kulhar, L. K. Mohan, N. K. Swami, A. L. Pandey, S. C. Bawa, Suman Kumar, K. S. Yadav, J. L. Goyal, Dipu, Babu, A. B. Samsi, Bharat Bhushan, T. K. Kaul, B. S. Gupta, S. B. Shah, I. P. Singh, R. S. Chauhan, Mukta Bihari, S. V. Kibe, A. P. Mathur, M. L. Goyal and all others friends and colleagues who made my stay in Pilani a lively and memorable experience in various fields of life.

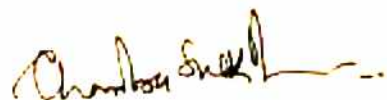
Thanks are due to Mr. S. S. Negi, and Mr. S. L. Sharma of the IPC staff of B.I.T.S. for extending unreserved help in the computational work.

I thank Mr. S. K. Sinha for efficient typing of the manuscript and Mr. S. D. Dewan for the drawing work.

I wish to express my deep sense of gratitude towards my parents for their stoic forbearance and continued encouragement.

I lovingly thank my younger brother Sudhir and sister Anita whose affection has been a constant source of inspiration to me.

I am thankful to the Director BITS, the Dean faculty of science and the Head Department of Physics for providing necessary facilities during the course of this work. I am thank-ful to U.G.C. and C. S. I. R. for providing financial assistance.



(CHANDRA SHEKHAR)

I N D E X

Introduction 1

Chapter-I.

ELECTRON TRANSPORT

I.	Introduction	4
II.	Band structure	8
III.	Boltzmann's equation	14
IV.	Scattering Mechanisms	17
V.	Techniques for solving Boltzmann's transport equation for GaAs.	29
VI.	Effect of various scattering mechanisms on the solution of Boltzmann's transport equation.	43
VII.	Effect of temperature on low field mobility and threshold field.	58

STUDY OF IMPACT IONIZATION 62

Chapter-II.

THRESHOLD ENERGY FOR IMPACT IONIZATION

I.	Threshold energy for impact ionization by electrons.	70
II.	Threshold energy for impact ionization by holes.	77
III.	Threshold energy for impact ionization by electrons including non parabolicity of the central valley.	81

Chapter-III.

TRANSITION PROBABILITY FOR IMPACT IONIZATION 88

Chapter-IV.

CALCULATION OF IONIZATION COEFFICIENT	103
---------------------------------------	-----

Chapter-V.

EFFECT OF MOBILE CHARGE CARRIERS ON JUNCTION POTENTIAL DISTRIBUTION, FIELD DISTRIBUTION AND CAPACITANCE.	
--	--

i. Setting up the generalized differential equation.	115
II. Boundary conditions and technique of obtaining solution.	116
III. Capacitance	120
IV. Results and Discussions.	122

Chapter-VI.

CONCLUSION	146
------------	-----

Appendix A	151
Appendix B	157

VALUES OF VARIOUS MATERIAL PARAMETERS USED IN THE
CALCULATIONS

The longitudinal optic phonon frequency at the centre of the zone. $\omega_0 = 5.37 \times 10^{13} \text{ rad sec}^{-1}$.

Static dielectric constant $\epsilon_0 = 12.53$.

High frequency dielectric constant $\epsilon_\infty = 10.32$.

Lattice constant $a = 5.64 \text{ \AA}$.

Effective mass in the central valley $m_1 = .473 m_0$.

Effective mass in the satellite valleys $m_2 = .364 m_0$.

Heavy hole mass $m_{v1} = .68 m_0$.

Light hole mass $m_{v2} = .12 m_0$.

Mass of the hole in the split-off band $m_{v3} = .20 m_0$.

Sound velocity $S = 5.22 \times 10^5 \text{ cm/sec}$.

Density $\rho = 5.37 \text{ g/cm}^3$.

Acoustic deformation potential $\Xi_a = 7 \text{ eV}$.

Band gap $E_g = 1.35 \text{ eV}$.

Energy separation between central and satellite minima $\Delta E_g = .33 \text{ eV}$.

Equivalent intervalley phonon frequency $\omega_e = 4.54 \times 10^{13} \text{ rad sec}^{-1}$.

Intervalley phonon frequency $\omega_{ij} = 4.54 \times 10^{13} \text{ rad sec}^{-1}$.

Equivalent intervalley deformation potential for impact

$$\Xi_e = 1 \times 10^9 \text{ eV/cm.}$$

Equivalent intervalley deformation potential for transport

$$\Xi_e = 10/a \text{ eV/cm.}$$

Intervalley deformation potential for impact $\Xi_{ij} = 1 \times 10^9 \text{ eV/cm}$.

Intervalley deformation potential for transport $\Xi_{ij} = 10/a \text{ eV/cm}$.

I N T R O D U C T I O N

The importance of III-V compound semiconductors particularly that of GaAs in the modern semiconductor technology is too well known to need any emphasis. Ever since the discovery of Gunn effect a great deal of effort has been devoted to exploit the advantages of the band structure of this material for microwave power generation. The electron transport in GaAs has therefore been a subject of active study during past few years. The current interest in IMPATT devices has laid much emphasis on the study of impact ionization in GaAs. It is in the light of these needs of technology and to provide a more complete basic understanding of the pertinent physical phenomena that the present study of transport properties and impact ionization in GaAs has been carried out.

Chapter I contains the study of electron transport. Important scattering mechanisms have been considered first and the Boltzmann's transport equation has been solved using them. Other scattering mechanisms have then been added one by one to see how they effect the distribution function and mobility. The effect of temperature on mobility has also been studied.

In chapter II an analytical method has been developed to predict threshold energy for impact ionization. Various

processes have been considered by which the electrons and holes in GaAs cause impact ionization. Corresponding threshold energies have been determined.

In chapter III, time dependent perturbation theory has been used to find out the transition probabilities for impact ionization by electrons in the central and satellite valleys as functions of electronic wave vector for processes with minimum and next minimum threshold energies for electrons in each valley.

In chapter IV the Monte Carlo technique has been used to simulate on a digital computer the motion of an electron in GaAs under electric fields strong enough to cause impact ionization. The ionization coefficient for electrons has been determined as a function of electric field therefrom.

Chapter V consists of a study of effect of space charge on junction potential-field distributions and capacitance for an abrupt symmetric p-n junction.

Chapter VI contains important conclusions drawn from the entire study and a discussion of some of the problems and difficulties in the field.

Chapter-I.

ELECTRON TRANSPORT

I.	Introduction	4
II.	Band structure	8
III.	Boltzmann's equation	14
IV.	Scattering Mechanisms	17
V.	Techniques for solving Boltzmann's transport equation for GaAs	29
VI.	Effect of various scattering mechanisms on the solution of Boltzmann's transport equation.	43
VII.	Effect of temperature on low field mobility and threshold field.	58

CHAPTER- I.

ELECTRON TRANSPORT

I. INTRODUCTION:

Gunn¹ observed microwave current oscillations in homogeneous samples of n-type Gallium Arsenide and Indium Phosphide subject to high electric fields. Similar oscillations have since been observed in n-type samples of Cadmium Telluride², Gallium Arsenide Phosphide alloys³ and Indium Arsenide under uniaxial stress⁴. The effect which has become known as the Gunn effect has aroused great interest because of its potential for the development of simple solid state sources of microwave power. Research into both the physical mechanism involved and microwave applications has proceeded rapidly. Most of the work has been concerned with Gallium Arsenide because of the relatively advanced state of the technology associated with the preparation of this material.

The Gunn effect occurs in its purest form in samples of Gallium Arsenide having length between 100 to 2500 μm subjected to a constant bias voltage. At low fields the current merely falls slightly below the value to be expected from Ohm's law as the field increases. The current oscillations occur when the field exceeds a threshold value of about 3 kv cm^{-1} . There is then a sharp drop in the time averaged value of the current and the current wave form consists of a

periodic train of spikes separated by plateau regions. The period of oscillation is close to the specimen length divided by the electron drift velocity corresponding to the plateau regions which is about 10^7 cm sec⁻¹. By making voltage probe measurements along the length of specimen Gunn⁵ and Heeks et al⁶ showed that a narrow region of high field was drifting through the sample. This region of high field has come to be called the high field domain or just domain. The spiky current waveform is due to the periodic recirculation of domains through the specimen.

The physical mechanism involved was the subject of considerable debate until the crucial experiment which picked out the precise mechanism was performed by Muston et al⁷. They subjected Gallium Arsenide to hydrostatic pressure and observed that the threshold field for the Gunn effect decreased. Out of the various possible instability mechanisms only one predicted this behaviour : the electron transfer mechanism proposed by Ridley and Watkins⁸ and independently by Hilsun⁹ before Gunn's original observations. They pointed out that semiconductors having multivalley band structures could exhibit a negative differential mobility at high fields as a result of the progressive transfer of hot carriers from high mobility valleys to low mobility valleys at higher energies. Gallium Arsenide has a conduction band structure of the required type and the energy separation

between the high mobility and low mobility valleys decreases with hydrostatic pressure¹⁰.

The Gunn effect thus marked the first success in the search for a negative differential conductivity mechanism capable of sustaining high frequency oscillations which began in early 1950s with Shockly^e and Ryder suggesting that a negative differential mobility could be realised if the negative effective mass states near the top of the conduction band could be sufficiently populated by imparting high energy to carriers by the application of high electric fields. However the attempts proved abortive with only a saturation of drift velocity at high fields being observed. Significant population of negative mass states could not be achieved because of the high energy losses associated with optical mode scattering which is now known to dominate the high field behaviour.

This failure led to fresh theoretical efforts the consequence of which was Ridley and Watkins⁸ and Hilsun⁹ independently realising that the population of negative mass states was not essential for the production of a negative differential mobility. All that was required was that carriers should transfer rapidly from low effective mass (high mobility) states to high effective mass (low mobility) states as the field increased.

Since the discovery of Gunn effect and the electron transfer as its mechanism the electron transport in GaAs has been a subject of active theoretical and experimental study. Before taking up the study of various scattering mechanisms and their effects on velocity field characteristic and distribution function in GaAs it is worth while to review the knowledge about band structure of this material, the theoretical formalism of Boltzmann's transport equation for solving transport problems and various techniques in the literature that have been applied to solve the Boltzmann's transport equation in the case of Gallium Arsenide.

II. BAND STRUCTURE:

The minimum of the conduction band of gallium arsenide occurs at the centre of the Brillouin zone and the effective mass ratio at the bottom of the band is $m^*/m_0 = .072$ ^{11,10}. The valley is spherical at all energies of interest but non parabolic. The non parabolicity can be taken into account by relating energy E to the wave vector \bar{k} through the relationship¹¹

$$\frac{\hbar^2 \bar{k}^2}{2m^*} = \gamma(E) = E(1 + \alpha E) \quad (1.1)$$

$$\text{where } \alpha = \frac{1}{E_g} \left(1 - \frac{m^*}{m_0}\right)^2 \quad (1.2)$$

using $E_g = 1.5 \text{ eV}$, α has a value 0.576 eV^{-1} in gallium arsenide.

Data concerning the subsidiary valleys in the conduction band of gallium arsenide are not yet very well established. Photo emission studies^{12,13} reveal transitions to subsidiary minima about .35, .45 and .95 eV above the (000) minimum and these were interpreted as being the minima at the X1, L1 and X3 points in the Brillouin zone. The identification of the lowest of these minima is consistent with the results of an analysis by Ehrenreich¹⁰ of several different kinds of data on the high temperature Hall coefficient, variation of resistivity with pressure

and behaviour of the band gap in Ga(As, P) alloys which showed that there are minima 0.36 eV above the (000) minimum with a combined density of states mass of about $1.2 m_0$. These experiments do not, unfortunately, give the location of the minima along (100) directions. According to theoretical calculations^{14,15} these minima appear to be at the edge of the Brillouin zone and to have X_1 symmetry. On the basis of this evidence it has been assumed that the lowest subsidiary minima lie in the (100) direction and are .36 eV above the central minimum at the edge of the Brillouin zone.

The band structure calculations¹⁴⁻¹⁹ available at the present time do not consistently predict the relative positions of the (100) minima and next higher minima in (111) directions with L_1 symmetry. The latter have been calculated to be from as much as .5 eV below to .4 eV above the (100) minima. Pseudo potential calculations by Cohen and Bergstresser¹⁴ predict the (111) minima to be .1 eV below the (100) minima where as Jones and Lettington¹⁶ using the same method but a different form of the pseudo potential have calculated the (111) minima to be .4 eV above the (100) minima. $\bar{k} \cdot \bar{p}$ calculations of Pollak et al¹⁵ place the (111) and (100) minima at about the same energy. Vanvechten¹⁷ and an OPW calculation by Collins et al¹⁸ place (111) minima

.48 eV and .44 eV below (100) minima. Herman¹³ has shown that it is possible to adjust the Fourier coefficients of the potential used in OPW calculation to obtain good agreement with the observed transition energies between the various minima through out the band structure if the X_1 and L_1 minima were .35 and .45 eV respectively above the (000) minimum which are the energies observed in photo emission experiments.

The calculations show another set of minima at the zone edge along the (100) directions not too far from the X_1 minima. These higher minima have X_3 symmetry. According to calculations¹⁵ $X_1 - X_3$ distance is about 1 eV. These are probably identical with the subsidiary minima at .95 eV above the (000) valley to which transitions have been observed in photo emission experiments. However in another calculation¹⁴ $X_1 - X_3$ distance is only a few tenths of an electron volt. Since in any case the density of states appears to be much smaller in X_3 minima than in X_1 minima, the neglect of this set of minima is justified.

For both X_1 and L_1 minima the constant energy surfaces in the neighbourhood of band edge are ellipsoidal. Pollak et al¹⁵ have calculated the transverse mass to be $0.23 m_0$ for X_1 minima. They could not however obtain the longitudinal mass m_t for these minima. For (100) minima in Si, $m_t = .19 m_0$

and $m_t = .98 m_0$, while for those of GaP the calculations of Pollak et al¹⁵ give $m_t = .28 m_0$ and $m_l = 1.5 m_0$. Thus m_+ of GaAs is intermediate between m_t of Si and GaP and expecting that m_l is similarly placed Conwell and Vassel¹¹ give a value $1.3 m_0$ for m_l of GaAs.

However we have assumed the (100) minima to have spherical constant energy surfaces. This is because of the uncertainty in principal effective masses and also because it is expected that anisotropic effects associated with these minima will be small due to strong intervalley scattering. (Absence of anisotropic effects and orientation dependence of Gunn effect testify to it). We have therefore used a scalar effective mass m_2 of $.364 m_0$ for these minima. The L1 minima have been neglected following an argument given by Fawcett et al²⁰. It may however be noted that in their work Conwell and Vassel¹¹ have used $1.2 m_0$ as the combined density of states mass for the (100) valleys. This though looks high for the case of 3 minima and a m_2 value of $.364 m_0$ for each of these minima may actually to go a long way in compensating for the neglect of L1 minima which at only .1 eV above X1 minima are expected to be well populated by them. But as Fawcett et al²⁰ argue, a reasonable choice of scattering strengths for various scattering mechanisms in X1 valley leads to only slight heating of the electrons in this valley until quite high fields and conse-

quently the number of electrons in L1 minima would be small for the fields of interest. We have therefore assumed 3 spherical parabolic minima at the band edge along (100) directions 0.36 eV above the (000) minimum. The effective mass ratio for each of the (100) minima has been taken to be .364 which gives a combined density of states mass value of .757 m_0 for these minima. The L1 minima have been neglected.

Considering the free hole absorption measurement data furnished by Braunstein^{21b} and the fact that the shape of fundamental absorption edge^{22,25} appears to be consistent with direct transitions. Ehrenreich¹⁰ concluded that valence bands in GaAs are similar to those of Ge. These experiments yielded a value of 0.33 eV for spin orbit splitting as well as ratios of the effective masses in the heavy mass, light mass and split off bands. Using Kanes²⁴ theory to untangle experimental valence band mass ratios Ehrenreich¹⁰ has given heavy hole mass $m_{v1} = 0.68 m_0$, light hole mass $m_{v2} = 0.12 m_0$ and split off band hole mass $m_{v3} = 0.20 m_0$. We have also assumed that the valence bands are spherical and parabolic. Fig. 1 depicts the band structure pictorially.

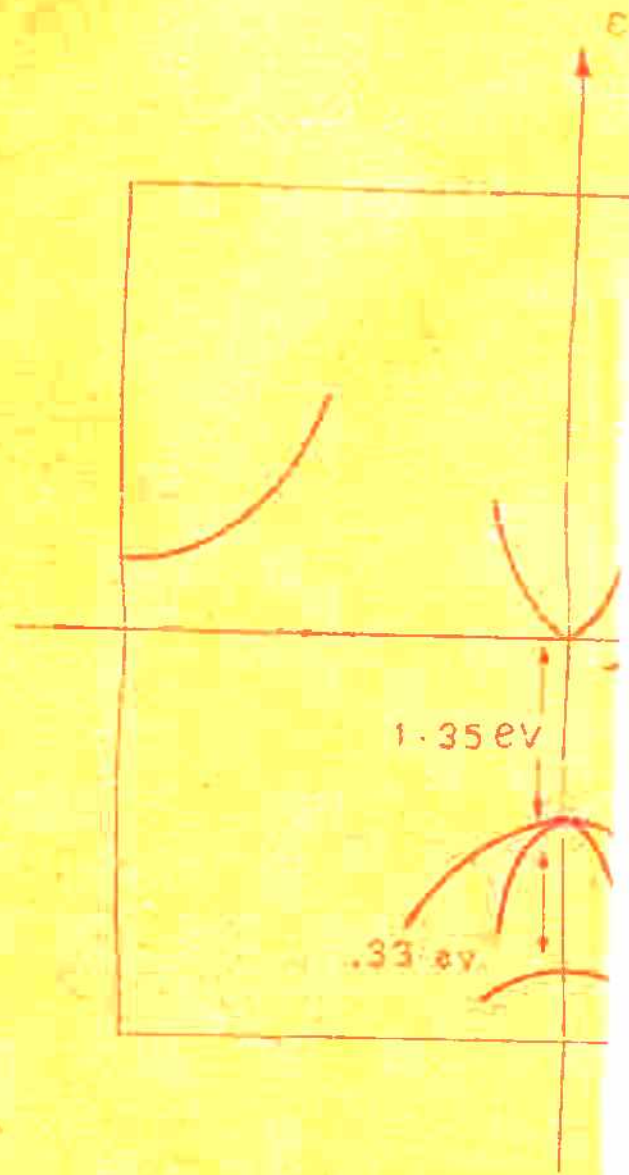
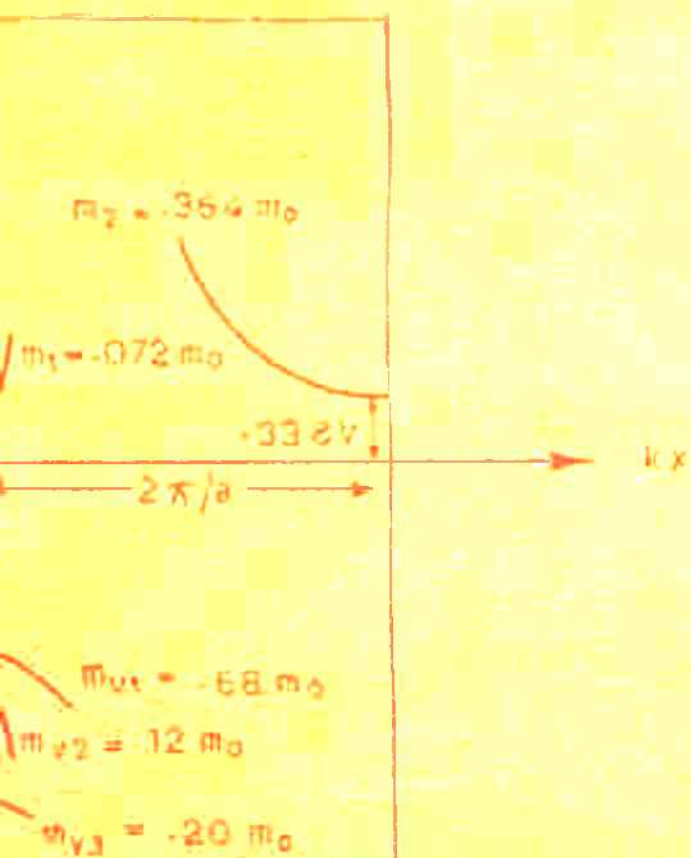


FIG. 1 BAND S



III. BOLTZMANN'S EQUATION:

In thermal equilibrium; the distribution of electrons in energy in a crystal is given in terms of the density of states function $N(E)$ and the Fermi function $F[(E - E_F)/k_B T]$. The probability that a state with wave vector \bar{k} is occupied is the same as that of a state with wave vector $-\bar{k}$ and no transport takes place. When we have transport of charge or transport of energy the distribution function must be modified by electric or magnetic fields or by temperature gradients. It is this modification of the distribution function which we will now calculate. A knowledge of this would enable us to know about the transport properties of the crystal. Let $f(\bar{k}, \bar{r}, t)$ be the probability at time t of occupation of the state corresponding to the wave vector \bar{k} at a point in the crystal given by the position vector \bar{r} . If we have a force \bar{F} whose components are F_x , F_y and F_z acting on the electrons, the value of \bar{k} will change at a rate given by $\frac{\hbar d\bar{k}}{dt} = \bar{F}$; at time $t + dt$, \bar{k} will have value $\bar{k} + \bar{k}^{-1} \bar{F} dt$. An electron which at time t has position vector \bar{r} and a wave vector \bar{k} will at time $t + dt$ have position vector $\bar{r} + \bar{v} dt$ and a wave vector $\bar{k} + \bar{k}^{-1} \bar{F} dt$. The function f is then given by

$f(\bar{k} + \bar{k}^{-1} \bar{F} dt, \bar{r} + \bar{v} dt, t + dt)$, so that the total rate of change of f is given by

$$\frac{df}{dt} = \frac{\partial f}{\partial t} + \hbar^{-1} \bar{k} \cdot \bar{F} \cdot \nabla_{\bar{k}} f + \bar{u} \cdot \nabla_{\bar{r}} f \quad (1.3)$$

This total rate of change in f must be brought about by collisions and we shall write the rate of change of f due to collisions in the form $\left. \frac{df}{dt} \right|_{coll}$

Thus we obtain the equation

$$\frac{\partial f}{\partial t} = \left. \frac{df}{dt} \right|_{coll} - \hbar^{-1} \bar{k} \cdot \bar{F} \cdot \nabla_{\bar{k}} f - \bar{u} \cdot \nabla_{\bar{r}} f \quad (1.4)$$

This equation is known as the Boltzmann's equation and is a fundamental equation in the theory of transport phenomena. In steady state conditions, $\frac{\partial f}{\partial t} = 0$ and we have

$$\left. \frac{df}{dt} \right|_{coll} = \hbar^{-1} \bar{k} \cdot \bar{F} \cdot \nabla_{\bar{k}} f + \bar{u} \cdot \nabla_{\bar{r}} f \quad (1.5)$$

The detailed form of $\left. \frac{df}{dt} \right|_{coll}$ varies from material to material and with wave vector \bar{k} (or energy E) for the same material. The exact solution of Boltzmann's equation is not possible except for some simple cases. A variety of techniques have been developed in the literature to obtain approximate solution to the equation. These techniques usually rely upon making some assumptions as to the form of the distribution function $f(\bar{k}, \bar{r}, t)$ which are physically reasonable under the given set of conditions for which a solution is desired. The collision term is then

$$\frac{df}{dt} = \frac{\partial f}{\partial t} + \bar{k}^{-1} \bar{F} \cdot \nabla_{\bar{k}} f + \bar{u} \cdot \nabla_{\bar{r}} f \quad (1.3)$$

This total rate of change in f must be brought about by collisions and we shall write the rate of change of f due to collisions in the form $\left. \frac{df}{dt} \right|_{coll}$

Thus we obtain the equation

$$\frac{\partial f}{\partial t} = \left. \frac{df}{dt} \right|_{coll} - \bar{k}^{-1} \bar{F} \cdot \nabla_{\bar{k}} f - \bar{u} \cdot \nabla_{\bar{r}} f \quad (1.4)$$

This equation is known as the Boltzmann's equation and is a fundamental equation in the theory of transport phenomena. In steady state conditions, $\frac{\partial f}{\partial t} = 0$ and we have

$$\left. \frac{df}{dt} \right|_{coll} = \bar{k}^{-1} \bar{F} \cdot \nabla_{\bar{k}} f + \bar{u} \cdot \nabla_{\bar{r}} f \quad (1.5)$$

The detailed form of $\left. \frac{df}{dt} \right|_{coll}$ varies from material to material and with wave vector \bar{k} (or energy E) for the same material. The exact solution of Boltzmann's equation is not possible except for some simple cases. A variety of techniques have been developed in the literature to obtain approximate solution to the equation. These techniques usually rely upon making some assumptions as to the form of the distribution function $f(\bar{k}, \bar{r}, t)$ which are physically reasonable under the given set of conditions for which a solution is desired. The collision term is then

calculated using quantum mechanical transition rates $S(\bar{k}, \bar{k}')$ and $S(\bar{k}', \bar{k})$ (for transition probability per second from state \bar{k} to state \bar{k}' and from state \bar{k}' to \bar{k} respectively) and summing over all transitions per second into and out of state \bar{k} . i.e.

$$\left. \frac{df}{dt} \right|_{\text{coll}} = \int \left[f(\bar{k}', \bar{v}, t) S(\bar{k}', \bar{k}) - f(\bar{k}, \bar{v}, t) S(\bar{k}, \bar{k}') \right] d\bar{k}' \quad (1.6)$$

This may seem to give the treatment a look of truly quantum mechanical approach. However it is not so. When-ever spatial variations like inhomogenities or temperature gradient are not present, the distribution function takes the form $f(\bar{k}, t)$. The rigorous quantum mechanical approach to the subject is through density matrix and it will not be considered in the present work. The Boltzmann's equation approach remains at best a semiclassical treatment.

IV. SCATTERING MECHANISMS:

For the sake of simplicity we shall be neglecting the non parabolicity of the central valley. Further the wave vector dependence of cell periodic part of Bloch functions shall be neglected and S-type wave functions shall be assumed.

Following scattering mechanisms are important in Gallium Arsenide:

Polar Optical Phonon Scattering:

Because gallium arsenide is a some what polar compound, the polar variety (due to polarization) of optical mode scattering is an important scattering mechanism.

The transition rate from wave vector \bar{k} to \bar{k}' for this process is given by^{10a, 25}

$$S_0(\bar{k}, \bar{k}') = \frac{2\pi}{\hbar} \cdot \frac{q\pi e^2 \hbar \omega_0}{V |\bar{k} - \bar{k}'|^2} \left(\frac{1}{\epsilon_\infty} - \frac{1}{\epsilon_0} \right) \times \begin{cases} N_0 \delta [E(\bar{k}') - E(\bar{k}) - \hbar \omega_0] & \text{(absorption)} \\ (N_0 + 1) \delta [E(\bar{k}') - E(\bar{k}) + \hbar \omega_0] & \text{(emission)} \end{cases} \quad (1.7)$$

where ω_0 is the optical phonon frequency, ϵ_∞ and ϵ_0 are the high frequency and static dielectric constants, V is the volume, N_0 is the optical phonon occupation number given by

$$N_0 = \left[\exp(\hbar \omega_0 / k_B T) - 1 \right]^{-1} \quad (1.8)$$

and T is the lattice temperature. One can sum expression (1.7) over all values of \vec{k}' to get the total transition rate from state \vec{k} (energy E) due to this process.

$$\lambda_0(k) = \sum_{\vec{k}'} S_0(\vec{k}, \vec{k}') = \frac{V}{8\pi^3} \int S_0(\vec{k}, \vec{k}') d\vec{k}'$$

This gives

$$\lambda_0(k) = \frac{e^2 m^{*1/2} \omega_0}{\sqrt{2} \hbar} \left(\frac{1}{\epsilon_\infty} - \frac{1}{\epsilon_0} \right) \frac{1}{E^{1/2}} \left[\ln \left| \frac{E^{1/2} + E'^{1/2}}{E^{1/2} - E'^{1/2}} \right| \right] \times \begin{cases} N_0 \text{ (absorption)} \\ (N_0 + 1) \text{ (emission)} \end{cases} \quad (1.9a)$$

where

$$E' = \begin{cases} E + \hbar\omega_0 & \text{(absorption)} \\ E - \hbar\omega_0 & \text{(emission)} \end{cases} \quad (1.9b)$$

The energies E and E' are measured from the minimum of the valley concerned.

Acoustic Phonon Scattering:

Since the energy of an acoustic phonon is small compared to $k_B T$, this process can be considered to be elastic. The scattering rate (including both absorption and emission) from \vec{k} to \vec{k}' for this process is given by²⁶

$$S_a(\vec{k}, \vec{k}') = \frac{2\pi \cdot \rho \cdot \hbar \Xi_a}{\hbar} |\vec{k} - \vec{k}'| N_a \delta[E(\vec{k}') - E(\vec{k})] \quad (1.10)$$

Where N_a is the acoustic phonon occupation number, ρ is the density, S is the velocity of sound and Ξ_a is the acoustic phonon deformation potential.

$$N_a = \left[\exp\left(\frac{\hbar S |\vec{k} - \vec{k}'|}{k_B T}\right) - 1 \right]^{-1} \approx \frac{k_B T}{\hbar S |\vec{k} - \vec{k}'|} \quad (1.11)$$

summing (1.10) over all \vec{k}' the total transition rate from state \vec{k} due to this process becomes

$$\lambda_a(k) = \frac{(2m^*)^{3/2} k_B T \Xi_a^2}{2\pi \rho S^2 \hbar^4} E^{1/2} \quad (1.12)$$

Non Equivalent Intervalley Scattering:

Transitions are possible between states in the central and satellite valleys with the absorption or emission of a suitable²⁷ phonon (the inter valley phonon). It is convenient to distinguish between the two types of valleys by suffices i and j . The transition rate from state \vec{k} in valley i to state \vec{k}' in valley j is given by²⁰

$$S_{ij}(\vec{k}, \vec{k}') = \frac{2\pi}{\hbar} Z_j \frac{\hbar}{2\rho\omega_{ij}V} \Xi_{ij}^2 \times \begin{cases} N_{ij} \delta[E_j(\vec{k}') - E_i(\vec{k}) + \Delta_j - \Delta_i - \hbar\omega_{ij}] \\ (N_{ij} + 1) \delta[E_j(\vec{k}') - E_i(\vec{k}) + \Delta_j - \Delta_i + \hbar\omega_{ij}] \end{cases} \quad (1.13)$$

(absorption)
(emission)

where ω_{ij} is the intervalley phonon frequency, Z_j is the number of valleys of type j , Ξ_{ij} is the intervalley deformation potential and N_{ij} is the intervalley phonon occupation number given by

$$N_{ij} = \left[\exp(\hbar\omega_{ij}/k_B T) - 1 \right]^{-1} \quad (1.14)$$

The energies E_i and E_j are measured from the minima of valleys denoted by i and j ; the minima are at energies Δ_i and Δ_j for valleys i and j respectively.

Summing over all \bar{k}' the total transition rate from state \bar{k} due to this process becomes

$$\lambda_{ij}(\bar{k}) = \frac{Z_j m_j^{*3/2} \Xi_{ij}^2}{\sqrt{2} \pi \rho \omega_{ij} \hbar^3} E_j'^{1/2} \times \begin{cases} N_{ij} & \text{(absorption)} \\ (N_{ij} + 1) & \text{(emission)} \end{cases} \quad (1.15a)$$

where

$$E_j' = \begin{cases} E_i - \Delta_j + \Delta_i + \hbar \omega_{ij} & \text{(absorption)} \\ E_i - \Delta_j + \Delta_i - \hbar \omega_{ij} & \text{(emission)} \end{cases} \quad (1.15b)$$

The Equivalent Intervalley Scattering Among Satellite Valleys:

Just as in Silicon, the scattering among equivalent (100) valleys of GaAs by absorption or emission of the phonons of optical branch is expected to be large. The transition rate from state \bar{k} to \bar{k}' for this process is given by

$$S_e(\bar{k}, \bar{k}') = \frac{2\pi}{\hbar} \frac{(Z_e - 1) \hbar}{2\rho \omega_e V} \Xi_e^2 \times \begin{cases} N_e \delta[E(\bar{k}') - E(\bar{k}) - \hbar \omega_e] & \text{(absorption)} \\ (N_e + 1) \delta[E(\bar{k}') - E(\bar{k}) + \hbar \omega_e] & \text{(emission)} \end{cases} \quad (1.16)$$

where

$$N_e = \left[\exp(\hbar \omega_e / k_B T) - 1 \right]^{-1} \quad (1.17)$$

ω_e is the inter valley phonon frequency, Ξ_e is the deformation potential for this process and Z_e is the number of equivalent valleys.

Summing over all \bar{k}' the total transition rate from state \bar{k} due to this process becomes

$$\lambda_e(k) = (Z_e^{-1}) \frac{m_a^{3/2} \omega_e^2 E'^{1/2}}{\sqrt{2\pi} \rho \omega_e \hbar^3} \times \left\{ \begin{array}{l} N_e \text{ (absorption)} \\ (N_e+1) \text{ (emission)} \end{array} \right\} \quad (1.18a)$$

where

$$E' = \left\{ \begin{array}{l} E + \hbar \omega_e \text{ (absorption)} \\ E - \hbar \omega_e \text{ (emission)} \end{array} \right. \quad (1.18b)$$

Figs. 2 and 3 depict the total transition rates from a state as functions of energy of the state for various scattering mechanisms. It can be seen from Fig. 2a and 2b that at low energies (and therefore at low fields) polar optical phonon scattering dominates in the central valley. Acoustic phonon scattering is very small at low energies and therefore it can be safely neglected until very high fields are reached. At higher fields when sufficient electrons have energies more than .35 eV, the most important scattering mechanism in the central valley is the intervalley (non equivalent) scattering. This is then the principal energy loss mechanism, and, since the intervalley scattering rate does not depend upon the direction of \bar{k}' , this is also the principal momentum randomizing mechanism. Acoustic phonon scattering is also momentum randomizing but its magnitude is very small in the central valley. By contrast, the polar optical phonon scattering is not randomizing. It is strongly

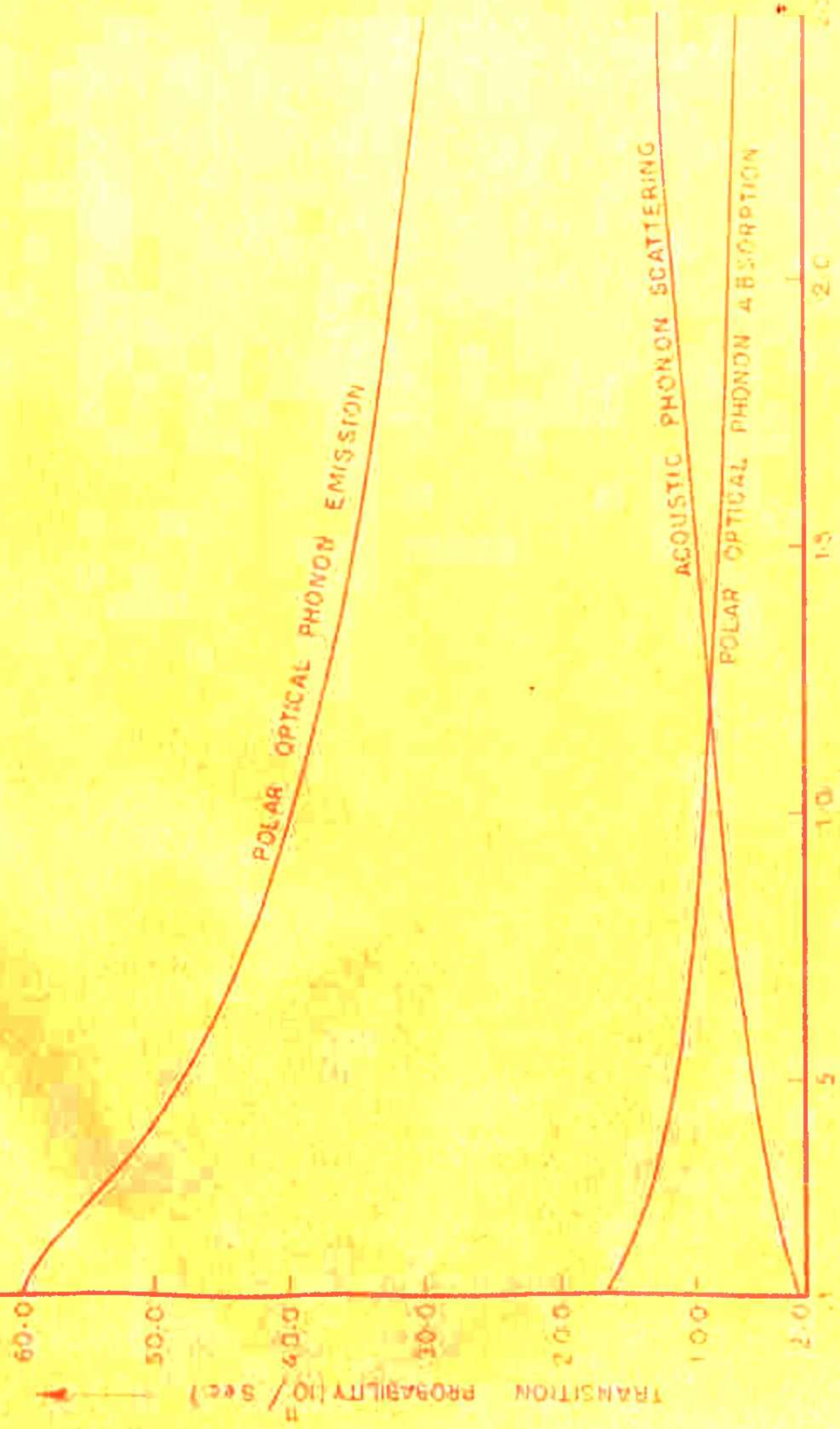


FIG 2 a ACOUSTIC AND POLAR OPTICAL SCATTERING IN CENTRAL VALLEY



FIG. 2b INTER VALLEY SCATTERING FOR AN ELECTRON IN CENTRAL VALLEY

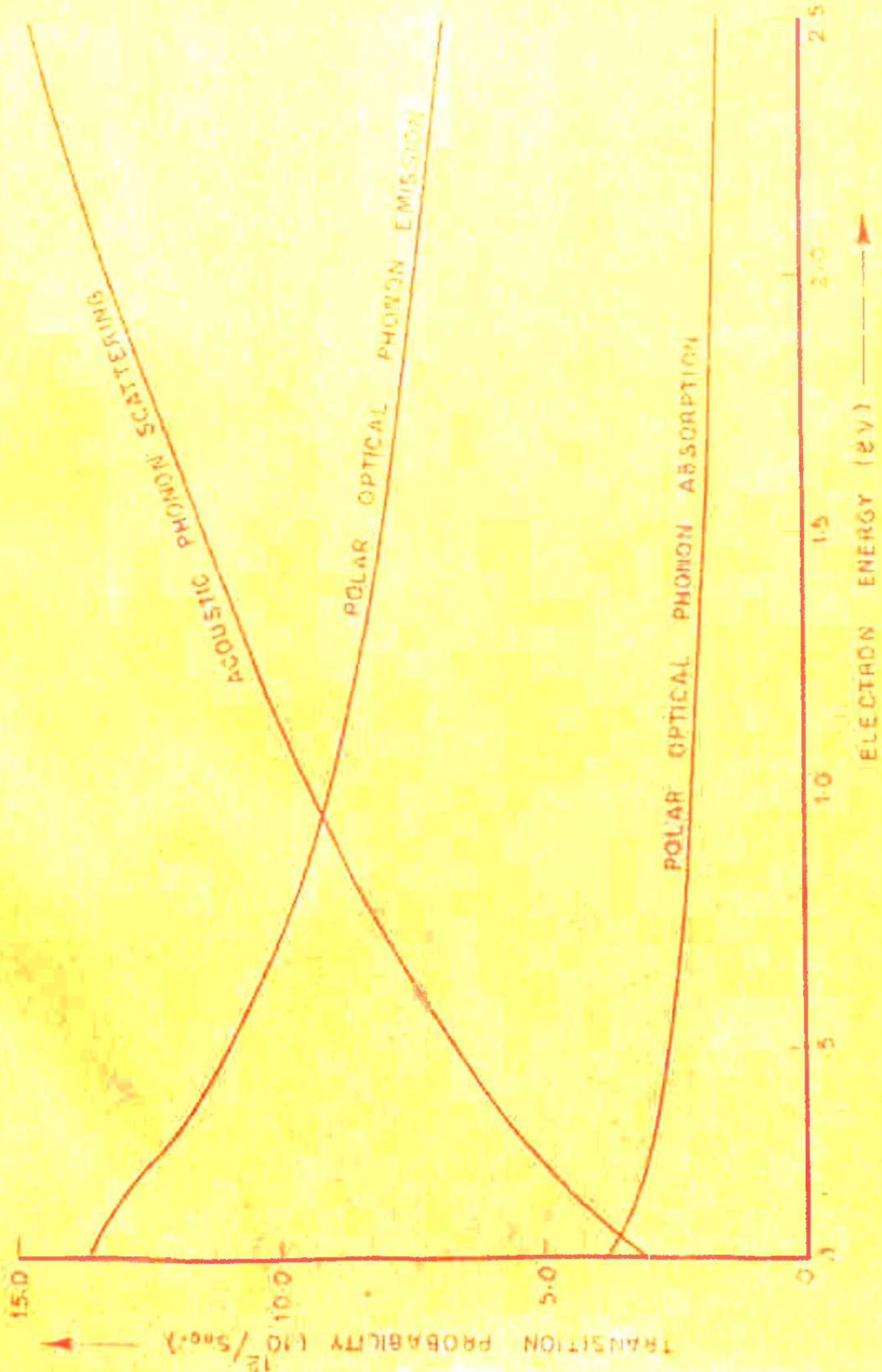


FIG. 3 a ACOUSTIC AND POLAR OPTICAL SCATTERING IN SATELLITE VALLEY

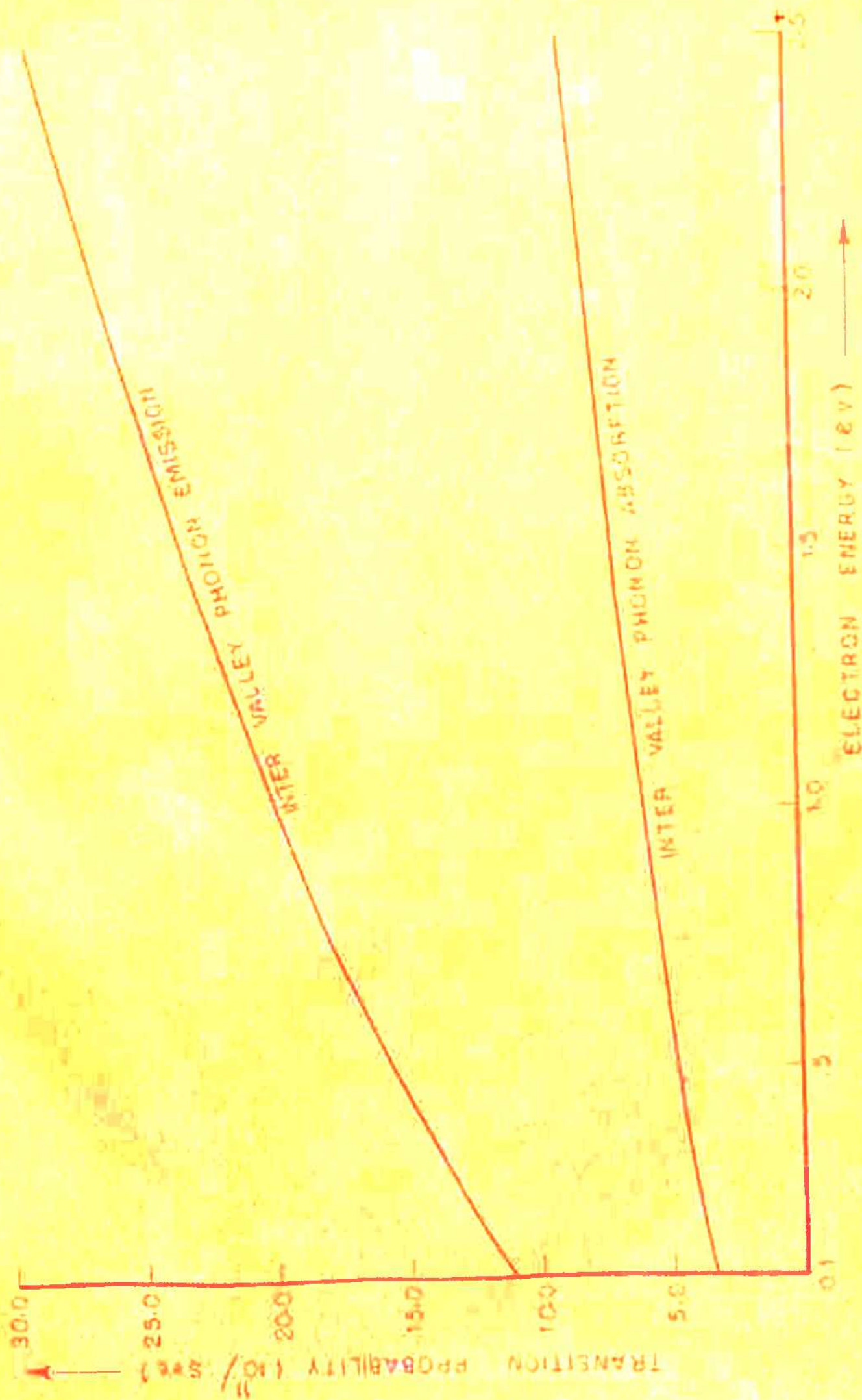


FIG. 3b INTER VALLEY SCATTERING FOR AN ELECTRON IN SATELLITE VALLEY.



FIG. 3C EQUIVALENT INTER - VALLEY SCATTERING BETWEEN SATELLITE VALLEYS.

directional. If \bar{k} and \bar{k}' are the initial and final states of the electron then from equn (1.7) it can be seen that for polar scattering the probability $p(\beta)d\beta$ that \bar{k}' lies in a small range $d\beta$ at angle β with \bar{k} is

$$p(\beta)d\beta \propto [E + E' - 2(EE')^{1/2} \cos\beta] E'^{1/2} \sin\beta d\beta \quad (1.19a)$$

$$\text{where } \left. \begin{array}{l} E' = E + \hbar\omega_0 \text{ (absorption)} \\ E' = E - \hbar\omega_0 \text{ (emission)} \end{array} \right\} \quad (1.19b)$$

The probabilities for both forward ($\beta=0$) and backward ($\beta=\pi$) scattering are zero and the direction of maximum scattering depends upon the energy of the electron.

In the satellite valleys, again, at low energies, the polar optical phonon scattering dominates. Next in line and quite close to it is the equivalent intervalley scattering. The acoustic phonon and the non equivalent intervalley scatterings are small.

With the increase of electron energy, the effectiveness of equivalent intervalley scattering rises very rapidly. The effectiveness of acoustic phonon scattering also rises fast. The non-equivalent intervalley scattering also increases though rather slowly; but the polar mode scattering decreases as can be seen from Fig. 3a.

At higher energies, the equivalent intervalley scattering is the dominant scattering. It is the principal energy loss mechanism. Both the equivalent intervalley scattering and the acoustic mode scattering mainly serve to randomize the momentum. The polar mode scattering is again non randomizing as in the case of central valley. However it is an important energy loss mechanism at lower electron energies.

V. TECHNIQUES FOR SOLVING BOLTZMANN'S TRANSPORT EQUATION FOR GALLIUM ARSENIDE:

Here we review briefly the various techniques that have been applied in the literature to solve the Boltzmann's transport equation for GaAs.

As mentioned earlier in section III, it is not possible to solve the Boltzmann's transport equation for Gallium Arsenide exactly because it takes the form of two complicated coupled integrodifferential equations for the distribution functions in the two valleys. When substitution is made for the collision term $\left(\frac{\partial f}{\partial t}\right)_{coll}$ in the Boltzmann's transport equation (eqn. 5) for each valley using eqn.(1.6) and the transition rates for various scattering mechanisms described in the previous section.

Approximations are therefore necessary to be made. One such approximation is the displaced Maxwellian approximation due to Butcher and Fawcett²⁸. In this, the distribution functions in the central and satellite valleys are approximated by two different displaced Maxwellian distribution functions. i.e.

$$f_i(\vec{k}) = n_i \left(\frac{h^3}{2\pi m_i k_B T_i} \right)^{3/2} \exp\left(-\frac{h^2 (\vec{k} - \vec{k}_i - \vec{d}_i)^2}{2m_i k_B T_i} \right) \quad (1.20)$$

where $i = 1$ denotes the central valley and $i = 2$ denotes the satellite valley. \vec{d}_i and T_i denote the displacement and the

electron temperature in the i th valley, k_B is the Boltzmann's constant, n_i is the number of electrons in the i th valley and \vec{k}_i is the position of energy minimum of the i th valley in wave vector space. The parameters n_i and T_i are identical in all the satellite valleys but have different values in the central valley. The Boltzmann's transport equation for distribution function in the i th valley established in the presence of steady electric field \vec{F} reads

$$\frac{\partial f_i(\vec{k})}{\partial t} = \left[\frac{\partial f_i(\vec{k})}{\partial t} \right]_F + \left[\frac{\partial f_i(\vec{k})}{\partial t} \right]_{ii} + \sum_{j \neq i} \left[\frac{\partial f_i(\vec{k})}{\partial t} \right]_{ij} \quad (1.21)$$

where the first term on the RHS denotes the rate of change of $f_i(\vec{k})$ due to the field. The second term is the rate of change of $f_i(\vec{k})$ produced by all intravalley (and also equivalent intervalley) scattering processes in valley i of which there are a large number. However, the important intravalley scattering mechanisms for each valley have already been mentioned in section IV and only those will be used for further consideration.

The third term on the RHS of equn. (1.21) represents the rate of change of $f_i(\vec{k})$ produced by all (non equivalent) intervalley scattering processes between valleys i and j , of which, again, there is a large number. However, we shall consider only the phonon induced transitions between the

central valley and the equivalent satellite valleys whose transition rates have already been given in the previous section. This term gives rise to the coupling between the distribution functions as we shall see later more explicitly.

After approximating the distribution functions in the two valleys by two different displaced Maxwellian forms (equation 1.20), Butcher and Fawcett evaluated the values of parameters n_i , \bar{d}_i and T_i as functions of the electric field from the conservation equations for electron number, wave vector and energy for each valley. For a steady electric field these conservation equations read

$$\int_i \left[\frac{\partial f_i(\bar{k})}{\partial t} \right] \phi_i(\bar{k}) d\bar{k} = \int_i \left[\frac{\partial f_{ij}(\bar{k})}{\partial t} \right]_F \phi_i(\bar{k}) d\bar{k} + \int_i \left[\frac{\partial f_{ij}(\bar{k})}{\partial t} \right]_{ij} \phi_i(\bar{k}) d\bar{k} = 0 \quad (1.22)$$

where, as before, $i = 1$ denotes the central valley and $i = 2$ denotes the satellite valley and $\phi_i(\bar{k})$ takes value 1, $\bar{k} - \bar{K}_i$ and $\epsilon_i(\bar{k}) - \Delta_i$ in turn to give the number conservation, wave vector conservation and energy conservation equations respectively. Eqns. (1.22) represent a total of 10 equations (one for the conservation of number in the central valley, three for the conservation of three components of $(\bar{k} - \bar{K}_1)$ in the central valley and one for the conservation of energy in the central valley - a total of five equations for the central valley and the same

number of equations for $i = 2$ i.e. the satellite valley) which can uniquely determine the ten parameters n_i , \bar{d}_i and T_i . However, since the displacements of the distribution functions in the two valleys are expected to be opposite to the direction of the electric field applied, the displacements become scalars when the direction of applied electric field is chosen as one of the coordinate axes in \bar{k} -space . This results in appreciable simplification and the number of equations to be solved becomes six.

Further, the electron number conservation equations for the central and satellite valleys are equivalent since the total number of electrons is automatically conserved.

It may here be noted that the substitution of displaced Maxwellian forms for the distribution functions in the conservation equations reduces the original set of ten integrodifferential equations that equn. (1.22) represents into ten simultaneous algebraic equations in the parameters n_i , \bar{d}_i and T_i which occur in the integrands of definite integrals. In particular, the integrals in the conservation equations can be evaluated exactly and the solutions can be obtained by an iterative numerical procedure. Further details and the procedure for obtaining the solution shall be described in the next section.

Another approach for solving the Boltzmann's transport equation for GaAs in the literature is due to Conwell and Vassel¹¹. This technique relies upon the assumption that a relaxation time exists for all the scattering mechanisms that are important in Gallium Arsenide. Conwell and Vassel expand the distribution function in terms of spherical harmonics and truncate the series after the second term assuming that the higher order terms are small. This implies that at low fields the distribution function can be thought of as composed of mainly a spherically symmetric part with the superposition of a small distortion that is maximum in the field direction and decreases as one moves away from this direction. i.e.

$$f_i(\vec{R}) = f_{0i}(k) + f_{1i}(k) \cos \theta \quad (1.23)$$

since the valleys are spherical, this can be written as

$$f_i(E, \theta) = f_{0i}(E) + g_i(E) k_E \quad (1.24)$$

where

$$g_i(E) = \frac{f_{1i}(k)}{k} \quad (1.25)$$

and $k_E = k \cos \theta$ is the component of wave vector in the field direction. The first term on the RHS of equn. (1.24) being spherically symmetric does not contribute to the electron transport.

The second term gives rise to net momentum in the direction of field and is responsible for the electric current. The mobility of a semiconductor depends upon the rate at which the net momentum (or the field directed momentum) is destroyed. Under certain conditions²⁹ the rate of destruction or relaxation of such momentum is proportional to the existing momentum in the field direction. The proportionality factor is the reciprocal of a time called the relaxation time and it is this time that must be used in the calculation of the mobility. However, a relaxation time may not always exist. One such example is the polar mode scattering at low energies. In this case, the net rate of change of momentum in the field direction due to polar mode scattering i.e. $\left. \frac{\partial [g_i(E) kE]}{\partial t} \right|_{p_0}$ is not proportional to $g_i(E) kE$ ¹¹. Only at energies much greater than the optical phonon energy is $\left. \frac{\partial [g_i(E) kE]}{\partial t} \right|_{p_0}$ proportional to $g_i(E) kE$ and a relaxation time exists¹¹.

When a relaxation time exists for all the scattering mechanisms, the transport problem is greatly simplified as described below.

The steady state transport equation for the *i*th valley reads

$$\left[\frac{\partial f_i(\vec{k})}{\partial t} \right]_F + \left[\frac{\partial f_i(\vec{k})}{\partial t} \right]_C = 0 \quad (1.25)$$

where the first term on the LHS is the rate of change of $f_i(\vec{k})$ due to field and the second term is the rate of change of $f_i(\vec{k})$ due to all sorts of collisions.

Now

$$f_i(\vec{k}) = f_{0i}(E) + g_i(E) k_E \quad (1.27)$$

When a relaxation time exists, the substitution of (1.27) in the collision term of equn. (1.26) permits that term to be written as

$$\left[\frac{\partial f_i(\vec{k})}{\partial t} \right]_c = \left(\frac{\partial f_{0i}}{\partial t} \right)_c - \frac{g_i(E) k_E}{\tau_i} \quad (1.28)$$

where τ_i is the combined relaxation time for all the processes in valley i . $\left(\frac{\partial f_{0i}}{\partial t} \right)_c$ does not contain k_E .

Similarly $\left[\frac{\partial f_i}{\partial t} \right]_F$ can also be written as a sum of terms independent of k_E and terms linear in k_E . The vanishing of $\left[\frac{\partial f_i(\vec{k})}{\partial t} \right]_F + \left[\frac{\partial f_i(\vec{k})}{\partial t} \right]_c$ then implies separate vanishing of coefficients of different powers of k_E and it yields four coupled equations in f_{01}, f_{02}, g_1 and g_2 . At this stage the utility of relaxation time approximation becomes evident.

As a direct result of this approximation one of these equations is of the form

$$A f_{01}' - \frac{g_1}{\tau_1} = 0$$

and another is of the form

$$B f_{02}' - \frac{g_2}{\tau_2} = 0$$

Where primes denote derivatives w.r.t. E . These two equations can be used to eliminate g_1 and g_2 from the other two equations. The result is two coupled second order differential equations for f_0 and f_{02} , which can be solved numerically. When relaxation times do not exist, a decoupling of the type mentioned above is not possible and the problem to solve the resulting four coupled ^{difference} differential equations (which then have terms like $g_1(E)$ and $g_1(E + \hbar\omega_c)$ occurring in the same expression) is a formidable one.

A detailed calculation of the collision integrals for various scattering mechanisms i.e. terms of the type $\left(\frac{\partial f_{0i}}{\partial t}\right)_{\text{polar mode}}$ etc. and the corresponding relaxation times is given by Conwell and Vassel¹¹. They have also discussed at length the appropriate boundary conditions for the solutions.

Both the displaced Maxwellian approach and the relaxation time approach are approximate techniques to solve the Boltzmann's transport equation, which, hitherto, has been considered to provide the necessary (and perhaps only) theoretical formalism for solving the transport problems.

However, Kurosawa³⁰ and Fawcett et al^{31,20} have carried out theoretical calculations of distribution function and transport properties without the use of Boltzmann's

transport equation. Their calculations termed the Monte-Carlo calculations consist of simulating the motion of an electron in momentum space on a digital computer. In the presence of an applied electric field this motion consists alternately of a drift with constant velocity in the electric field followed by a scattering by phonons. The time for which the electron drifts in the electric field, the type of scattering process which terminates the drift and the final state after scattering are random quantities with probability distributions which can be expressed in terms of the transition rates due to various scattering processes and the strength of the electric field.

For example, the probability that an electron will drift for a time t in the electric field F and will then be scattered in the next second is given by

$$P(t) = \lambda[\vec{k}(t)] \exp \left\{ - \int_0^t \lambda[\vec{k}(t')] dt' \right\} \quad (1.29a)$$

where

$$\vec{k}(t) = \vec{k}_0 + \frac{e\vec{F}t}{\hbar} \quad (1.29b)$$

$$\lambda(\vec{k}) = \sum_{q=1}^N \lambda_q(\vec{k}) \quad (1.29c)$$

and $\lambda_q(\vec{k}) = \int S_q(\vec{k}, \vec{k}') d\vec{k}'$ is the total transition rate from state \vec{k} due to the q th process. Also, \vec{k}_0 is the wave vector at $t = 0$; at the beginning of the flight i.e. the final state after the previous scattering event. The probability

that q th process has terminated the flight is

$$\frac{\lambda_q [\bar{r}(t)]}{\sum_{q=1}^N \lambda_q [\bar{r}(t)]} \quad (1.30)$$

Random times of flight which obey the probability distribution (1.29) can be generated using the Monte Carlo technique^{32, 33, 54, 55}. This technique provides for generating random numbers from any given probability distribution with the help of a 'basic sequence' of random numbers from another probability distribution. The 'basic sequence' usually used is a sequence of random numbers r generated with equal (uniform) probability between 0 and 1. This is because it is only straight forward to generate such a sequence on a computer. The random times of flight t from the probability distribution (1.29) are then obtained by solving the equation

$$r = \int_0^t P(t') dt' \quad (1.31)$$

However, further discussions in detail shall be taken at a later stage. Here it will suffice to summarise the procedure of simulation. First of all, a random time of flight t is generated from the probability distribution (1.29) using the Monte Carlo technique as described above. After we have known the time of flight, another random number is generated from the discrete probability distribution (1.30)

to determine which process has terminated the flight. A further random number generated from the angular probability distribution of final states after scattering determines angle θ between the scattered wave vector and $\bar{k}(t)$. The azimuthal angle ϕ is obtained by generating another uniform random number between 0 and 2π (This is because for all the scattering mechanisms mentioned in section IV the final states after scattering are uniformly distributed in ϕ). Once again a new time of flight is generated and the cycle repeated. This way a large number (several tens of thousands) of collisions are studied. Entire \bar{k} space is divided (meshed) into a large number of fine cells. The total time that electron spends in each cell during the entire course of collisions is recorded and it is proportional to the value of distribution function in that cell. Separate meshes are made for the central and satellite valleys and the recording switches from one mesh to another in the appropriate cell whenever the electron suffers a transition from the central valley to the satellite valley or vice-versa. The population ratio of the two valleys is simply the ratio of total times that the electron has spent in the two meshes. The drift velocity in the j th valley is

$$v_j = \frac{1}{\kappa K_j} \sum (E_f - E_i)$$

where \bar{K}_j is the total length of the k space trajectory in the j th valley i.e. $K_j = \frac{eFT_j}{\kappa}$, where T_j is the total

time that the electron spends in the mesh for the j th valley. E_i and E_f are the initial and final values of energy for a particular flight and the summation is over all the flights.

That the technique is equivalent to the Boltzmann's transport equation approach in the limit when the number of collisions considered is large has been shown by Fawcett et al²⁰.

It is now worthwhile to review the relative merits and demerits of these three approaches. In the displaced Maxwellian approach, first and foremost it is very difficult to justify the assumption that the electron distributions in the two valleys can be represented by the displaced Maxwellian functions. It is to be expected that when electron densities are large, electron-electron collisions are very frequent and any momentum and energy gained by the electrons from the field is much more rapidly distributed among themselves than it is lost to the phonons. A displaced Maxwellian form may well represent the electron distribution then. However, the electron density in GaAs is quite small and the assumption is not very justified. Stratton³³ also points out that an electron density at which the rate of loss of energy by fast electrons to slow electrons is equal to the rate of loss

of energy by electrons to phonons need not be sufficient to balance the rate of loss of momentum to the two processes. Higher electron densities are required in the case of GaAs to balance the two momentum loss rates. And since it is the rate of loss of momentum by fast electrons to slow electrons that must be larger than the rate of loss of momentum by electrons to phonons for ensuring a displaced Maxwellian distribution, much higher electron densities than what actually are in GaAs are required for the purpose. That makes the assumption quite unjustified in case of GaAs. However, since no further approximations are required (at least in the simple case with parabolic valleys and s-type wave functions) the method permits to take a full account of the inelastic scattering (by polar modes) which is dominant at low energies.

In the relaxation time approximation on the other hand, the assumption that a relaxation time exists for all the scattering mechanisms is far from realistic at low energies, and at higher energies, the neglect of terms beyond the second term in the spherical harmonic expansion of the distribution function becomes extremely unjustified. In such cases there is a strong streaming of electrons in the field direction and the Maximum anisotropy approximation due to Baraff³⁹ must be used with a suitable higher value of N .

Both these approaches have given qualitatively correct results but quantitative agreements are not very satisfactory. The best quantitative agreements come from the Monte Carlo calculation²⁰ which permits a wider dimension for the theoretical study of transport at all fields. Here no form is assumed for the distribution function, instead, the distribution function builds up in the natural course of collisions that the electron suffers. Also the effects of nonparabolicity, and the wave vector dependence of the cell periodic part of Bloch functions can be exactly taken into account which is nearly impossible in the earlier two analytical approaches. The method is much more simple and direct compared to the analytical approaches. However fast computers are required and one must study a very large number of collisions to get the desired accuracies in the results.

VI. EFFECT OF VARIOUS SCATTERING MECHANISMS ON THE SOLUTION OF BOLZMANN'S TRANSPORT EQUATION:

To study the effect of various scattering mechanisms on the solution of Boltzmann's transport equation and the velocity field characteristic for GaAs, we shall start with the solution considering only those scattering mechanisms which are most important at low energies. The displaced Maxwellian approach shall be used. From Figs. 2 and 3 it can be seen that the most important scattering mechanism at low energies is the polar optical phonon scattering in both the central and satellite valleys. One must ofcourse take into account the intervalley (non equivalent) scattering since the electron transfer from central to satellite valleys is the most important feature of electron transport in GaAs. Considering only these two scattering mechanisms in both the central and satellite valleys the conservation equations (1.22) for the steady state for number, wave vector and energy for the two valleys become:

$$\int_i \left[\frac{\partial f_i(\vec{k})}{\partial t} \right]_F \overline{d\vec{k}} + \int_i \left[\frac{\partial f_i(\vec{k})}{\partial t} \right]_{p_0} \overline{d\vec{k}} + \sum_{j \neq i} \int_i \left[\frac{\partial f_i(\vec{k})}{\partial t} \right]_{ij} \overline{d\vec{k}} = 0 \quad (1.32a)$$

$$\int_i \left[\frac{\partial f_i(\vec{k})}{\partial t} \right]_F (\vec{k} - \vec{k}_i) \overline{d\vec{k}} + \int_i \left[\frac{\partial f_i(\vec{k})}{\partial t} \right]_{p_0} (\vec{k} - \vec{k}_i) \overline{d\vec{k}} + \sum_{j \neq i} \int_i \left[\frac{\partial f_i(\vec{k})}{\partial t} \right]_{ij} (\vec{k} - \vec{k}_i) \overline{d\vec{k}} = 0 \quad (1.32b)$$

$$\int_i \left[\frac{\partial f_i(\vec{k})}{\partial t} \right]_F (E_{i1}(\vec{k}) - \Delta_i) \overline{d\vec{k}} + \int_i \left[\frac{\partial f_i(\vec{k})}{\partial t} \right]_{p_0} (E_{i1}(\vec{k}) - \Delta_i) \overline{d\vec{k}} + \sum_{j \neq i} \int_i \left[\frac{\partial f_i(\vec{k})}{\partial t} \right]_{ij} (E_{i1}(\vec{k}) - \Delta_i) \overline{d\vec{k}} = 0 \quad (1.32c)$$

The integrals in equns. (1.3) can be evaluated using the displaced Maxwellian forms for $f_i(\vec{k})$ and the

transition rates for polar optical phonon and intervalley scatterings given in section IV. Necessary mathematical details of the procedure are given in appendix (A). Using the results (A12, A15 and A28) of appendix (A), the number conservation equation for the central valley becomes:

$$-\frac{n_1 \Omega_{12}}{(k_B T_1)^2} \int_0^\infty V \left\{ \left(\frac{2E}{m_1} \right)^{1/2} \frac{\hbar d_1}{k_B T_1} \right\} H_{12}^{(1)}(E) dE + \frac{n_2 \Omega_{21}}{(k_B T_2)^2} \int_0^\infty V \left\{ \left(\frac{2E}{m_2} \right)^{1/2} \frac{\hbar d_2}{k_B T_2} \right\} H_{21}^{(1)}(E) dE = 0 \quad (1.33a)$$

The number conservation equation for the satellite valley turns out to be identical with equn. (1.33a). After dividing out by $n_1 d_1$ and $n_2 d_2$ respectively the conservation equations for the component of momentum antiparallel to the field in central and satellite valleys read.

$$\frac{e F d_1}{\hbar} - \frac{2}{3} \frac{\Omega_1}{(k_B T_1)^2} \int_0^\infty \exp\left(-\frac{E}{k_B T_1}\right) \times U \left\{ \left(\frac{2E}{m_1} \right)^{1/2} \frac{\hbar d_1}{k_B T_1} \right\} Q(E) E dE - \frac{2 \Omega_{12}}{(k_B T_1)^3} \int_0^\infty U \left\{ \left(\frac{2E}{m_1} \right)^{1/2} \frac{\hbar d_1}{k_B T_1} \right\} H_{12}^{(1)}(E) dE = 0 \quad (1.33b)$$

$$\frac{e F d_2}{\hbar} - \frac{2}{3} \frac{\Omega_2}{(k_B T_2)^2} \int_0^\infty \exp\left(-\frac{E}{k_B T_2}\right) \times U \left\{ \left(\frac{2E}{m_2} \right)^{1/2} \frac{\hbar d_2}{k_B T_2} \right\} Q(E) dE - \frac{2}{3} \frac{\Omega_{21}}{(k_B T_2)^3} \int_0^\infty U \left\{ \left(\frac{2E}{m_2} \right)^{1/2} \frac{\hbar d_2}{k_B T_2} \right\} H_{21}^{(1)}(E) dE = 0 \quad (1.33c)$$

and after dividing out by n_1 and n_2 respectively the energy conservation equations for the central and satellite valleys

become:

$$\frac{e \hbar F d_1}{m_1} - \left(\frac{\hbar \omega_0}{k_B T_1} \right) \Omega_1 \int_0^\infty \exp\left(-\frac{E}{k_B T_1}\right) \times V \left\{ \left(\frac{2E}{m_1} \right)^{1/2} \frac{\hbar d_1}{k_B T_1} \right\} \left\{ (N_0 + 1) \phi(E - \hbar \omega_0) - N_0 \phi(E) \right\} dE - \frac{3 \Omega_{12}}{(k_B T_1)^2} \int_0^\infty V \left\{ \left(\frac{2E}{m_1} \right)^{1/2} \frac{\hbar d_1}{k_B T_1} \right\} H_{12}^{(1)}(E) dE + \frac{3 n_2 \Omega_{21}}{n_1 (k_B T_2)^2} \int_0^\infty V \left\{ \left(\frac{2E}{m_2} \right)^{1/2} \frac{\hbar d_2}{k_B T_2} \right\} H_{21}^{(1)}(E) dE = 0 \quad (1.33d)$$

$$\frac{eA}{m_2} F d_2 = \left(\frac{k_B \omega_0}{k_B T_2} \right) \Omega_2 \int_0^\infty \exp\left(\frac{-E}{k_B T_2}\right) \times V \left\{ \left(\frac{2E}{m_2} \right)^{1/2} \frac{k d_2}{k_B T_2} \right\} \left\{ (N_0 + 1) \phi(E - k\omega_0) - N_0 \phi(E) \right\} dE$$

$$-\frac{\Omega_{21}}{(k_B T_2)^2} \int_0^\infty V \left\{ \left(\frac{2E}{m_2} \right)^{1/2} \frac{k d_2}{k_B T_2} \right\} H_{21}(E) dE + \frac{\Omega_{12}}{m_2 (k_B T_1)^2} \int_0^\infty V \left\{ \left(\frac{2E}{m_1} \right)^{1/2} \frac{k d_1}{k_B T_1} \right\} H_{12}(E) dE = 0$$

(1.33e)

Equation (1.33a) gives the ratio n_2/n_1 as a function of d_1 , d_2 , T_1 and T_2 . Substituting this function for n_2/n_1 in equns. (1.33 b, c, d and e) we get equations of the form

$$F/d_1 = M_1(d_1, T_1) \quad (1.34a)$$

$$F/d_2 = M_2(d_2, T_2) \quad (1.34b)$$

$$F d_1 = E_1(d_1, d_2; T_1, T_2) \quad (1.34c)$$

$$F d_2 = E_2(d_1, d_2; T_1, T_2) \quad (1.34d)$$

These four equations determine d_1 , d_2 , T_1 and T_2 as functions of F . However, in solving these equations it is more convenient to regard T_1 as the independent variable and to replace one of the four equations by the equation obtained by eliminating F , d_1 and d_2 from the left hand sides:

$$M_1(d_1, T_1) E_1(d_1, d_2; T_1, T_2) = M_2(d_2, T_2) E_2(d_1, d_2; T_1, T_2) \quad (1.34e)$$

An iterative numerical solution can be obtained by assigning T_1 a value above room temperature and giving d_1 and d_2 their starting value zero in equn. (1.34e) and in the right hand sides of equns. (1.34 ^{a, b, c and d}). Equn. (1.34e) can then be solved numerically for T_2 and the solution can be substituted in equns. (1.34a, b, c and d) which yield value for F

and new values for d_1 and d_2 . The process is repeated with these new values of d_1 and d_2 and continued until convergence is achieved. Usually six iterations sufficed to give a reasonable accuracy. In the seventh iteration the change in the values of various quantities was often less than 1 %.

The velocity field characteristic resulting from this calculation for a lattice temperature of 300°K is shown as curve (a) in Fig. 5a. Curves (a) and (c) of Fig. 5b depict the electron temperatures in the central and satellite valleys respectively as functions of the electric field. Curve (a) of Fig. 5c shows the fraction of electrons in the central valley as a function of the electric field. It can be seen from these curves that the threshold field is about 3.1kV/cm and the valley field is about 5.2 kV/cm . The low field mobility is $7800\text{ cm}^2/\text{V sec}$ and the high field mobility is about $750\text{ cm}^2/\text{V sec}$. There is a very steep region of negative differential mobility between the threshold and valley fields. The average negative differential mobility has a magnitude of about $5400\text{ cm}^2/\text{V sec}$. The electron distribution in the central valley first heats up slowly with the applied field; between the threshold and valley fields the rate of heating is very high; thereafter, the rate of heating slows down, the electron temperature rises almost linearly with the field reaching about 4000°K at

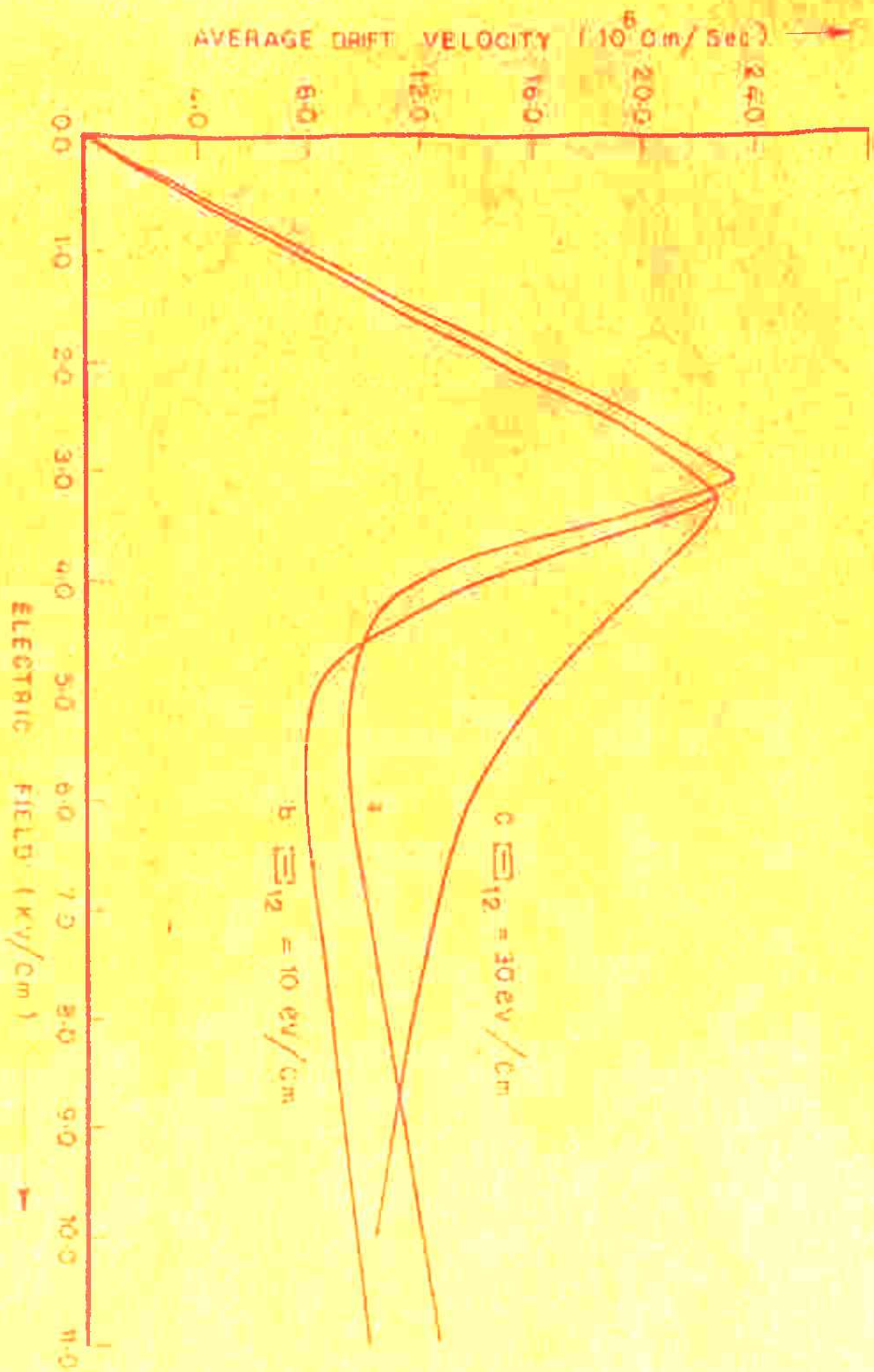


FIG. 5 a

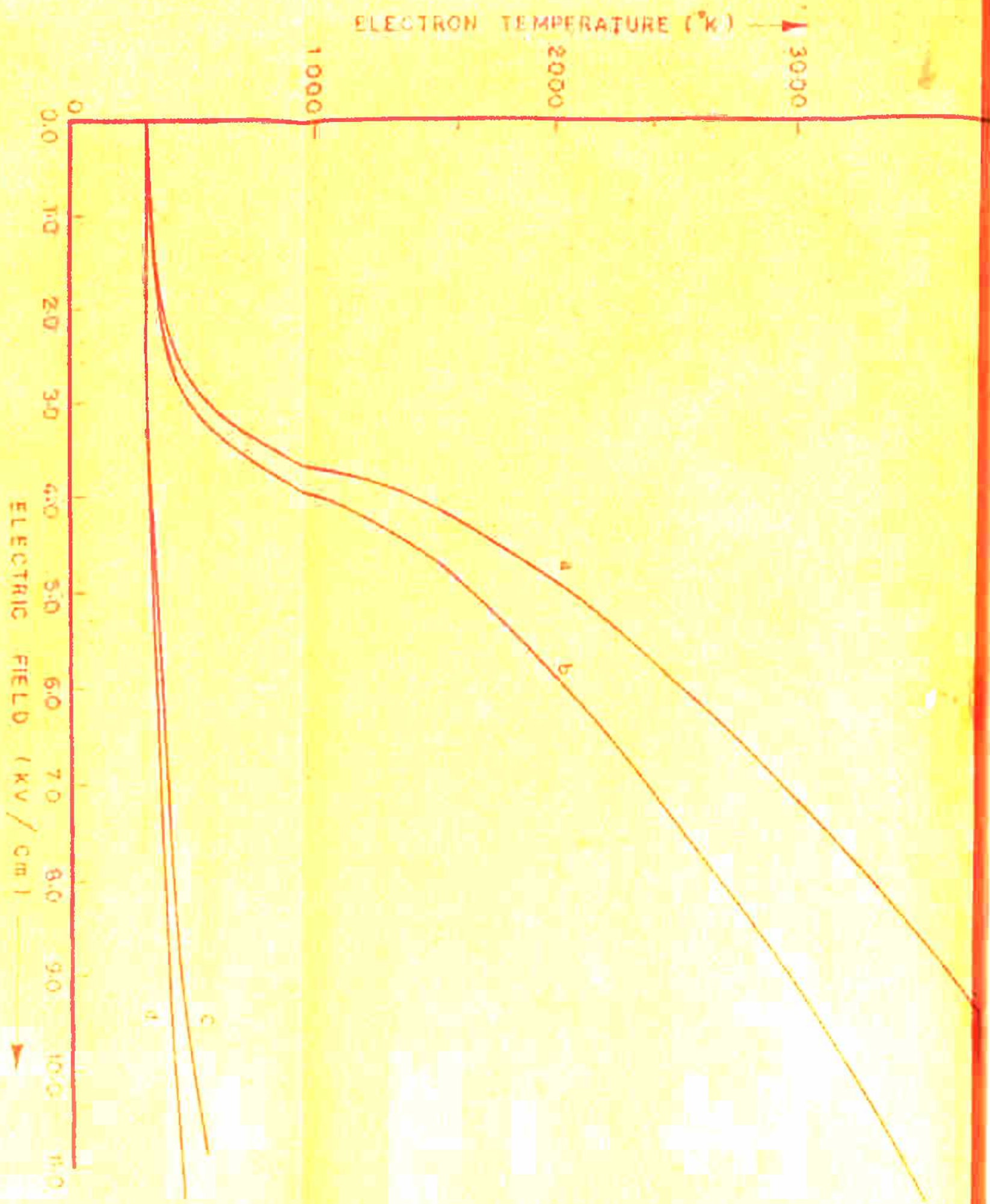
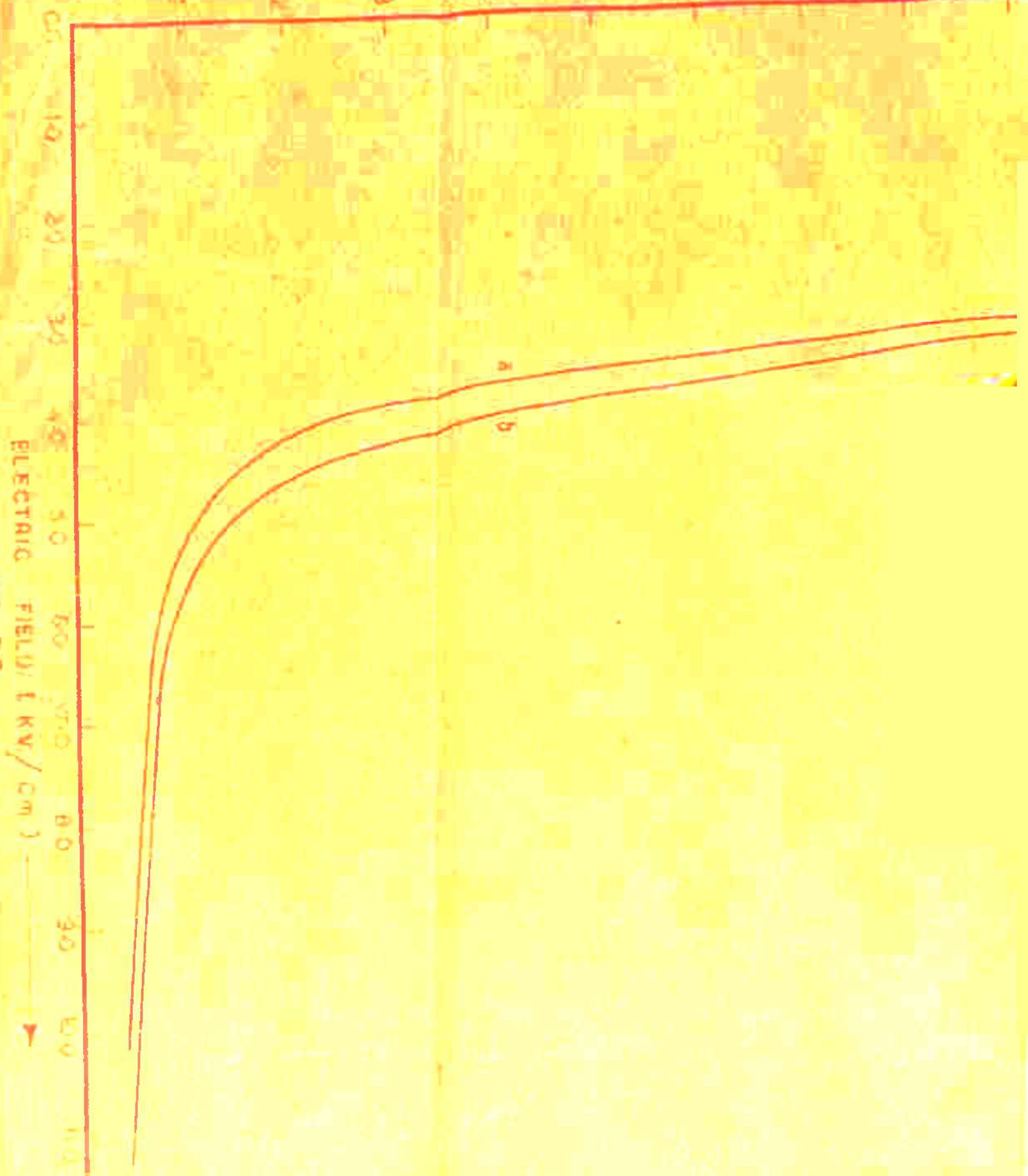


FIG. 5B

FRACTION OF ELECTRONS IN 1000 Å VALLEY



ELECTRIC FIELD (kV/cm)

FIG. 5C

10 kV/cm. Much less heating takes place in the satellite valleys. The electron temperature in the satellite valleys is only 490°K for a field of 10 kV/cm. Beyond the threshold field there is rapid transfer of electrons to the satellite valleys resulting in a steep negative differential mobility region and a small value of valley field. There are only about 5% of the total electrons in the central valley at 10 kV/cm.

The low field mobility and threshold field values are in very good agreement with the experimental results of Ruch and Kino³² who have reported a low field mobility of $7500\text{ cm}^2/\text{V sec}$ and a threshold field of 3.3 kV/cm. However, the calculated negative differential mobility and high field mobility values are much higher and the valley field is much lower as compared to the experimental results. Ruch and Kino report a negative differential mobility of magnitude $2600\text{ cm}^2/\text{V sec}$ at the onset of negative differential mobility region. They have found no evidence of a valley field upto 14 kV/cm. It may be mentioned here that because of the strong instability associated with the negative differential mobility the measurement of velocity field characteristic for GaAs in the negative differential mobility region had been very difficult. Out of all the experimental investigations only those due to Ruch and Kino³² provide the most reliable and direct measurements of drift velocity as a

function of field. All earlier measurements⁴⁵ were indirect and for obtaining a relation between the drift velocity and applied field from the experimental data one had to rely upon assumptions which are now known to be rather crude. We shall therefore make comparisons only to the experimental results of Ruch and Kino.

Next we include the equivalent intervalley scattering among the satellite valleys in our calculation of velocity field characteristic. One can include respectively terms like $\int_2 \left[\frac{\partial f_2(\vec{k})}{\partial t} \right]_e d\vec{k}$, $\int_2 \left[\frac{\partial f_2(\vec{k})}{\partial t} \right]_e (\vec{k} - \vec{k}_2) d\vec{k}$, $\int_2 \left[\frac{\partial f_2(\vec{k})}{\partial t} \right]_e (E_2(\vec{k}) - \Delta_2) d\vec{k}$

in the left hand sides of equns. (1.32a), (1.32b) and (1.32c) for $i = 2$ to take into account the net rate of change of number, momentum and energy in the satellite valley because of the equivalent intervalley scattering. Explicit expressions for these integrals can be substituted from equns (A2a to A3a) of appendix (A) and the conservation equations can be solved as discussed earlier.

The resulting velocity field characteristic is shown as curve (b) of Fig. 5a. Curves (b) and (d) of Fig. 5b show the variation of electron temperatures in the central and satellite valleys with the electric field and curve (b) of Fig. 5c shows the variation of fractional electron population in the central valley with the applied electric field.

Curve (b) of Fig. 5a shows a low field mobility value of about $7200 \text{ cm}^2/\text{V sec}$ which is about $600 \text{ cm}^2/\text{V sec}$ less than that shown by curve (a) of Fig. 5a. The threshold field is about 3.3 kV/cm . The magnitude of negative differential mobility is some what less and the valley field is some what higher in curve (b) as compared to curve (a). Finally, the slope of velocity field characteristic beyond the valley field is significantly less in curve (b) as compared to curve (a). The high field mobility from curve (b) is about $440 \text{ cm}^2/\text{V sec}$ (as compared to about $750 \text{ cm}^2/\text{V sec}$ in curve (a)) which is in good agreement with a value of $400 \text{ cm}^2/\text{V sec}$ reported from Hall mobility measurements²⁰. Other experimental measurements²⁰ give values varying as much as from $110 \text{ cm}^2/\text{V sec}$ to $350 \text{ cm}^2/\text{V sec}$. Curves (b) and (d) of Fig. 5b show that the electron distributions in the two valleys are significantly cooled by the inclusion of equivalent intervalley scattering. Electron temperature in the satellite valleys is about 415°K for a field of 10 kV/cm from curve (d) of Fig. 5b as compared to 480°K from curve (c). Similarly the electron temperature in the central valley for a field of 10 kV/cm is about 3200°K in curve (b) as compared to 4000°K in curve (a). A comparison of curves (a) and (b) of Fig. 5c shows that there is a relatively larger fraction of electrons in the central valley at all fields when equivalent intervalley scattering among the satellite valleys is included.

However, the magnitude of negative differential mobility is still much larger and the valley field is still much smaller as compared to the experimental results. We see from curves (a) and (b) of Fig. 5a and curves (c) and (d) of Fig. 5b that the inclusion of equivalent intervalley scattering greatly lowers the high field mobility and electron temperature in the satellite valleys. This is to be expected since the equivalent intervalley scattering is the principal scattering mechanism for energy loss and momentum randomization in the satellite valleys at higher energies. Other effects due to the inclusion of equivalent intervalley scattering which are of smaller magnitude, such as the lowering of low field mobility and electron temperature in the central valley, increase in the fractional population of the central valley and the valley field can be understood as follows:

The intervalley transitions by absorption or emission of an intervalley phonon can take an electron of energy E ($E > \Delta E - \hbar\omega_{ij}$ for absorption, and $E > \Delta E + \hbar\omega_{ij}$ for emission) in central valley to an energy $E + \hbar\omega_{ij}$ or $E - \hbar\omega_{ij}$ in the satellite valley or vice versa. The transition rate for this process (section IV) is independent of the wave vectors of initial and final states of the electron. Thus for the intervalley scattering the total probability of

transition from a state of energy E in one valley depends upon the number of states that correspond to energies $E + \hbar\omega_j$ and $E - \hbar\omega_j$ in the other. Now the ratio of states in the central and satellite valleys that correspond to an energy

E is

$$R = \frac{\gamma m_1^{3/2}}{3\gamma m_2^{3/2}} \frac{E^{1/2}}{(E - \Delta E)^{1/2}} \quad (1.35)$$

$$R = \frac{1}{34} \frac{1}{\left(1 - \frac{\Delta E}{E}\right)^{1/2}} \quad (1.36)$$

For large values of E (i.e. $E \gg \Delta E$) $R \approx \frac{1}{34}$ (this provides a lower limit to the population ratio) and it increases with decreasing E . If we neglect $\hbar\omega_j$ in comparison to E , then (1.36) gives the ratio between transition rates for an electron of energy E from central to satellite valley and vice-versa. In steady state it also determines the ratio of electron populations in the two valleys at energy E . The fraction R thus plays an important role in determining the population ratio. Now R increases as E decreases . Thus if equivalent intervalley scattering among the satellite valleys is included the electron distribution in the satellite valleys can be kept more cool; the satellite electrons can be confined to lower E values and hence there will be more transitions to the central valley than those when equivalent intervalley scattering is neglected. Thus

the inclusion of equivalent intervalley scattering will give more electrons in the central valley for a given field than those resulting from without its inclusion. Since the electrons in the satellite valleys can be confined to lower energies, the electrons that are scattered into central valley shall also be scattered to lower energies where polar mode scattering is more effective. This results in cooling of the electron distribution in the central valley and lowering of the low field mobility. Since both the distributions are cooled down, there is a slower transfer of electrons to the satellite valleys with the increase in electric field and consequently the magnitude of negative differential mobility is some what lowered and the valley field is some what increased.

The inclusion of acoustic phonon scattering in the satellite valleys did not make any significant differences and the resulting curves were not appreciably different from curves (b) of Figs. 5a, 5b and 5c. This was to be expected since for energies that are of interest in the range of field considered here the equivalent intervalley scattering among the satellite valleys is about 6 times as strong as the acoustic phonon scattering. The acoustic phonon scattering in the central valley is far too weak as compared

to other scattering mechanisms in the valley to be of any significant importance. It was not included in the calculation.

It is interesting to note that the strength of nonequivalent intervalley scattering has appreciable effects on the velocity field characteristic. For a comparison, we have included the results of a calculation by Butcher and Fawcett⁶⁷ as curve (c) in Fig. 5a. This curve was obtained by considering the same scattering mechanisms that we have considered for obtaining curve (b). However, for non equivalent intervalley scattering Butcher and Fawcett used a deformation potential field of $30/a$ eV/cm as against $10/a$ eV/cm used by us. This resulted in a nine-fold increase in the transition rate for non equivalent intervalley scattering. As a result the number of electron in the central valley with energy greater than ΔE was far less in their case. The electron distribution in the satellite valleys is already confined to lower energies because of the heavy electron mass and strong scattering mechanisms in the satellite valleys. This increased the factor R of equn. (1.36) and resulted in much higher fraction of electron population in the central valley and a slower transfer of electrons to the satellite valleys with an increase in the electric field. As a consequence the negative differential mobility was

substantially reduced and the valley field was increased. Since the non equivalent intervalley scattering is also an energy loss mechanism an increase in its strength significantly cooled down the central valley distribution, as a result, the electron temperature in the central valley rose to only about 1500°K at 10 kV/cm .

Thus we see that the velocity field characteristic upto the threshold field is primarily governed by the polar mode scattering in the central valley. Other scattering mechanisms in the central and satellite valleys have only very small effect on this part of the characteristic. The curve beyond the threshold field is governed primarily by the non equivalent intervalley scattering. The greater the strength of this mechanism the slower the transfer of electrons to the satellite valleys . Consequently, lesser is the magnitude of post threshold negative slope and hence a higher valley field. Beyond the valley field, the characteristic is dominated by the equivalent intervalley scattering among the satellite valleys and to a lesser extent by acoustic and polar mode scatterings.

VII. EFFECT OF TEMPERATURE ON LOW FIELD MOBILITY AND THRESHOLD FIELD:

Since the low field mobility and the threshold field are correctly predicted by taking into account only the polar mode and intervalley scatterings., we shall be considering only these scattering mechanisms for the present study. A change of lattice temperature effects the distribution functions in the two valleys in the following ways..

a) Through the change in number of phonons:

This is the most important factor and effects both the polar optical phonon and intervalley scattering rates.

b) Through the change in ΔE - the energy separation between minima of central and satellite valleys:

This factor has not been measured very accurately. However, despite the large error bars, we have used the values given by James and Moll⁴⁹ and have extrapolated for higher temperatures from their curve. Table II gives the list of ΔE values for various lattice temperatures.

Any changes in the effective masses, deformation potentials and low and high frequency dielectric constants with temperature have been neglected.

As before, the displaced Maxwellian approach was used to solve the Boltzmann's transport equation. The calculated velocity field characteristics for various lattice

temperatures are shown in Fig. 6. It can be seen from the figure that the threshold field decreases with the increase of lattice temperature. It is an interesting result in that the calculations by Ruch and Fawcett⁵⁰ predict results which are on the contrary. However, the experimental observations of Ruch and Kino^{32a,b} confirm a decrease in the threshold field with increasing lattice temperature. An increase in the efficiency of Gunn oscillators with temperature observed by Bott et al⁵¹ has also been explained^{32a,b} in terms of the decrease of threshold field with increasing lattice temperature.

This calculation therefore brings out the salient role that the variation of ΔE with temperature plays. In their calculation Ruch and Fawcett⁵⁰ have neglected the variation of ΔE with temperature and hence they predict an increase in the threshold field with temperature since at higher temperatures polar optical phonon scattering in the central valley becomes stronger and therefore larger electric fields are required for heating up the electron distribution in the central valley sufficiently to start the intervalley transfer. However, a decrease in ΔE with temperature more than compensates for this effect and lowers the threshold field. Thus the variation of ΔE with temperature is of crucial importance in determining the variation of threshold field with temperature.

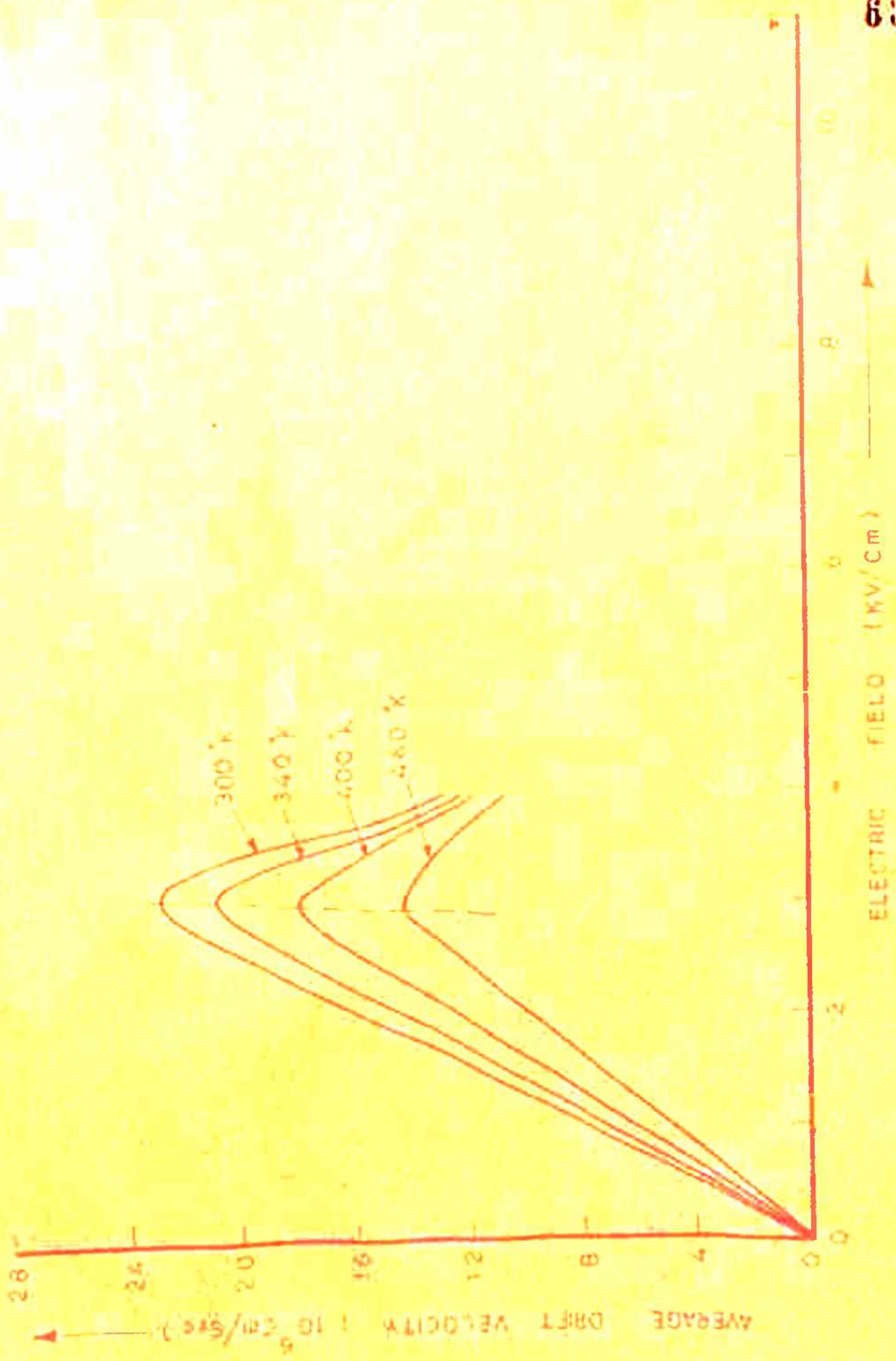


FIG. 6

The low field mobility decreases with increasing lattice temperature. Its values are 7800, 7250, 6300 and 4900 $\text{cm}^2/\text{V sec}$ respectively for lattice temperatures of 300, 340, 400 and 460 $^{\circ}$ K respectively.

Table-II.

Lattice temperature θ	E eV
300	.33
340	.32
400	.30
460	.28

The low field mobility decreases with increasing lattice temperature. Its values are 7800, 7250, 6300 and 4900 $\text{cm}^2/\text{V sec}$ respectively for lattice temperatures of 300, 340, 400 and 460^oK respectively.

Table-II.

Lattice temperature _o K	E eV
300	.33
340	.32
400	.30
460	.28

STUDY OF IMPACT IONIZATION

Our study of electron transport in GaAs so far has been restricted to electric fields that are not very high so that the energy picked up by the carriers from the field is lost to optical phonon collisions of various kinds. As a result a steady state is always possible under such fields. The mean free path for optical phonon collisions is essentially a constant quantity independent of the electron energy (This is because the scattering matrix elements for collisions of various kinds involving optical phonons can be taken energy independent. Using the usual argument that the total scattering rate from a state depends upon the available phase space leads to the conclusion that the mean free path for optical phonon collisions λ is essentially independent of energy) . The existence of a constant mean free path means the existence of a threshold electric field below which an average carrier is never accelerated to energies much higher than the optical phonon energy. In other words, if the energy gained from the field in travelling a mean free path λ is less than the optical phonon energy ϵ_R , then as soon as electron reaches energy ϵ_R it is returned to about zero energy in the next collision after which it accelerates again and so on. Thus the time average energy of the electron is $\epsilon_R/2$ implying a time average constant velocity. This is the origin of the well known velocity saturation

effect in semiconductors. However, if the energy gained between the collisions is greater than ϵ_R , the electron energy steadily increases on the average. Thus we see that a threshold field can be defined by $\epsilon_R/e\lambda'$, where e is the electron charge and λ' is the mean distance travelled by electrons in the field direction between optical phonon collisions. For random velocities $\lambda' < \lambda$; but since at very high fields the motion of an electron is almost rectilinear in field direction $\lambda' \approx \lambda$. However, for fields above the threshold field, the rise in electron energy is not unrestricted. As the energy of a carrier increases, it can eventually attain the threshold energy for pair production ϵ_T , whereafter, a new process of energy loss that of impact ionization sets in. The high energy conduction band electron (usually called the primary electron) gives up its energy to a valence band electron in their coulomb interaction to elevate the valence band electron to the conduction band, thus producing an electron hole pair. This amounts to a very high energy loss for the primary electron. Once the electrons has achieved an energy greater than ϵ_T , it will have a mean free path λ_i for ionization usually assumed independent of energy. In addition to electron optical phonon and ionizing collisions the electrons may also undergo electron electron collisions. Energy and momentum are exchanged in such collisions which

therefore serve to randomise the velocity distribution. Clearly the frequency of such collisions depends upon the electron density. The density needed for the velocity distribution to be maintained roughly spherically symmetric by this means (and therefore electron-electron collisions to be important) at pre breakdown fields has been estimated by Stratton³⁵. However , in the field swept space charge regions of reverse biased p-n junctions where impact ionization and charge multiplication phenomena are usually observed, the density of electrons is rather small for electron-electron collisions to be important. The theoretical treatments for electron transport in such cases leading to the determination of ionization coefficient α - which is the number of electron-hole pairs generated by a carrier per unit path length travelled - as a function of the applied electric field are due to Wolff³⁵, Shockley³⁶, Moll and Overstraeten³⁷, Baraff^{38,39} and Moll and Mayer⁴⁰.

The theoretical treatment and determination of the critical field for the case when electron-electron collisions are dominant (collective electron breakdown) has been given by Frolich and Paranjpe⁴¹ and Stratton⁴².

However, we shall be considering here only the first case where electron electron collisions can be neglected.

Wolff³⁵ was the first to give a theoretical treatment of impact ionization in semiconductors and determine α as a

function of E . His theory is essentially an application of Wannier's⁴³ gas discharge theory to semiconductors in which the carriers through the course of collisions slowly gather energy from the field and 'diffuse' to energies beyond ϵ_T . Wolff also assumed that the mean free path for ionizing collisions was considerably less than that for phonon collisions and that this would result in a considerable attenuation of the distribution function in the high energy tail for $\epsilon > \epsilon_T$. The theory gave an $\exp(-1/E^2)$ dependence of α on the electric field and successfully explained the experimentally observed dependence of α on E for very high fields. However, it failed at comparatively lower fields.

Experimental results of Bartelink et al⁴⁴ showed the inaccuracy of the assumption that $\lambda_i \ll \lambda$ made by Wolff. Subsequently Moll and R. Van. Overstraten repeated Wolff's theory dropping the assumption $\lambda_i \ll \lambda$. Their results are qualitatively similar to Wolff's but different in detail. The parameters involved in the theory are $\epsilon_R, \lambda, \epsilon_T$ and λ_i .

Shockley³⁶ gave a 'ballistic' theory of ionization which successfully explained the observed $\exp(-1/E)$ dependence of α on the electric field at relatively lower fields. Shockley argued that at lower fields the effective electron temperature is so small that an electron which suffers its normal share of phonon collisions will never achieve an energy ϵ_T .

Only those electrons attain an energy \mathcal{E}_T which have happened to escape any phonon collisions while being accelerated. The electrons that cause ionization therefore reside in a high velocity spike in the otherwise spherical distribution. Shockley assumed that an electron gives up all its energy when it encounters an optical phonon collision and makes a start afresh- a cold start. After several cold starts does it happen that the electron can avoid optical phonon collisions and reach beyond energy \mathcal{E}_T and ionize. Subsequent improvements in the theory were attempted by Moll and Meyer⁴⁰ who also included multiple ionization processes. By a multiple ionization process we mean a process of ionization in which an electron with energy less than the threshold energy is first accelerated to energies equal to the threshold energy plus one or more number of times the optical phonon energy, and then emits one or more optical phonons before ionizing. This resulted in a better quantitative agreement but large changes in the values of parameters λ_i and λ were required to fit the experimental data to theoretical curves.

However the most general treatments so far are due to Baraff^{38,39} who obtained exact³⁸ and almost exact³⁹ solutions of the Boltzmann's transport equation under the following assumptions:

1. There are no electron-electron interactions.
2. Acoustic phonon scattering is elastic.

3. Electrons emit optical phonon and lose a fixed amount of energy.
4. The probability that an electron is scattered from momentum \vec{p} to \vec{p}' depends only on its initial and final energy.
5. An electron causing ionization gives up all of its energy in the ionization process.
6. Scattering is spherically symmetric.
7. The hot electron has a constant mean free path.

His results in the form of universal curves are plots of $\log(\alpha\lambda)$ versus $\epsilon_T/eE\lambda$ for various values of parameter ϵ_R/ϵ_T . This parameter is constant for a given material. Hence there will be a single curve for each material. Experimentally α is determined as a function of field E . By finding the curve that gives best fit, the two adjustable parameters λ and ϵ_T are found. The curves obtained were for a value .5 for r -the ratio of scattering cross sections for ionization and optical phonon emission. Calculations were performed using other values of this ratio and α was found only weakly dependent on it. Baraff's theory gave an $\exp(-1/E)$ dependence for α on E for lower fields and an $\exp(-1/E^2)$ dependence for higher fields. It also gave correct dependence of α on E for intermediate fields where both 'ballistic' and 'diffusion' processes are important.

However in all the theoretical treatments so far the quantities $\epsilon_T, \epsilon_R, \lambda_i, \lambda$ and r have been taken as adjustable parameters. Besides the assumption that the mean free path for impact ionization is constant is open to question. In particular, all the above mentioned mathematical models have been developed for a simple band structure with a single valley (or equivalent valleys at best) and effective mass in the conduction band. Their application to GaAs which has two valleys in the conduction band with vastly different effective masses for the electrons, quite different scattering strengths and a field dependent population ratio looks quite unjustified. The quantities λ, λ_i and ϵ_T are expected to have quite different values for the two valleys. The use of a single λ_i, λ and ϵ_T amounts to the loss of any information regarding the relative importance of the two valleys for ionization. It includes rather crude and unrealistic averaging. With a view to go into some depth of the problem we first have considered various processes by which electrons in the central and satellite valleys ionize and have found the corresponding threshold energies for impact ionization. Thereafter, to determine the relative importance of each of these processes we have carried out a time dependent perturbation calculations of transition probability for impact ionization for several of these processes. Finally under certain assumptions a Monte Carlo calculation of the ionization coefficient for electrons has been carried out.

Chapter-II.

THRESHOLD ENERGY FOR IMPACT IONIZATION

I.	Threshold energy for impact ionization by electrons.	70
II.	Threshold energy for impact ionization by holes.	77
III.	Threshold energy for impact ionization by electrons including non parabolicity of the central valley.	81

CHAPTER -II.

THRESHOLD ENERGY FOR IMPACT IONIZATIONI. THRESHOLD ENERGY FOR IMPACT IONIZATION BY ELECTRONS:

For the calculation of the threshold energy for impact ionization, it is assumed that the ionization event involves only the primary electron and the secondary pair with or without a phonon. Also all the bands are assumed parabolic. The energy conservation alone requires that the minimum energy of primary electron for ionization must be at least equal to the energy gap. Conservation of momentum in the ionizing collision, however, places a still higher limit on ionization threshold. We have considered various types of ionization processes that are possible. The corresponding states of the primary electron, the secondary electron and the hole are listed in cols. 1 to 4 of Table 2.1 and 2.2. Both normal and Umklapp processes have been considered. The latter process reduces the energy requirement for ionization in such cases where large momentum transfers are involved in the ionization process. This is because a phonon carries with it a large momentum but negligible energy and thus transfers large momenta without appreciable energy. The momentum conservation equations for normal and Umklapp processes respectively are

$$\vec{k}_1 + \vec{k}_2 = \vec{k}_1' + \vec{k}_2' \quad (2.1a)$$

$$\vec{k}_1 + \vec{k}_2 = \vec{k}_1' + \vec{k}_2' \pm \vec{G} \quad (2.1b)$$

where \vec{k}_1 is the wave vector of the primary electron before

before ionization; \vec{k}_2 the wave vector of the electron in the valence band that is knocked out, i.e. the wave vector of the hole; \vec{k}_1' and \vec{k}_2' , the wave vectors of the two electrons after ionizing collision; and \vec{G} , a reciprocal lattice vector. The energies of these electrons depend upon the valley they lie in. For the central valley, the electron energy ϵ is related to the electron wave vector \vec{k} by the relation $\hbar^2 k^2 / 2m_1 = \epsilon$ and for the satellite valley, $\epsilon = \hbar^2 (\vec{k} - \vec{k}_0)^2 / 2m_2$ where \vec{k}_0 gives the minimum of the satellite valley in the wave vector space. For GaAs, \vec{k}_0 has values $(\pm 2\pi/a, 0, 0)$, $(0, \pm 2\pi/a, 0)$, $(0, 0, \pm 2\pi/a)$. Since the energy minima lie along equivalent $(1, 0, 0)$ directions, we shall search the minimum energy required for ionization along these directions and can, therefore, treat the wave vectors as scalars. Thus for the process corresponding to the first energy in Table 2.1, the momentum and energy conservation equations become

$$k_1 + k_2 = k_1' + k_2' \quad (2.2)$$

$$\frac{\hbar^2 k_1'^2}{2m_1} - E_g - \frac{\hbar^2 k_2'^2}{2m_h} = \frac{\hbar^2 (k_1' - 2\pi/a)^2}{2m_2} + \frac{\hbar^2 (k_2' - 2\pi/a)^2}{2m_2} + 2\Delta E_g \quad (2.3)$$

where m_1, m_2 are the effective masses of electrons in central and satellite valleys respectively; m_h , the mass of the hole; E_g , the band gap; and ΔE_g , the energy difference between

the minima of central and satellite valleys. For processes involving the hole of mass $0.20 m_0$, the appropriate value of the band gap would be 1.68 eV since the corresponding split off band lies 0.33 eV below the top of the valence band and consequently this quantity should be added to the band gap value 1.35 eV.

In eqs. (2) and (3), there are four variables namely k_1, k_2, k_1', k_2' . Thus one can treat two of them as independent variables and the other two as dependent variables. We treat k_1' and k_2' as independent variables and find out k_1 and k_2 in terms of them. Since we are interested in the minimum value of the primary electron energy, we have to get the minimum possible value of k_1 , i.e. the value of k_1 such that

$$\frac{\partial k_1}{\partial k_1'} = 0; \quad \frac{\partial k_1}{\partial k_2'} = 0 \quad (2.4)$$

For this we adopt the following procedure:

Eliminating k_2 from Eq. (3) with the help of Eq.

(2) we have

$$\frac{\hbar^2 k_1^2}{2m_1} - E_g - \frac{\hbar^2}{2m_A} (k_1' + k_2' - k_1)^2 = \frac{\hbar^2}{2m_2} (k_1' - 2\pi/a)^2 + \frac{\hbar^2}{2m_2} (k_2' - 2\pi/a)^2 + 2\Delta E_g \quad (2.5)$$

Differentiating Eq. (5) partially with respect to k_1' and k_2' respectively and using Eq. (4) we have

$$-\frac{\hbar^2}{m_1} (k_1' + k_2' - k_1) = \frac{\hbar^2}{m_2} (k_1' - 2\pi/a) \quad (2.6)$$

$$-\frac{\hbar^2}{m_1} (k_1' + k_2' - k_1) = \frac{\hbar^2}{m_2} (k_2' - 2\pi/a) \quad (2.7)$$

from Eqs. (6) and (7) eliminating k_1' and k_2' in turn we have:

$$k_1' = k_2' = \frac{(k_1 + 2\pi/a) m_h/m_2}{(2 + m_h/m_2)} \quad (2.8)$$

Substituting these back in Eq. (5) and multiplying out by $2m_0/k_1^2$ we have,

$$\frac{m_0}{m_1} k_1^2 - (E_g + 2\Delta E_g) \frac{2m_0}{k_1^2} - \frac{m_0 m_h}{m_2^2} \frac{(k_1 - 4\pi/a)^2}{(2 + m_h/m_2)^2} - \frac{2m_0}{m_2} \frac{(k_1 - 4\pi/a)^2}{(2 + m_h/m_2)^2} = 0 \quad (2.9)$$

Eq. (9) is a quadratic equation in k_1 and can be solved to give two values of k_1 . The one with smaller absolute value is chosen and corresponding k_1' and k_2' are determined from Eq. (8). In the case considered above, it must result in positive values of k_1' and k_2' (since both electrons after ionizing collision lie in the satellite valley at $(2\pi/a, 0, 0)$) if it is to be acceptable. If it is not so, it is rejected and the other value of k_1 is chosen.

For processes involving the primary electron in the satellite valley at $(2\pi/a, 0, 0)$ only positive value of k_1 is to be accepted if there are both positive and negative values

resulting from the solution of equations like (9). In case of both values being positive, the one which gives a $k_1 < 2\pi/a$ is chosen.

The procedure for determining k_1 in processes involving Umklapp is identical except that the momentum conservation equation becomes:

$$k_1 + k_2 = k'_1 + k'_2 \pm 4\pi/a \quad (2.10)$$

The calculated values of ionization thresholds for the primary electron in the central and the satellite valleys are shown in Table 2.1 and 2.2 respectively. For the Umklapp process, (out of the plus and minus signs in Eq. (2.10)), the results are reported only for the one which gives a lesser value of energy. Also for processes which give ionization thresholds in excess of 10 eV, results are not reported (blanks in cols. 5 and 6 of Tables 2.1 and 2.2) since such processes are of no interest.

Table-2.1

Threshold energy for impact ionization for an electron
in the central valley

Position of the valley of			Hole mass (m_0)	ionization threshold for	
Primary electron before impact	Secondary electron	Primary electron after impact		Normal process (eV)	Umklapp process (eV)
(000)	(000)	(000)	0.68	1.48	-
(000)	(000)	(100)	0.68	4.09	-
(000)	(100)	(-100)	0.68	2.18	-
(000)	(100)	(100)	0.68	-	-
(000)	(000)	(000)	0.12	1.86	-
(000)	(000)	(100)	0.12	5.88	-
(000)	(100)	(-100)	0.12	2.26	-
(000)	(100)	(100)	0.12	-	2.26
(000)	(000)	(000)	0.20	2.12	-
(000)	(000)	(100)	0.20	5.73	-
(000)	(100)	(-100)	0.20	2.60	-
(000)	(100)	(100)	0.20	-	2.60

Table-2.2

Threshold energy for impact ionization an electron
in the satellite valley

Position of the valley of			Hole mass m_0	Threshold energy for impact ionization	
Primary electron before impact	Secondary electron	Primary electron after impact		Normal process (eV)	Umklapp process (eV)
(1,00)	(1,00)	(100)	0.68	-	-
(1,00)	(-100)	(100)	0.68	2.70	-
(1,00)	(-100)	(-100)	0.68	-	-
(1,00)	(000)	(100)	0.68	2.00	7.73
(1,00)	(000)	(-100)	0.68	7.73	2.00
(1,00)	(000)	(000)	0.68	2.69	-
(1,00)	(100)	(100)	0.12	-	-
(1,00)	(-100)	(100)	0.12	3.15	-
(1,00)	(-100)	(-100)	0.12	-	3.15
(1,00)	(000)	(100)	0.12	3.91	-
(1,00)	(000)	(-100)	0.12	-	3.91
(1,00)	(000)	(000)	0.12	4.76	-
(1,00)	(100)	(100)	0.20	-	-
(1,00)	(-100)	(100)	0.20	3.29	-
(1,00)	(-100)	(-100)	0.20	-	3.29
(1,00)	(000)	(100)	0.20	3.93	-
(1,00)	(000)	(-100)	0.20	-	3.93
(1,00)	(000)	(000)	0.20	4.02	-

II. THRESHOLD ENERGY FOR IMPACT IONIZATION BY HOLES:

Once again, by the arguments of section I the wave vectors can be regarded as scalars for the purpose of determination of the threshold energy for impact ionization.

The momentum conservation equations for the normal and Umklapp processes respectively then read:

$$k_1 + k_2 = k'_1 + k'_2 \quad (2.11a)$$

$$k_1 + k_2 = k'_1 + k'_2 \pm 4\pi/a \quad (2.11b)$$

where k_1 is the wave vector of primary hole, k'_1 that of the primary hole after impact, k'_2 that of the secondary hole and k_2 that of the secondary electron. It should be noted that the momentum of a hole of wave vector k is given by $-kR$.

Assuming parabolic bands, the energy conservation equation becomes

$$E_{hp} + \frac{\hbar^2 k_1^2}{2m_{hp}} = E_{hpc} + \frac{\hbar^2 k'^2_1}{2m_{hpc}} + E_{hs} + \frac{\hbar^2 k'^2_2}{2m_{hs}} + E_e + \frac{\hbar^2}{2m_e} (k_e - k_2)^2 \quad (2.12)$$

where E_{hp} , E_{hpc} , E_{hs} are the positions of tops of the branches of valence band in which respectively primary hole, primary hole after collision and secondary hole lie measured downward positive with respect to the top of valence band chosen as the reference level for energy measurements. E_e is the position of the minimum of the valley of secondary electron

with respect to the reference level measured positive upwards and k_0 the wave vector corresponding to the energy minimum.

Equations (2.11) and (2.12) can be solved for the minimum energy of the primary hole (The threshold energy for impact ionization) as described in section. The results for various possible processes are shown in Table 2.3 and 2.4.

Table- 4.3

Effective mass of the primary hole in units of m_0	Effective mass of the primary hole after collision in units of m_0	Effective mass of the secondary hole in units of m_0	Effective mass of the secondary electron in units of m_0	Threshold energy for impact ionization	
				Normal process eV	Umklapp process eV
0.68	0.68	0.68	0.072	2.57	5.45
0.68	0.68	0.12	0.072	6.13	6.35
0.68	0.68	0.20	0.072	5.88	6.77
0.68	0.12	0.20	0.072	not possible	9.72
0.68	0.12	0.12	0.072	-do-	-
0.68	0.20	0.20	0.072	-do-	9.21
0.12	0.12	0.12	0.072	2.19	-
0.12	0.12	0.68	0.072	1.56	-
0.12	0.12	0.20	0.072	2.42	-
0.12	0.68	0.20	0.072	1.92	-
0.12	0.68	0.68	0.072	1.47	8.99
0.12	0.20	0.20	0.072	2.69	-
0.20	0.20	0.20	0.072	2.91	-
0.20	0.20	0.12	0.072	2.76	-
0.20	0.20	0.68	0.072	1.71	-
0.20	0.12	0.68	0.072	1.32	-
0.20	0.12	0.12	0.072	2.84	-
0.20	0.68	0.68	0.072	1.18	7.74

Table-2.4

Effective mass of the primary hole in units of m_0	Effective mass of the primary hole after collision in units of m_0	Effective mass of the secondary hole in units of m_0	Effective mass of the secondary electron in units of m_0	Threshold energy for impact ionization	
				Normal process eV	Umklapp process eV
0.68	0.68	0.68	0.364	2.23	2.23
0.68	0.68	0.12	0.364	2.40	2.40
0.68	0.68	0.20	0.364	2.61	2.61
0.68	0.12	0.20	0.364	2.90	2.90
0.68	0.12	0.12	0.364	2.77	2.77
0.68	0.20	0.20	0.364	3.07	3.07
0.12	0.12	0.12	0.364	4.96	4.96
0.12	0.12	0.68	0.364	3.67	3.67
0.12	0.12	0.20	0.364	4.92	4.92
0.12	0.68	0.20	0.364	3.84	3.84
0.12	0.68	0.68	0.364	3.12	3.12
0.12	0.20	0.20	0.364	4.95	4.95
0.20	0.20	0.20	0.364	4.13	4.13
0.20	0.20	0.12	0.364	4.07	4.07
0.20	0.20	0.68	0.364	3.22	3.22
0.20	0.12	0.68	0.364	3.05	3.05
0.20	0.12	0.12	0.364	4.06	0.06
0.20	0.68	0.68	0.364	2.60	2.60

III. THRESHOLD ENERGY FOR IMPACT IONIZATION BY ELECTRONS INCLUDING NONPARABOLICITY OF THE CENTRAL VALLEY:

It is possible to include the non parabolicity of the central valley in the calculation of threshold energy for impact ionization. As mentioned in section II of chapter I, the energy wave vector relationship for this valley can be written in the form

$$\frac{\hbar^2 k^2}{2m_1} = E(1 + \alpha E) \quad (2.13)$$

where $\alpha = .576 \text{ eV}^{-1}$ and m_1 is the effective mass of an electron in the central valley.

To be particular, let us consider a normal process of impact ionization in which the primary electron before impact is in the central valley of the conduction band, both the primary and secondary electrons after impact are in the central valley and the hole produced is in the heavy hole band (effective mass ratio 0.68).

The wave vector and energy conservation equations for this process read

$$k_1 + k_2 = k_1' + k_2' \quad (2.14)$$

$$E(k_1) + E(k_2) = E(k_1') + E(k_2') \quad (2.15)$$

where k_1 , k_2 , k_1' and k_2' are respectively the wave vectors of

primary electron before impact, the hole, primary electron after impact and the secondary electron and $E(k)$'s are the corresponding energies.

$$E = \frac{-1 + \sqrt{1 + ck^2}}{2\alpha} \quad (2.16)$$

where

$$c = \frac{2\alpha\hbar^2}{m_l}$$

Only positive sign has been taken with the square root term in equn. (2.16). This is because E being the energy measured from the minimum of the central valley is always positive for all k values. Using equn. (2.16), equn. (2.15)

becomes

$$-\frac{1 + \sqrt{1 + ck_1^2}}{2\alpha} - E_g - \frac{\hbar^2 k_1^2 k_2^2}{4m_h} = \frac{-1 + \sqrt{1 + ck_1'^2}}{2\alpha} + \frac{-1 + \sqrt{1 + ck_2'^2}}{2\alpha} \quad (2.17)$$

where E_g is the band gap and m_h is the effective mass value for the hole. One can now follow the procedure laid down in.

Differentiating equn. (2.17) (after eliminating k_2 from it with the help of equn. (2.14)) w.r.t. k_1' and k_2' and setting

$$\frac{\partial k_1}{\partial k_1'} = 0 \text{ and } \frac{\partial k_1}{\partial k_2'} = 0 \text{ one has}$$

$$-b(k_1' + k_2' - k_1) = (1 + ck_1'^2)^{-1/2} ck_1' \quad (2.18)$$

$$-b(k_1' + k_2' - k_1) = (1 + ck_2'^2)^{-1/2} ck_2' \quad (2.19)$$

where

$$b = \frac{2\alpha\hbar^2}{m_h}$$

From equns. (2.18) and (2.19) one has

$$k_2' = k_1' \quad (2.20)$$

and

$$k_1 = \frac{2}{b} k_1' + \frac{c}{b} k_1' (1 + c k_1'^2)^{-1/2} \quad (2.21)$$

also from equns. (2.14), (2.20) and (2.21)

$$k_2 = -\frac{c}{b} k_1' (1 + c k_1'^2)^{-1/2} \quad (2.22)$$

substitution can be made in equn. (2.17) for k_1 , k_2 and k_2' in terms of k_1' from equns. (2.21), (2.22) and (2.20) and the resulting equation can be solved for k_1' by an iterative procedure. The corresponding value of k_1 can then be determined from equn. (2.21) and using this value of k_1 , the threshold energy can be determined from equn. (2.16). One can proceed in a similar way for other processes also.

The threshold energies for three processes which result in lowest threshold energies for central and satellite valley electrons are given in table (2.5)..

It can be seen from table (2.1) that the lowest threshold energy for impact ionization for central valley electrons is 1.48 eV. There are several other threshold energies close to 2.0 eV. The lowest threshold energy for satellite valley electrons is 2.00 eV. The next lowest values are 2.69 and 2.70 eV respectively.

Table-2.5

Valley of the			Threshold energy ev			
Primary electron before impact	Primary electron after impact	Secondary electron	Effective mass of the hole	Process	Non parabolic central valley	Parabolic central valley
(000)	(000)	(000)	$0.68 m_0$	Normal	1.62	1.48
(100)	(100)	(000)	$0.68 m_0$	Normal	1.93	2.00
(100)	(000)	(000)	$0.68 m_0$	Normal	2.69	2.69

The calculated values of threshold energies are for the case when the primary electron is moving in the (100) direction. They are the lowest possible values for a given process. Under the assumption of spherical constant energy surfaces for all bands the threshold energies for impact ionization for processes involving only the electrons of the central valley will be independent of the direction of motion of the primary particle. However, this will not be so for processes involving the electrons of the satellite valley; different threshold energies will exist for primary particles moving in different directions.

At lower fields the process with lowest threshold energy will be the most effective process (provided it has a good enough transition probability). With an increase in the electric field, the average energy of the electron distribution will increase and processes with higher threshold energies will start becoming important. This perhaps explains the range of threshold energy values (between $1.7 \pm .3$ eV) required by Logan et al⁶⁰ to fit their experimental data to theoretical curves.

The inclusion of non parabolicity of the central valley results in about 10% increase in the threshold energy for impact ionization for the process with lowest threshold energy. In processes where only the secondary electron or the primary electron after impact are in the central valley,

the non parabolicity of this valley is not likely to make any significant differences in the threshold energy values. This is because the energy and momentum associated with these electrons are small enough for the parabolic band to lie close to the non parabolic band.

One can expect that Shockley kind (ballistic) impact ionization will first initiate in the central valley. It is because the threshold energy is lowest in this valley and the electrons being light accelerate faster and have more chances to escape to energies greater than ϵ_T .

At higher fields where Wolff type impact ionization dominates, the satellite valley may have an advantage of its higher population. However one must first see the transition probabilities for various processes before conjecturing any further.

Chapter-III.

TRANSITION PROBABILITY FOR IMPACT IONIZATION 88

CHAPTER III - III.

TRANSITION PROBABILITY FOR IMPACT IONIZATION

Let us consider an energetic electron with energy $\epsilon(\bar{k}_1)$ and wave vector \bar{k}_1 which is scattered to an energy $\epsilon(\bar{k}_1')$ with wave vector \bar{k}_1' , producing an electron hole pair of energies $\epsilon(\bar{k}_2')$ and $\epsilon(\bar{k}_2)$ with wave vectors \bar{k}_2' and \bar{k}_2 respectively. We seek the total transition probability per unit time for processes of this type. To be specific, let us consider the process that gives the lowest threshold energy for impact ionization for an electron in the central valley.

We shall treat the problem using time dependent perturbation theory assuming that the perturbing Hamiltonian is the difference (due to the coulomb interaction of electrons) between the complete Hamiltonian for the crystal and the Hamiltonian which is used in the one electron approximation^{47,48}. In the latter, the coulomb interaction is replaced by a self consistent field, containing exclusively terms which depend on single electron coordinates. The coulomb interaction terms in the complete hamiltonian are explicitly taken into account only for electrons of the conduction and valence bands. Electronic interactions in which the remaining electrons participate give rise to polarizability, and their effects are represented by the use of an effective dielectric constant ϵ . In order to be in a position to estimate the effect of electron screening on the impact ionization we shall assume the perturbing Hamiltonian to be

$$H' = \frac{1}{2} \sum_{ij} \frac{e^2}{4\pi\epsilon|\bar{r}_i - \bar{r}_j|} \exp(-q|\bar{r}_i - \bar{r}_j|) \quad (3.1)$$

where \vec{r}_i and \vec{r}_j are the position vectors of the i th and j th electrons, q is the screening constant and \sum_{λ} the summation is over all λ pairs of electrons. In accordance with the one electron approximation the electron wave functions for the conduction and valence bands of the crystal are described by Bloch functions, and the electrons that do not take part in a transition are supposed to have their states unaltered by the transition.

Let the electrons taking part in a transition be labeled 1 and 2. Then under the conditions stated only the term involving $e^{\lambda} \exp(-q|\vec{r}_1 - \vec{r}_2|) / 4\pi\epsilon |\vec{r}_1 - \vec{r}_2|$ of the perturbation operator H' can have a non zero matrix element. The transition probability is then given by^{7,56}

$$P(\vec{k}_1 \rightarrow \vec{k}_1'; \vec{k}_2 \rightarrow \vec{k}_2') = \frac{2}{\hbar^2} \frac{\sin \omega_1 t}{\omega_1} \left[|H_{\vec{k}_1, \vec{k}_2'}^{\lambda}|^2 + |H_{\vec{k}_2, \vec{k}_1'}^{\lambda}|^2 + |H_{\vec{k}_1, \vec{k}_2'}^{\lambda} - H_{\vec{k}_2, \vec{k}_1'}^{\lambda}|^2 \right] \quad (3.2)$$

where $H_{\vec{k}_1, \vec{k}_2'}^{\lambda}$ and $H_{\vec{k}_2, \vec{k}_1'}^{\lambda}$ are the matrix elements of the perturbation given by

$$H_{\vec{k}_1, \vec{k}_2'}^{\lambda} = \frac{1}{4\pi\epsilon} \iint \phi_{\vec{k}_1'}^*(\vec{r}_1) \phi_{\vec{k}_2'}^*(\vec{r}_2) \frac{e^{\lambda} \exp(-q|\vec{r}_1 - \vec{r}_2|)}{|\vec{r}_1 - \vec{r}_2|} \phi_{\vec{k}_1}(\vec{r}_1) \phi_{\vec{k}_2}(\vec{r}_2) d\vec{r}_1 d\vec{r}_2 \quad (3.3)$$

$$H_{\vec{k}_2, \vec{k}_1'}^{\lambda} = \frac{1}{4\pi\epsilon} \iint \phi_{\vec{k}_2'}^*(\vec{r}_2) \phi_{\vec{k}_1'}^*(\vec{r}_1) \frac{e^{\lambda} \exp(-q|\vec{r}_1 - \vec{r}_2|)}{|\vec{r}_1 - \vec{r}_2|} \phi_{\vec{k}_1}(\vec{r}_1) \phi_{\vec{k}_2}(\vec{r}_2) d\vec{r}_1 d\vec{r}_2 \quad (3.4)$$

In equn. (3.2) the terms in the bracket are due to spin considerations; the first two arise for antiparallel and the third for parallel spins, and

$$\omega_l = \frac{1}{\hbar} \left[\epsilon(\vec{k}_1') + \epsilon(\vec{k}_2') - \epsilon(\vec{k}_1) - \epsilon(\vec{k}_2) \right] \quad (3.5)$$

The wave functions for the various states are given in terms of their respective Bloch functions as follows :

$$\phi_{\vec{k}_1}(\vec{r}_1) = \frac{1}{\sqrt{V}} \sum_{\vec{n}_1} A(\vec{n}_1, \vec{k}_1) \exp[i(\vec{k}_1 + \vec{n}_1) \cdot \vec{r}_1] \quad (3.6a)$$

$$\phi_{\vec{k}_2}(\vec{r}_2) = \frac{1}{\sqrt{V}} \sum_{\vec{n}_2} B(\vec{n}_2, \vec{k}_2) \exp[i(\vec{k}_2 + \vec{n}_2) \cdot \vec{r}_2] \quad (3.6b)$$

$$\phi_{\vec{k}_1'}(\vec{r}_1) = \frac{1}{\sqrt{V}} \sum_{\vec{n}_1'} A(\vec{n}_1', \vec{k}_1') \exp[i(\vec{k}_1' + \vec{n}_1') \cdot \vec{r}_1] \quad (3.6c)$$

$$\phi_{\vec{k}_2'}(\vec{r}_2) = \frac{1}{\sqrt{V}} \sum_{\vec{n}_2'} A(\vec{n}_2', \vec{k}_2') \exp[i(\vec{k}_2' + \vec{n}_2') \cdot \vec{r}_2] \quad (3.6d)$$

where $\vec{n}_1, \vec{n}_2, \vec{n}_1'$ and \vec{n}_2' are reciprocal lattice vectors. Substituting these functions into equns. (3.3) and (3.4) followed by integration by standard methods yield

$$H_{\vec{k}_1', \vec{k}_2'} = \frac{e^2}{\epsilon V} \sum_{\vec{n}_1, \vec{n}_2, \vec{n}_1', \vec{n}_2'} A(\vec{n}_1, \vec{k}_1) B(\vec{n}_2, \vec{k}_2) A^*(\vec{n}_1', \vec{k}_1') A^*(\vec{n}_2', \vec{k}_2') \times \frac{\delta(\vec{k}_1 + \vec{k}_2 - \vec{k}_1' - \vec{k}_2' + \vec{n}_1 + \vec{n}_2 - \vec{n}_1' - \vec{n}_2')}{q^2 + (\vec{k}_1 - \vec{k}_1' + \vec{n}_1 - \vec{n}_1')^2} \quad (3.7)$$

$$H_{\vec{k}_2', \vec{k}_1'} = \frac{e^2}{\epsilon V} \sum_{\vec{n}_1, \vec{n}_2, \vec{n}_1', \vec{n}_2'} A(\vec{n}_1, \vec{k}_1) B(\vec{n}_2, \vec{k}_2) A^*(\vec{n}_1', \vec{k}_1') A^*(\vec{n}_2', \vec{k}_2') \times \frac{\delta(\vec{k}_1 + \vec{k}_2 - \vec{k}_1' - \vec{k}_2' + \vec{n}_1 + \vec{n}_2 - \vec{n}_1' - \vec{n}_2')}{q^2 + (\vec{k}_1 - \vec{k}_2' + \vec{n}_1 - \vec{n}_2')^2} \quad (3.8)$$

The above expressions for $H_{\vec{k}_1', \vec{k}_2'}$ and $H_{\vec{k}_2', \vec{k}_1'}$ are maximum when the denominators

$$q^2 + (\vec{k}_1 - \vec{k}_1' + \vec{n}_1 - \vec{n}_1')^2$$

and

$$q^2 + (\vec{k}_1 - \vec{k}_2' + \vec{n}_1 - \vec{n}_2')^2$$

are minimum. That is when

$$\vec{n}_1 = \vec{n}_1' \quad \text{and} \quad \vec{n}_2 = \vec{n}_2' \quad (3.8b)$$

Only the contribution of such terms is important and we shall consider only these terms.

The delta function on the right hand side of equns. (3.7) and (3.8) yields momentum conservation relations of types.

$$(i) \quad \vec{k}_1 + \vec{k}_2 = \vec{k}_1' + \vec{k}_2' \quad \text{for} \quad \vec{n}_1 + \vec{n}_2 - \vec{n}_1' - \vec{n}_2' = 0 \quad (3.9)$$

$$(ii) \quad \vec{k}_1' + \vec{k}_2' = \vec{k}_1 + \vec{k}_2 + \vec{n} \quad \text{for} \quad \vec{n}_1 + \vec{n}_2 - \vec{n}_1' - \vec{n}_2' = \vec{n} \quad (3.10)$$

The first one is normal process and the second one is an Umklapp process. We shall consider only normal processes here since the processes that yield lowest threshold energies for central and satellite valley electrons in GaAs (chapter II) are normal processes. Thus for a normal process and under the conditions $\vec{n}_1 = \vec{n}_1'$ and $\vec{n}_2 = \vec{n}_2'$ (3.8b), the matrix elements $H_{\vec{k}_1', \vec{k}_2'}$ and $H_{\vec{k}_2', \vec{k}_1'}$ (equn. 3.7 and 3.8) become

$$H_{\vec{k}_1', \vec{k}_2'} = \frac{e^2}{\epsilon V} \frac{F_1 F_2 \cdot \delta(\vec{k}_1 + \vec{k}_2 - \vec{k}_1' - \vec{k}_2')}{q^2 + (\vec{k}_1 - \vec{k}_1')^2} \quad (3.11)$$

$$H_{\vec{k}_2', \vec{k}_1'} = \frac{e^2}{\epsilon V} \frac{F_1 F_2 \cdot \delta(\vec{k}_1 + \vec{k}_2 - \vec{k}_1' - \vec{k}_2')}{q^2 + (\vec{k}_1 - \vec{k}_2')^2} \quad (3.12)$$

where F_1 and F_2 are the overlap integrals for the cell periodic parts of the Bloch functions

$$F_1 = \int u_{\vec{k}_1}^*(\vec{r}) u_{\vec{k}_1'}(\vec{r}) d\vec{r} = \sum_{\vec{m}_1} A(\vec{m}_1, \vec{k}_1) A^*(\vec{m}_1, \vec{k}_1') \quad (3.13)$$

$$F_2 = \int u_{\vec{k}_2}^*(\vec{r}) u_{\vec{k}_2'}(\vec{r}) d\vec{r} = \sum_{\vec{m}_2} B(\vec{m}_2, \vec{k}_2) A^*(\vec{m}_2, \vec{k}_2') \quad (3.14)$$

Using relations (3.11) and (3.12) the transition probability (equn. (3.2)) becomes.

$$P(\vec{k}_1 \rightarrow \vec{k}_1'; \vec{k}_2 \rightarrow \vec{k}_2') = \frac{2e^4}{k^2 \epsilon^2 v^2} \frac{\sin \omega_2 t}{\omega_2} \chi \left[F_1 F_2 \delta(\vec{k}_1 + \vec{k}_2 - \vec{k}_1' - \vec{k}_2') \right]^2 Q(\vec{k}_1, \vec{k}_2, \vec{k}_1', \vec{k}_2') \quad (3.15)$$

$$\text{where } Q(\vec{k}_1, \vec{k}_2, \vec{k}_1', \vec{k}_2') = \left[\frac{1}{\{q^2 + (\vec{k}_1 - \vec{k}_1')^2\}^2} + \frac{1}{\{q^2 + (\vec{k}_1 - \vec{k}_2')^2\}^2} \right. \\ \left. + \left\{ \frac{1}{q^2 + (\vec{k}_1 - \vec{k}_1')^2} - \frac{1}{q^2 + (\vec{k}_1 - \vec{k}_2')^2} \right\}^2 \right] \quad (3.16)$$

To be able to obtain the total transition probability for impact ionization ($P(\vec{k}_1)$) for an electron with wave vector \vec{k}_1 , we must sum the probability (3.15) over all the possible final states \vec{k}_1' and all the possible electron hole pairs \vec{k}_2, \vec{k}_2' that can be produced by this electron. i.e.

$$P(\vec{k}_1) = \sum_{\vec{k}_1'} \sum_{\vec{k}_2'} \sum_{\vec{k}_2} P(\vec{k}_1 \rightarrow \vec{k}_1'; \vec{k}_2 \rightarrow \vec{k}_2') \quad (3.17)$$

We first evaluate the sum over \vec{k}_1' and \vec{k}_2' keeping \vec{k}_2 fixed. i.e.

$$\vec{k}_1 + \vec{k}_2 = 2\vec{k}_0 \quad (3.18)$$

The non vanishing of the kroncker delta function in the expression for $P(\vec{k}_1 \rightarrow \vec{k}_1'; \vec{k}_2 \rightarrow \vec{k}_2')$ requires the relation

$$\vec{k}_1 + \vec{k}_2' = \vec{k}_1 + \vec{k}_2 = 2\vec{k}_0 \quad (3.19)$$

Thus out of \bar{k}'_1 and \bar{k}'_2 only one is independent. One can eliminate \bar{k}'_2 with the help of equn. (3.19) and drop the summation over \bar{k}'_2 . The summation over \bar{k}'_1 (and later also over \bar{k}_0) can be replaced by integration as follows.

$$\sum_{\bar{k}'} = \frac{V}{8\pi^3} \int d\bar{k}' \quad (3.20)$$

One therefore has

$$\begin{aligned} P(\bar{k}_1, \bar{k}_2) &= \sum_{\bar{k}'_1} \sum_{\bar{k}'_2} P(\bar{k}_1 \rightarrow \bar{k}'_1; \bar{k}_2 \rightarrow \bar{k}'_2) = \sum_{\bar{k}'_1} P(\bar{k}_1 \rightarrow \bar{k}'_1; \bar{k}_2 \rightarrow (2\bar{k}_0 - \bar{k}'_1)) \\ &= \frac{V}{8\pi^3} \frac{2e^4}{\hbar^2 \epsilon^2 V^2} \int \frac{\sin \omega_1 t}{\omega_1} (F_1 F_2)^2 Q(\bar{k}_1, \bar{k}_2, \bar{k}'_1, (2\bar{k}_0 - \bar{k}'_1)) d\bar{k}'_1 \quad (3.21) \end{aligned}$$

To simplify the computation F_1 and F_2 are assumed to be constants⁴⁸. It is convenient to change the variable of integration from \bar{k}'_1 to \bar{k} as follows

$$\bar{k} = \bar{k}'_1 - \bar{k}_0 \quad (3.22)$$

$$d\bar{k} = d\bar{k}'_1 \quad (3.23)$$

In terms of the new variable \bar{k} one has

$$\bar{k}'_1 = \bar{k}_0 + \bar{k} \quad (3.24a)$$

$$\bar{k}'_2 = \bar{k}_0 - \bar{k} \quad (3.24b)$$

and

$$P(\bar{k}_1, \bar{k}_2) = \frac{V}{8\pi^3} \frac{2e^4}{\hbar^2 \epsilon^2 V^2} (F_1 F_2)^2 \int \frac{\sin \omega_1 t}{\omega_1} Q(\bar{k}_1, \bar{k}_2, (\bar{k}_0 + \bar{k}), (\bar{k}_0 - \bar{k})) d\bar{k} \quad (3.25)$$

From (3.5), (3.24a) and (3.24b) one has

$$\omega_l = \frac{1}{\hbar} \left[\frac{\hbar^2}{m_1} (k_0^2 + k^2) - \epsilon(\vec{k}_1) - \epsilon(\vec{k}_2) \right] \quad (3.26)$$

Where minimum of the central valley of conduction band has been taken as the reference point for energy measurements. From (3.26)

$$d\omega_l = \frac{\hbar}{m_1} 2k dk \quad (3.27)$$

Using (3.26) and (3.27) the variable of integration in integral (3.25) can be changed from k, θ, ϕ to ω_l, θ, ϕ .

Since

$$\frac{\sin \omega_l t}{\omega_l} = \pi \delta(\omega_l) \quad (3.28)$$

integration of (3.25) over ω_l can be immediately carried out leaving the integration over angular variables.

∴ choice of polar axis \hat{z} along $(\vec{k}_1 - \vec{k}_0)$ makes the angular part of (3.25) independent of ϕ . A final integration over θ yields

$$P(\vec{k}_1, \vec{k}_2) = \frac{V \pi^2 e^4 (F_1 F_2)^2}{8 \pi^3 \hbar^2 \epsilon^2 V^2} \left[\frac{m_1 k}{\hbar} \frac{8}{A^2 - B^2} - \frac{2 m_1 k}{\hbar} \frac{1}{AB} \ln \left(\frac{A+B}{A-B} \right) \right] \quad (3.29)$$

where

$$A = q^2 + (\vec{k}_1 - \vec{k}_0)^2 + k^2 \quad (3.30a)$$

$$B = 2 |\vec{k}_1 - \vec{k}_0| k \quad (3.30b)$$

and

$$k = k \Big|_{\omega_l = 0} \quad (3.30c)$$

To obtain $P(\bar{k}_1)$, we should integrate (3.29) over that region of \bar{k}_2 space which participates in impact ionization (i.e. over all the possible holes).

It is convenient to transform the variable of integration from \bar{k}_2 to \bar{r} so that the region of \bar{k}_2 space for which ionization is possible becomes a sphere in \bar{r} space. The required transformation is (see Appendix B):

$$\bar{r} = \bar{k}_2 + Y\bar{k}_1 \quad (3.31)$$

$$\text{where } Y = \frac{1}{1 + 2m_1/m_h} \quad (3.32)$$

and the radius of the sphere is given by

$$r_{\max} = \frac{1}{\sqrt{\frac{k^2}{2m_h} + \frac{k^2}{4m_1}}} \times \sqrt{\varepsilon(\bar{k}_1) - E_g - \frac{k^2}{2m_h} \bar{k}_1^2 Y} \quad (3.33)$$

Also

$$\bar{k}_0 = \frac{\bar{k}_1 + \bar{k}_2}{2} = \frac{1}{2} (\bar{r} + (1-Y)\bar{k}_1) \quad (3.34)$$

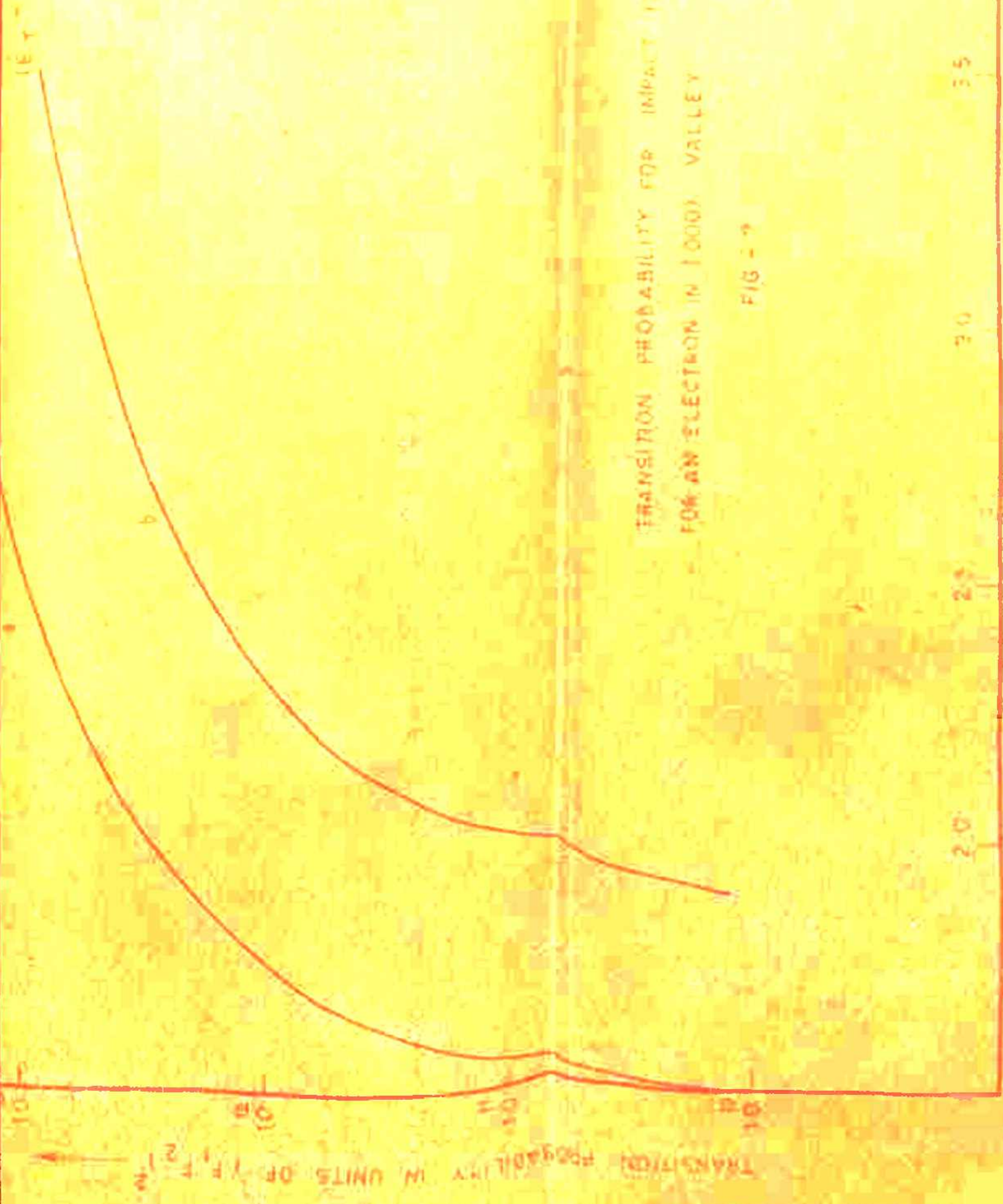
and

$$k^2 = (m_1/2m_h + 1/4) (r_{\max}^2 - r^2) \quad (3.35)$$

Using this transformation scheme, one can integrate (3.29) over a spherical volume of \bar{r} space with radius r_{\max} to obtain $P(\bar{k}_1)$.

For the present case, contribution of the logarithmic term in (3.29) comes out to be negligible. For the first

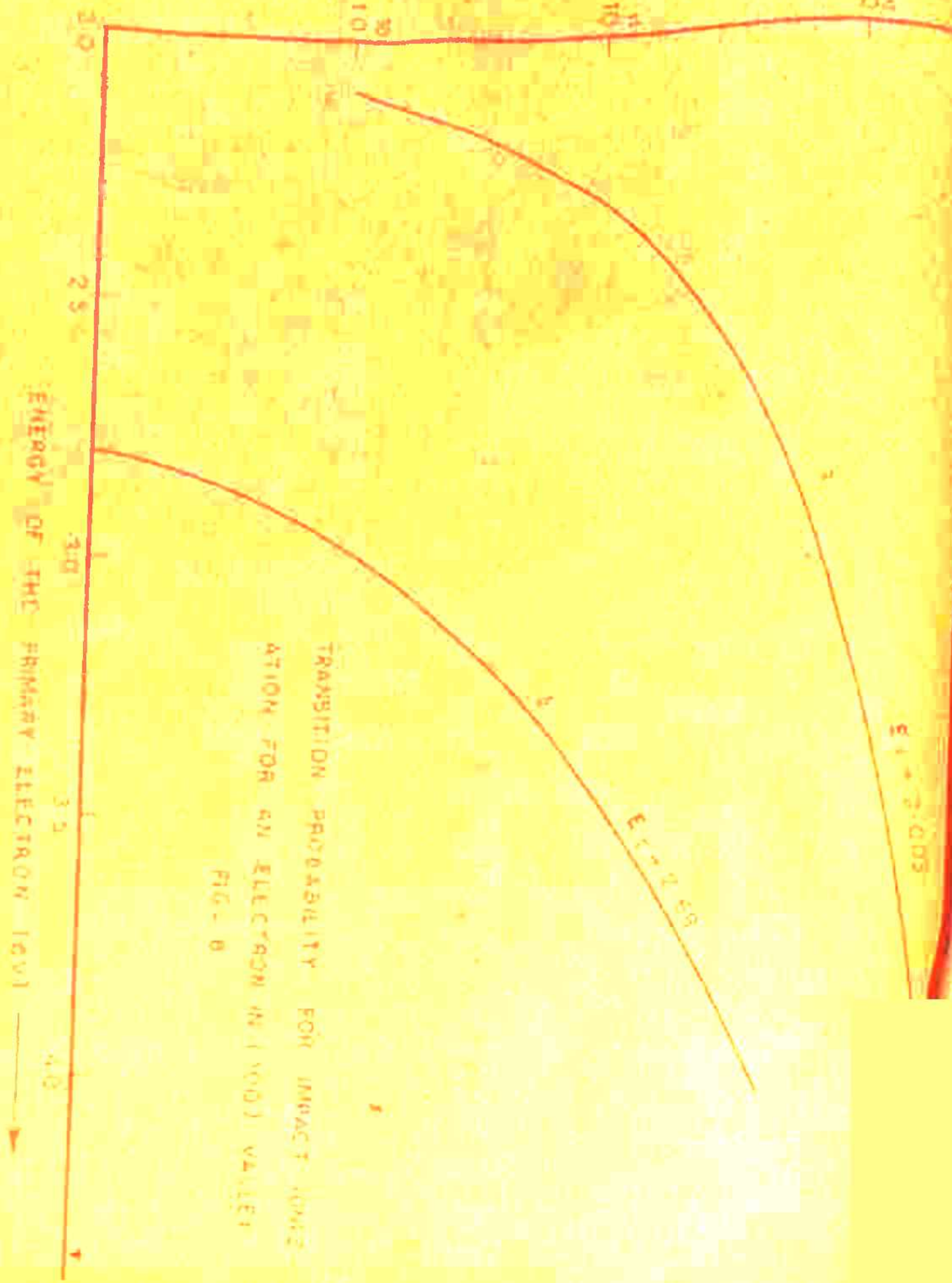
term, an angular integration can be carried out analytically and a final numerical integration over the radial coordinate gives $P(\bar{k}_1)$. Similar techniques are used to obtain $P(\bar{k}_1)$ for other processes. The required transformations are given in appendix B. For the process that gives the lowest threshold energy for a satellite valley electron, it is very difficult to find the contribution to $P(\bar{k}_1)$ from the product term that comes when the last term in Q (expression 3.16) which is the square of difference in two terms is opened up. However, the contributions of the first and second terms in Q can be found out using techniques similar to those described above. Since (3.16) is of the form $X^2 + Y^2 + (X - Y)^2$ with both X and Y positive, one gets a lower limit of $P(\bar{k}_1)$ if one neglects the last term and uses only the first two terms. If one neglects the XY term, one gets an upper limit which is twice the lower limit. We have calculated the lower limit of $P(\bar{k}_1)$ for this case. Curves (a) and (b) of Fig. 7 show $P(\bar{k}_1)$ for central valley electrons for the process with lowest and next lowest threshold energies respectively. Curve (a) of Fig. 8 shows the lower limit of $P(\bar{k}_1)$ for the process with lowest threshold energy for a satellite valley electron and curve (b) of Fig. 8 shows $P(\bar{k}_1)$ for the process with next lowest threshold energy for a satellite valley electron. The transition probabilities have been plotted in units of $(F_1 F_2)^2$ which was assumed to be a constant. The evaluation of $(F_1 F_2)^2$



TRANSITION PROBABILITY FOR IMPACT IONIZATION
FOR AN ELECTRON IN 1000Å VALLEY

FIG - 9

TRANSITION PROBABILITY IN UNITS OF $(F_1 F_2)^2$



TRANSITION PROBABILITY FOR IMPACT IONIZATION FOR AN ELECTRON IN (100) VALLEY
FIG. 6

is a rather delicate problem. In the absence of a knowledge of exact wave functions for the conduction and valence band electrons it is not possible to estimate this quantity directly. Indirect methods which circumvent the necessity of knowing exact wave function have been proposed by Antoncik and Landsberg⁴⁴. They have shown that it is possible to deduce information about overlap integrals from the oscillator strength or effective mass data. They have also shown that the overlap integrals between two Bloch states of the same band are close to unity. The quantity $(F_1 F_2)^2$ has different values for different curves in Fig. 7 and 8 since it involves different overlap integrals in each case.

For curve (a) of Fig. 7 a value of about .16 is obtained for $(F_1 F_2)^2$ using an isotropic effective mass, wave vectors $(k_2$ and $k_1')$ corresponding to threshold energy and results of Antoncik and Landsberg⁴⁵. The overlap integrals involved in this case are those between two conduction band (central valley) states which is close to unity and between conduction band (central valley) and heavy hole valence band states.

For curve (a) of Fig. 8 the value of $(F_1 F_2)^2$ should also be approximately .16 since it involves the overlap integrals between two conduction band (satellite valley) states which is close to unity and between conduction band

(central valley) and heavy hole valence band states.

$(F_1F_2)^2$ for curve (b) of Fig. 8 should be less than that for the two cases mentioned above . This is because it involves the overlap integrals between wave functions of central valley electrons and satellite valley electrons and between central valley electrons and heavy hole valence band.

$(F_1F_2)^2$ for curve (b) of Fig. 7 should also be less compared to that for curve (a) of Fig. 7.

With this knowledge of $(F_1F_2)^2$ a comparison of transition probabilities is now possible from Figs. 7 and 8. Highest transition probability exists for the process for which the primary electron is in the central valley, both primary after collision and secondary electrons are in the central valley and the hole involved is heavy hole (curve (a) of Fig. 7). Transition probability is highest for a satellite valley electron when the electron after impact remains in the same satellite valley, the hole involved is a heavy hole and the secondary electron produced is in the central valley (curve (a) of Fig. 8). However, the transition probability for this process is only about one twentieth^e of that of a central valley electron for process with highest transition probability.

More accurate values of $(F_1 F_2)^2$ are desirable for determining the transition probabilities accurately. However there seems to be little doubt as to the importance of the central valley for impact ionization. At high fields only about 5% of the electrons may be expected to remain in the central valley, yet the high transition probability for impact ionization in this valley may well make it comparable in importance to the satellite valley for impact ionization. Besides, the transition probability for the process that corresponds to curve (a) of Fig. 7 does not depend upon the direction of \bar{k}_1 - the wave vector of primary electron. However, this is not so for the process that corresponds to curve (a) of Fig. 8. As mentioned earlier, different threshold energies and transition probabilities may exist for different directions of \bar{k}_1 . Curve (a) of Fig. 8 shows the transition probability for a direction of \bar{k}_1 for which the threshold energy is minimum. For other directions the transition probabilities are expected to be lower.

Chapter IV.

CALCULATION OF IONIZATION COEFFICIENT.

103

CHAPTER- IV.CALCULATION OF IONIZATION COEFFICIENTS

We now apply the Monte Carlo technique to determine the ionization coefficient of electrons as a function of the applied electric field. Following assumptions have been made:

1. The electron loses all its energy in an ionizing collision.
2. In the central valley, the ratio of transition probability for impact ionization and non equivalent intervalley scattering by emission of an optical phonon is a constant

i.e.

$$\frac{\lambda_{1i}(k)}{\lambda_{ij}(k)_{\text{emission}}} = Ak_1$$

and for the satellite valley the ratio of transition probability for ionization and equivalent intervalley scattering by emission of an optical phonon is a constant

i.e.

$$\frac{\lambda_{2i}(k)}{\lambda_{ij}(k)_{\text{emission}}} = Ak_2$$

3. There is a single threshold energy for impact ionization for each valley.

The first of these assumptions has to be made since it is not possible to find the angular distribution of the final states after impact ionization in a closed form. And

therefore final states could ^{not} be generated using the Monte Carlo technique. One could have made an alternative assumption that the electron after impact is left with an energy which is a certain fraction of its energy before impact. But we have followed Baraff³⁸ in making this assumption.

The second assumption is necessary because the transition probability for impact ionization is known only for the case of an electron with wave vector in the (100) direction. As discussed earlier, for all other directions, there will be different threshold energies and transition probabilities. Besides, the overlap integrals are not accurately known. It therefore only looks reasonable to make assumption 2, with different Ak_1 and Ak_2 .

Assumption 3 has been made to simplify the calculation and in view of the reasons for which assumptions 1 and 2 had to be made.

As described in section V of chapter I, the principle of Monte Carlo method as applied to the transport problems consists of simulating the motion of an electron in momentum space. However, since for the present, we are not interested in the determination of the distribution function, no meshing of \bar{k} space into fine cells is attempted. Rather, we separately keep track of the following quantities for each valley.

1. Number of collisions of each type .
2. The time electron spends in the valley.
3. The distance electron travels in the field direction while it remains in the valley.

By knowing the total distance (S) travelled by the electron in the field direction and the total number of ionizing collisions (RNI) suffered in travelling this distance, the ionization coefficient α can be easily found from the relation.

$$\alpha = \frac{RNI}{S}$$

The population ratio R can be found from the times T_1 and T_2 that the electron spends in the central and satellite valleys respectively. i.e.

$$R = T_1/T_2$$

It is also possible to find out the mean distance that an electron travels in the field direction before suffering an optical phonon collision for each of the valleys. This factor also makes an interesting study in that in the earlier theories it was assumed that $\lambda \approx \lambda$ i.e. the average distance λ travelled by an electron in the field direction before suffering an optical phonon collision is the same as the optical ^{phonon} mean free path because of an expected streaming of the electronic motion in the field direction.

As described in chapter I, to simulate the motion of an electron, a random time of flight t is first generated from the probability distribution (1.29a) by solving equation (1.31). After substituting for $P(t)$ from equn.(1.29a) and carrying out the integration over t , equn.(1.31) becomes

$$r = 1 - \exp \left\{ - \int_0^t \lambda[\bar{k}(t')] dt' \right\} \quad (4.4)$$

where $\lambda[\bar{k}(t)]$ now includes the transition probability for impact ionization also.

For some scattering processes the integral in equation (4.4) can be evaluated analytically and t determined from the random number r analytically or numerically. However, the complicated form of $\lambda_0(\bar{k})$ for some of the scattering processes (section IV chapter I) makes it impossible to evaluate the integral analytically and t can then be determined from r only by solving the integral equation or by interpolation in a numerical table of λ as a function of t and initial components of \bar{k} . However both these procedures will prove to be prohibitively inefficient. We therefore follow an alternative technique^{52,53} to generate the random times of flight. Suppose in addition to the real scattering processes present in the semiconductor we include a fictitious process for which

$$S_0(\bar{k}, \bar{k}') = \lambda_0(\bar{k}) \delta(\bar{k} - \bar{k}') \quad (4.5)$$

since the delta function does not allow the electron wave vector to change in the scattering event, this self scattering process is of no physical significance and then the function $\lambda_0(\vec{k})$ is completely arbitrary. Including this fictitious process equation (1.29a) becomes

$$P(t) = \left\{ \lambda_0[\vec{k}(t)] + \lambda[\vec{k}(t)] \right\} \times \exp \left\{ - \int_0^t \left(\lambda_0[\vec{k}(t')] + \lambda[\vec{k}(t')] \right) dt' \right\} \quad (4.6)$$

and we can now choose $\lambda_0(\vec{k})$ in such a way that the exponential factor becomes simple. The particular choice that we have made in our work is

$$\lambda_0(\vec{k}) = \Gamma - \lambda(\vec{k}) \quad (4.7)$$

where Γ is a constant.

This choice of $\lambda_0(\vec{k})$ has the advantage that equn. (4.6) becomes simply

$$P(t) = \Gamma e^{-\Gamma t} \quad (4.8)$$

and so has the effect of simulating the motion of an electron that has an energy independent relaxation time $\frac{1}{\Gamma}$. The constant Γ is taken to be at least as large as the largest value of $\lambda(\vec{k})$ of interest in order to avoid negative values of $\lambda_0(\vec{k})$. It has been shown in an entirely mathematical way²⁰ that the introduction of self scattering

does not alter the distribution (1.29a) of times of flights terminated by a real scattering process; its effect is only to subdivide the real flight of the electron into shorter flights of durations governed by the probability distribution (4.8).

Having determined the time of free flight, it is necessary to determine the scattering process responsible for terminating the flight. Since the probability of the electron being scattered by process q is proportional to $\lambda_q(\vec{k})$, and since $\sum_{q=0}^N \lambda_q = \Gamma$, it is only necessary to generate a random number s between 0 and Γ and test the inequality

$$s < \sum_{q=0}^m \lambda_q(\vec{k}) \quad (4.9)$$

for all m .

When this inequality is satisfied, the scattering process m is selected. To increase the efficiency of calculation it is desirable to minimise the number of self scattering events since they are of no physical interest. This is achieved by making Γ as small as possible. For all real processes, further random numbers are required to determine the final state after scattering. It is convenient to regard the phonon absorption and emission as separate processes in (4.9). Then the energy of the final state

is also determined by this inequality, since the energy change is either independent of the change in momentum as in polar and intervalley scatterings or zero as in acoustic scattering, and, for impact ionization, we have already made the assumption that an electron loses all its energy in the process.

It only remains to determine the components of \bar{k} corresponding to the final energy after scattering. Acoustic scattering and all the intervalley scattering processes are randomizing, so that once the energy of the final state has been determined, all states on that energy surface are equally probable final states. Hence the probability that the angle between \bar{k}' and the field direction z has some value θ is proportional to the number of states on a circle with radius $|\bar{k}'| \times \sin\theta$. We can then write

$$P(\theta) = A \sin\theta \quad (4.10)$$

where A is a normalizing constant. If r is a uniformly distributed random number between 0 and 1 then from the Monte Carlo technique ^{54,55} angle θ from the probability distribution (4.10) is given by

$$r = \int_0^\theta P(\theta) d\theta = \frac{1}{2} (1 - \cos\theta) \quad (4.11a)$$

$$\text{i.e.} \quad \cos\theta = 1 - 2r \quad (4.11b)$$

A further random number generated between 0 and 2π determines angle ϕ . For polar mode scattering it is more convenient to first determine the angle β between \bar{k} and \bar{k}' . From equn. (1.7) of chapter I

$$P(\beta) d\beta = B \left[E + E' - 2(E E')^{1/2} \cos\beta \right]^{-1} E'^{1/2} \sin\beta d\beta \quad (4.12)$$

where B is a normalizing constant. Using random number r equally distributed between 0 and 1, β can be obtained from the equn.

$$r = \int_0^\beta P(\beta) d\beta = \frac{\ln \left[1 + f \times (1 - \cos\beta) \right]}{\ln [1 + 2f]} \quad (4.13)$$

or solving for $\cos\beta$

$$\cos\beta = \left[(1+f) - (1+2f)^r \right] / f \quad (4.14)$$

A further random number between 0 and 2π determines the azimuthal angle and \bar{k}' is completely specified in the coordinate system in which \bar{k} is z axis. From this system of coordinates one can transform to the system of coordinates in which applied field is z axis by Euler rotations. The choice of X and Y axes is arbitrary since there is symmetry about the field direction.

For our simulation, we have used assumption (2) in a slightly different form. Rather than take a single value of Ak_1 for central valley, we have used the following values.

$$\begin{aligned}
 Ak_1 &= .1 & E < 7 \text{ eV} \\
 &= .25 & 7 \text{ eV} \leq E < 12 \text{ eV} \\
 &= .5 & 12 \text{ eV} \leq E < \infty
 \end{aligned}$$

Similarly for the satellite valley we have used

$$\begin{aligned}
 Ak_2 &= .005 & E < 7 \text{ eV} \\
 &= .02 & 7 \text{ eV} \leq E < 12 \text{ eV} \\
 &= .1 & 12 \text{ eV} \leq E < \infty
 \end{aligned}$$

This allows to take a better account of the transition probabilities for impact ionization in the two valleys. We have used 1.8 eV and 2.3 eV as the threshold energies for impact ionization in the central and satellite valleys respectively. These may appear some what higher in view of the calculated values of 1.48 eV and 2.00 eV for these valleys. However, a look at the curves of transition probabilities for impact ionization (curves (a) of Figs. 7 and 8) for the two processes shows that the transition probabilities become appreciable only at about 1.8 eV and 2.3 eV respectively.

Fig. 9 shows the calculated variation of α with E . The results are in good agreement with the experimental

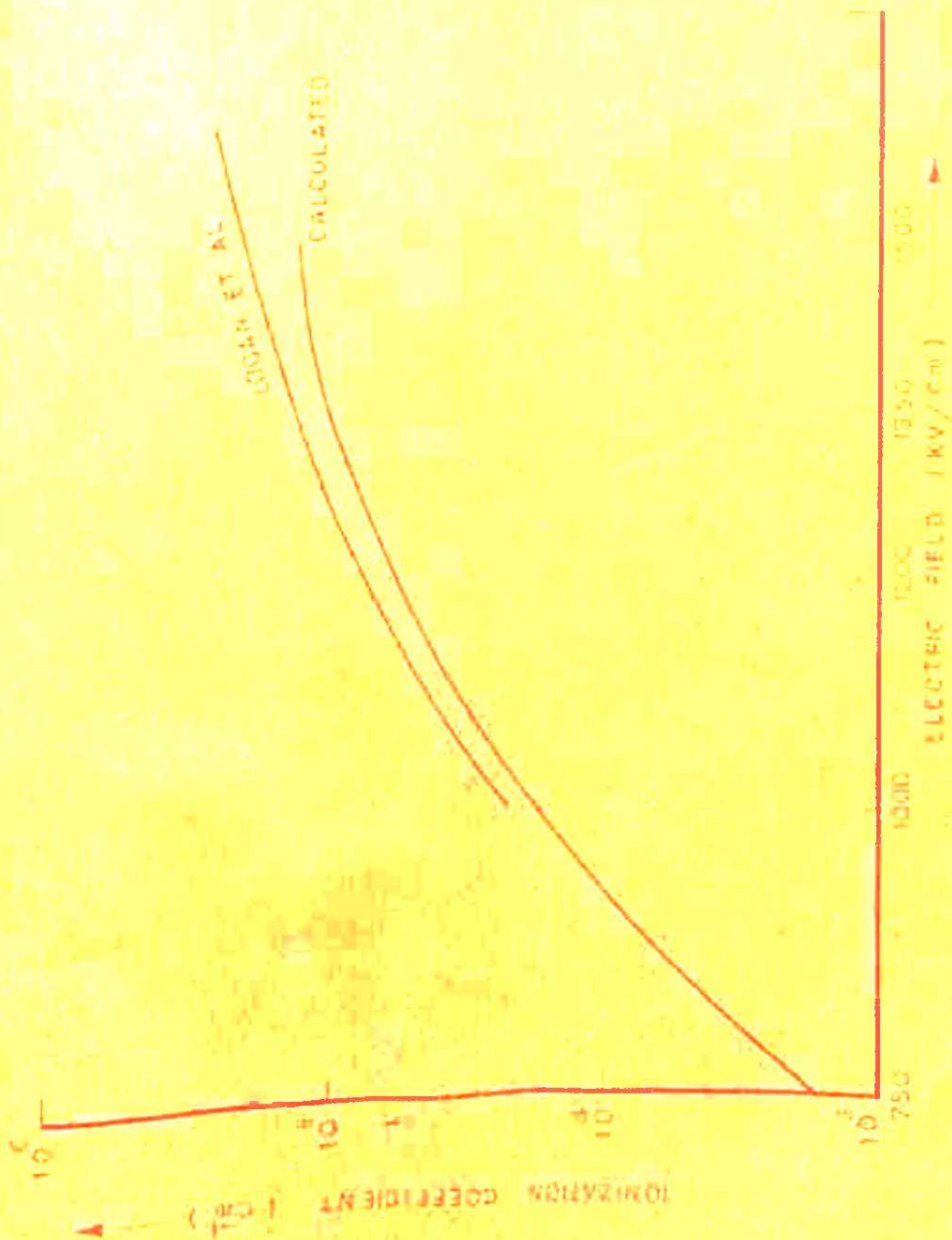


FIG. 11

results of Logan et al.⁶⁰ For higher fields about 25% of the ionizing collisions took place in the central valley. This fraction increased at lower fields. The mean free distance travelled by an electron before suffering an optical phonon collision increased with the electric field. In the central valley it increased from about 770 \AA° at 750 kV/cm to about 830 \AA° at 1500 kV/cm. In the satellite valley its value changed from about 17 \AA° to 23 \AA° . The mean free path value used by Logan et al in fitting their data to Baraff's curve is 17 \AA° . This is close to the values obtained by us for the satellite valley electrons. However, Logan et al have assumed the mean free path to be a constant independent of the electric field where as our calculation shows an increase in the mean free path with an increase in the electric field. A possible reason for this increase appears to be the increasing anisotropy of the electronic distribution function with the increase in the electric field.

Chapter-V.EFFECT OF MOBILE CHARGE CARRIERS ON JUNCTION
POTENTIAL DISTRIBUTION, FIELD DISTRIBUTION AND
CAPACITANCE.

I.	Setting up the generalized differential equation.	115
II.	Boundary conditions and technique of obtaining solution.	116
III.	Capacitance	120
IV.	Results and Discussions.	122

CHAPTER-7.EFFECT OF MOBILE CHARGE CARRIERS ON JUNCTION POTENTIAL DISTRIBUTION, FIELD DISTRIBUTION AND CAPACITANCE.

In this chapter we discuss and calculate the effect of mobile charge carriers on the potential, field distributions and capacitance in an abrupt symmetric p-n junction.

In the conventional complete depletion approximation the presence of mobile charge carriers in the depletion region is neglected and sharp boundaries are assumed for the space charge region. We have examined the validity of this approximation under various bias conditions, particularly the forward bias when heavy injection of mobile charge carriers in the depletion region makes their neglect unjustified.

I. SETTING UP THE GENERALIZED DIFFERENTIAL EQUATION:

In the quasi fermilevel theory, the electron density n and the hole density p are expressed by

$$n = n_i \exp[\beta(\psi - \phi_n)] \quad (5.1a)$$

$$p = n_i \exp[\beta(\phi_p - \psi)] \quad (5.1b)$$

where ψ is the potential, $\beta = q/k_B T$ and all other symbols have their usual meanings.

Assuming complete ionization of donors, the charge density ρ on n-side becomes

$$\rho = q(N_d + p - n) \quad (5.2)$$

We introduce the normalized potential U defined by $U = \beta[\psi - \frac{1}{2}(\phi_n + \phi_p)]$. Using equations (5.1) and the property $(\phi_p - \phi_n) = V$, V being the applied voltage, eqn. (5.2) gives

$$\rho = q \left[N_d - n_i \exp(\beta V/2) \sinh(U) \right] \quad (5.3)$$

Inserting the expression for ρ from eqn. (5.3) in the poisson's equation and making transformations

$$Z = \left(\frac{8\pi n_i q \beta}{\epsilon} \exp(\beta V/2) \right)^{1/2} x \quad (5.4a)$$

and

$$K = \frac{N_d}{n_i} \exp(-\beta V/2) \quad (5.4b)$$

We get the one parameter differential equation for the generalized potential distribution in the junction as

$$d^2U/dz^2 = \sinh(U) - K \quad (5.5)$$

K being the parameter.

II. BOUNDARY CONDITIONS AND TECHNIQUE OF OBTAINING SOLUTION:

The boundary conditions for U are: (1) $U(0) = 0$, and (2) $U(z) \rightarrow \bar{U} = \sinh^{-1}(K)$ as $z \rightarrow \infty$. The second condition comes from the neutrality of the regions far off from the junction. \bar{U} is an upper bound for the potential function. Also $U = 0$ is a

lower bound for the potential function on n-side.

The solution of the generalized differential equation (5.5) by numerical integration however encounters the difficulty that one boundary condition is specified at infinity and for large values of z the obtained solution diverges rapidly from the desired solution. To overcome this difficulty of the we shall be following Morgan's ⁵⁷ procedure of calculating close upper and lower bounds for the generalized potential function. Let $U_s(z)$ denote the solution of equation (5.5) which satisfies the boundary conditions $U_s(0) = 0$ and $U'_s(0) = s$, where s is some real number and prime denotes the derivative with respect to z . It can be seen from equation (5.5) and the Taylor series expansion of $U_s(z)$ about the origin that

$$U_{s_2}(z) - U_{s_1}(z) > (s_2 - s_1) \sinh(z) > 0$$

Thus if s is the slope of the desired solution with boundary conditions mentioned at the beginning of section II, then, $U_{s_1}(z)$ is an upper bound for the true solution if $s_1 > s$ and a lower bound if $s_1 < s$. This is pictorially depicted in FIG. (10). In Morgan's procedure some arbitrary value s is assumed for the derivative of U at the origin. A solution is then constructed using $U(0) = 0$ and $U'(0) = s$. We have used the fourth order Runge Kutta method for constructing solutions. A check is made whether the constructed solution crosses the

upper bound \bar{U} or bends down to meet the lower bound $U = 0$. If a constructed curve crosses the upper bound \bar{U} , it can never recross it because henceforth it has a positive second derivative and therefore remains concave upwards whereas \bar{U} is a constant. The constructed curve thus is a better upper bound than \bar{U} in the region where it lies below it. Beyond the point of its crossing \bar{U} , \bar{U} is a better upper bound. Similar deliberations apply to an integral curve which once crosses $U = 0$. In the region before crossing z -axis the constructed curve is an improvement over the lower bound $U = 0$. Beyond the point of crossing, $U = 0$ is a better lower bound. So if a curve identifies itself by having crossed the upper bound, it is rejected and the initial slope s is decreased to construct another curve. Similarly if a curve identifies by crossing the lower bound $U = 0$, the curve is rejected and the value of initial slope s is increased to construct another curve. The computation is limited by computer accuracy and time. We stopped the computation when the initial slopes for the upper bound and lower bounds differed by less than 10^{-5} . Fig.10 depicts the technique of obtaining the solution.

If one neglects $\sinh(U)$ term in eqn. (3.5) and integrates twice assuming electrical neutrality and vanishing of the electric field at some $z = z_m$, one gets the usual space charge approximation potential

$$U(z) = s_1 z - K z^2 / 2 \quad 0 \leq z \leq z_m \quad (5.6a)$$



z

FIG. 10.

$$U(z) = \sinh^{-1}(K) \quad z > z_m \quad (5.6b)$$

with the space charge boundary z_m given by

$$z_m = \left(\frac{2 \sinh^{-1}(K)}{K} \right)^{1/2} \quad (5.7a)$$

and

$$s_a = K z_m \quad (5.7b)$$

III. CAPACITANCE:

A change in the voltage between two contacts say $x = -l$ and $x = +l$ is associated with a change in the total number of mobile carriers stored in the structure. The two types of carriers are equivalent to the charges on the two plates of a capacitor and therefore the capacitance of the structure becomes

$$C = \frac{d}{dV} \left(q \int_{-l}^{+l} p dx \right) \quad (5.8)$$

Because the junction is symmetric, we can write

$$C = \frac{d}{dV} \left(q \int_0^l [(p+n) - N_d] dx \right) \quad (5.9)$$

which on using eqn. (5.2) becomes.

$$C = \frac{d}{dV} \left(2q \int_0^l p dx \right) - \frac{d}{dV} \left(\int_0^l p dx \right) \quad (5.10)$$

The total capacitance is thus split into two parts:

The neutral capacitance C_n given by

$$C_n = \frac{d}{dV} \left(2q \int_0^l p dx \right) \quad (5.11)$$

and the space charge capacitance C_p given by

$$C_p = -\frac{d}{dV} \left(\int_0^l p dx \right) \quad (5.10)$$

The expression for the space charge capacitance converges very strongly as l tends to infinity. Thus only negligible error will be made if we replace the upper limit of the integral by infinity in expression (5.12). Using (5.4b) one has

$$\frac{d}{dV} = -\beta/2 K \frac{d}{dK} = -\beta/2 \frac{d}{d(\log K)} \quad (5.13)$$

Also using equations (5.1b), and the relation $\phi_p - \phi_n = V$ one can write

$$p = n_i \exp(\beta V/2) \exp(-U) \quad (5.14)$$

The values of p and ρ from equations (5.1a) and (5.3) are substituted in equations (5.11) and (5.12). The variable of integration is then changed from x to z using (5.4a). Finally the derivatives with respect to V are changed to derivatives with respects to K with the help of (5.13). This results in following expressions for C_n and C_p :

$$C_n = \frac{C_0}{K^{1/2}} \left[-2 \frac{\partial}{\partial(\log K)} \int_0^{z_l} e^{-U} dz + z_l e^{-U(z_l)} + \int_0^{z_l} e^{-U} dz \right] \quad (5.15)$$

$$C_p = C_0/K^{1/2} \frac{\partial}{\partial z} \left[2 \frac{\partial U}{\partial(\log K)} - U \right]_{z=0} = \frac{C_0}{K^{1/2}} \left[2 \frac{\partial U'(0)}{\partial(\log K)} - U'(0) \right] \quad (5.16)$$

Where z_l is the z value corresponding to $x = l$ and C_0 is the normalising capacitance defined by

$$C_0 = \left(\frac{2q n_i \epsilon}{4\pi\beta} \right)^{1/2} \left(\frac{N_d}{2n_i} \right)^{1/2} \quad (5.17)$$

In equation (5.15) the differentiation with respect to $(\log K)$ is to be carried out for a fixed value of z . We have taken $z = 4z_m$ for our calculations. To evaluate the first term on right hand side of equation (5.15), we evaluated the integral expression numerically for the value of K for which C_n is required and two values adjacent to it one on either side. (For example to find C_n for $K = 1$, we evaluated the integral for K values .9, 1, 1.1) the results were fitted to a second degree polynomial in $\log K$ which was then differentiated at the value of K for which C_n was required. The second and third terms in equation (5.15) were also evaluated numerically for the value of K for which C_n was required. To evaluate C_e a similar technique is applied.

IV. RESULTS AND DISCUSSIONS:

Table 5.1 to 5.15 contain the calculated values of close upper and lower bounds for U and U' for different z . Table 5.16 contains the calculated neutral, space charge and total capacitances for different K together with the capacitance obtained by using complete depletion approximation which has been included for comparison. Figs. 11 and 13 show the comparison between calculated generalized potential and field distributions and those obtained by using complete depletion approximation for $K = 10$. Under the curves marked

Table-5.1

K = .1

U	U		U'	
	Upper bound	Lower bound	Upper bound	Lower bound
0	0	0	.099958	.099958
.2	.013119	.013119	.081831	.081831
.4	.032951	.032951	.066928	.066928
.6	.045093	.045093	.054835	.054835
.8	.055032	.055032	.044885	.044885
1.0	.063167	.063167	.036738	.036738
1.4	0.75275	.075275	.024611	.024611
1.8	.083386	.083386	.014485	.016485
2.2	.088819	.088819	.011041	.011041
2.6	.092457	.092457	.007394	.007394
3.0	.094894	.094894	.004952	.004952
3.4	.096526	.096526	.003316	.003316
3.8	.097619	.097619	.002221	.002221
4.2	.098351	.098350	.001487	.001487
4.6	.098841	.098840	.000996	.000996

Table-8.2

K = .2

Z	Upper bound	Lower bound	Upper bound	Lower bound
0	0	0	.199670	.199670
.2	.036187	.036187	.163410	.163410
.4	.065801	.065801	.133713	.133713
.8	.109852	.109852	.089482	.089432
1.0	.126064	.126064	.073183	.073183
1.4	.150163	.150163	.048932	.048932
1.8	.166273	.166273	.032703	.032703
2.2	.177039	.177039	.021850	.021850
2.6	.184230	.184230	.014595	.014595
3.0	.189034	.189034	.009748	.009748
3.4	.192242	.192242	.006510	.006510
3.8	.194385	.194385	.004347	.004347
4.2	.195816	.195815	.002903	.002902
4.6	.196771	.196770	.001938	.001937

Table-5.3

K = .5

Z	U		U'	
	Upper bound	Lower bound	Upper bound	Lower bound
0	0	0	.495120	.495120
.2	.089652	.089652	.404394	.404394
.4	.162842	.162842	.329966	.329966
.6	.222532	.222532	.268955	.268955
.8	.271161	.271161	.219004	.219004
1.0	.310741	.310740	.178164	.178164
1.4	.369079	.369073	.117634	.117633
1.8	.407550	.407549	.077477	.077476
2.2	.432867	.432866	.050941	.050939
2.6	.449503	.449500	.033453	.033450
3.0	.460423	.460419	.021952	.021948
3.4	.467583	.467381	.014398	.014391
3.8	.472286	.472277	.009442	.009432
4.2	.475367	.475353	.006193	.006178

Table-5.4

S K = 1.0

Z	U		U'	
	Upper bound	Lower bound	Upper bound	Lower bound
0	0	0	.966603	.966602
.2	.174547	.174547	.784711	.784709
.4	.316014	.316013	.634817	.634815
.6	.430255	.430254	.511668	.511666
.8	.522176	.522175	.410962	.410960
1.0	.595889	.595888	.329027	.329025
1.2	.654826	.654824	.262696	.262694
1.4	.701826	.701823	.209242	.209238
1.6	.739225	.739221	.166334	.166330
1.8	.768931	.768926	.132009	.132004
2.0	.792491	.792485	.104628	.104621
2.2	.811154	.811147	.082837	.082828
2.4	.825924	.825915	.065528	.065517
2.6	.837604	.837592	.051800	.051786
2.8	.846834	.846819	.040927	.040909
3.0	.854126	.854106	.032323	.032300
3.2	.859884	.859859	.025521	.025492

Table-5.5

$$K = 2.0$$

Z	U		U'	
	Upper bound	Lower bound	Upper bound	Lower bound
0	0	0	1.81725	1.81725
.2	.325758	.325758	1.45136	1.45136
.4	.584633	.584633	1.14696	1.14696
.6	.788140	.788140	.895569	.895569
.8	.946433	.946433	.693757	.693757
1.0	1.06839	1.06839	.532075	.532075
1.2	1.16157	1.16157	.405046	.405046
1.4	1.23230	1.23230	.306487	.306487
1.6	1.28569	1.28569	.230799	.230799
1.8	1.32582	1.32582	.173154	.173153
2.0	1.35588	1.35588	.129532	.129531
2.2	1.37835	1.37835	.096687	.096686
2.6	1.40753	1.40758	.053624	.053622
2.8	1.41687	1.41686	.039873	.039870
3.2	1.42839	1.42838	.022003	.021998
3.6	1.43552	1.43551	.012124	.012116
4.0	1.43917	1.43916	.006678	.006663

Table-5.6

K = 5.0

Z	U		U'	
	Upper bound	Lower bound	Upper bound	Lower bound
0	0	0	3.86346	3.86346
.2	.677640	.677640	2.93717	2.93717
.4	1.18462	1.18462	2.15765	2.15765
.6	1.55094	1.55094	1.53130	1.53130
.8	1.80714	1.30714	1.05453	1.05453
1.0	1.98152	1.98152	.709049	.709048
1.2	2.09775	2.09775	.468386	.468385
1.4	2.17406	2.17406	.305573	.305572
1.6	2.22363	2.22363	.197669	.197668
1.8	2.25561	2.15560	.127148	.127146
2.0	2.27614	2.27613	.081484	.081481
2.4	2.29768	2.29767	.033255	.033248
2.8	2.30645	2.30643	.013517	.013498
3.2	2.31001	2.30999	.005487	.005442

ple-5.7

K = 10.0

Z	U		U'	
	Upper bound	Lower bound	Upper bound	Lower bound
0	0	0	6.47029	6.47029
.2	1.10258	1.10258	4.59968	4.59968
.4	1.86048	1.86048	3.03933	3.03933
.6	2.34462	2.34462	1.87015	1.87015
.8	2.63450	2.63450	1.08737	1.08757
1.0	2.89143	2.89143	.332664	.332663
1.2	2.94110	2.94110	.179372	.179371
1.4	2.96779	2.96779	.095989	.095988
1.6	2.98204	2.98204	.051157	.051154
1.8	2.98963	2.98962	.027201	.027196
2.0	2.99366	2.99365	.014443	.014432
2.2	2.99580	2.99579	.007656	.007636

Table-5.8

K = 20.0

Z	U		U'	
	Upper bound	Lower bound	Upper bound	Lower bound
0	0	0	10.4657	10.4657
.2	1.70800	1.70800	6.70143	6.70143
.4	2.73144	2.73144	3.70034	3.70034
.6	3.26200	3.26200	1.78610	1.78610
.8	3.50754	3.50754	.790352	.790346
1.0	3.61382	3.61382	.334458	.334444
1.2	3.65835	3.65834	.138710	.138674
1.4	3.67674	3.67672	.057060	.056974
1.6	3.68430	3.68425	.023461	.023247
1.8	3.68742	3.68731	.009807	.009234

Table-5.9

K = 50.0

β	Upper bound	Lower bound	Upper bound	Lower bound
0	0	0	19.0396	19.0396
.1	1.65740	1.65740	14.1493	14.1493
.2	2.84313	2.84313	9.66551	9.66550
.3	3.61796	3.61796	5.99994	5.99993
.4	4.07069	4.07069	3.41791	3.41790
.5	4.33489	4.33489	1.82964	1.82964
.6	4.46395	4.46395	.942590	.942567
.7	4.53730	4.53729	.475357	.475312
.8	4.57157	4.57155	.237079	.236936
.9	4.58862	4.58859	.117616	.117426
1.0	4.59706	4.59701	.058281	.057896
1.1	4.60126	4.60115	.029037	.028256
1.2	4.60337	4.60314	.014858	.013275

Table-5.10

 $K = 100.0$

Z	U		U'	
	Upper bound	Lower bound	Upper bound	Lower bound
0	0	0	29.3540	29.3540
.05	1.34334	1.34334	24.3943	24.3943
.10	2.44160	2.44160	19.5683	19.5683
.15	3.30495	3.30495	15.0317	15.0317
.20	3.95329	3.95329	11.0057	11.0057
.25	4.41737	4.41737	7.68601	7.68601
.30	4.73504	4.73504	5.15044	5.15044
.35	4.94456	4.94456	3.34104	3.34103
.40	5.07891	5.07891	2.11698	2.11697
.45	5.16336	5.16336	1.32011	1.32010
.50	5.21576	5.21575	.814648	.814632
.60	5.26770	5.26769	.304877	.304833
.70	5.28703	5.28701	.112833	.112715
.80	5.29416	5.29413	.041481	.041162
.90	5.29677	5.29668	.014930	.014065

Table-5.11

K = 200.0

Z	U		U'	
	Upper bound	Lower bound	Upper bound	Lower bound
0	0	0	44.7055	44.7055
.05	1.98636	1.98636	34.7774	34.7774
.10	3.48354	3.48354	25.2145	25.2145
.15	4.52514	4.52514	16.6987	16.6987
.20	5.18501	5.18501	10.0579	10.0579
.25	5.56770	5.56770	5.59812	5.59812
.30	5.77518	5.77518	2.96254	2.95254
.35	5.88290	5.88290	1.50836	1.50835
.40	5.93746	5.93745	.757409	.757393
.45	5.96474	5.96473	.377123	.377089
.50	5.97830	5.97829	.187337	.187269
.55	5.98505	5.98504	.093694	.093555
.60	5.99031	5.99027	.028537	.027965
.70	5.99156	5.99148	.023409	.022250

Table-5.12

K = 500.0

Z	U		U'	
	Upper bound	Lower bound	Upper bound	Lower bound
0	0	0	76.8750	76.8750
.05	3.22132	3.22132	52.0725	52.0725
.10	5.23844	5.23844	29.2866	29.2866
.15	6.26136	6.26136	13.0513	13.0513
.20	6.68115	6.68115	4.88343	4.88342
.25	6.83183	6.83183	1.67862	1.67860
.30	6.88286	6.88285	.561056	.560977
.35	6.89999	6.89998	.193392	.193149
.40	6.90644	6.90641	.090702	.089958

Table-5.13

$$K = 1000.0$$

Z	U		U'	
	Upper bound	Lower bound	Upper bound	Lower bound
0	0	0	114.908	114.908
.05	4.50178	4.50178	65.4862	65.4862
.10	6.68925	6.68925	25.0405	25.0405
.15	7.39014	7.39014	6.43397	6.43397
.20	7.55632	7.55632	1.39948	1.39946
.25	7.59167	7.59167	.291404	.291293
.30	7.59901	7.59899	.063462	.059809
.35	7.60055	7.60047	.013601	.010993

Table-5.14

K = 2000.0

Z	U		U'	
	Upper bound	Lower bound	Upper bound	Lower bound
0	0	0	170.816	170.816
.02	3.01667	3.01667	130.882	130.882
.04	5.23964	5.23964	91.6856	91.6856
.06	6.70832	6.70832	56.2329	56.2329
.08	7.54895	7.54895	29.6512	29.6511
.10	7.96744	7.96744	13.8540	13.8539
.12	8.15624	8.15623	6.02560	6.02534
.14	8.23694	8.23693	2.53062	2.52999
.16	8.27057	8.27054	1.04672	1.04518
.18	8.28445	8.28436	.430781	.427010
.20	8.29016	8.28995	.178429	.169208

Table-5.15

K = 5000.0

Z	U		U'	
	Upper bound	Lower bound	Upper bound	Lower bound
0	0	0	286.541	286.541
.01	2.61547	2.61547	236.565	236.565
.02	4.73193	4.73193	186.810	186.810
.03	6.35551	6.35551	138.290	138.290
.04	7.51127	7.51127	93.9125	93.9124
.05	8.26194	8.26194	57.9525	57.9524
.06	8.70677	8.70677	32.8674	32.8673
.07	8.95163	8.95163	17.5502	17.5500
.08	9.07995	9.07995	9.03212	9.03183
.09	9.14531	9.14530	4.55439	4.55381
.10	9.17808	9.17806	2.27224	2.27106
.11	9.19438	9.19435	1.12785	1.12546
.12	9.20247	9.20240	.559042	.554202
.13	9.20648	9.20634	.278243	.268430
.14	9.20849	9.20821	.141467	.121572

Table-5.16

K	C_n/C_o	C/C_o	C_t/C_o	C_{cd}/C_o
.1	35.327	.317	35.644	.445
.2	24.490	.445	24.935	.622
.5	14.013	.676	14.689	.912
1.0	7.823	.776	8.599	1.065
2.0	3.466	.933	4.429	1.053
5.0	.917	.949	1.866	.912
10.0	.356	.880	1.236	.813
20.0	.110	.813	.923	.735
50.0	.028	.718	.746	.659
100.0	$.114 \times 10^{-1}$.675	.686	.614
200.0	$.468 \times 10^{-2}$.630	.635	.578
500.0	$.153 \times 10^{-2}$.580	.581	.538
1000.0	$.688 \times 10^{-3}$.550	.551	.513
2000.0	$.316 \times 10^{-3}$.523	.523	.491
5000.0	$.119 \times 10^{-3}$.493	.493	.466



FIG. 11



FIG. 11.

exact actually the average value of calculated upper and lower bounds has been plotted since it is not possible in the plot to show the two bounds separately because they are very very close. Figs. 12 and 14 show similar comparison for $K = 5000$. From these curves it can be seen that the complete depletion approximation results are in poor agreement for $K = 10$ but they are in fairly good agreement for $K = 5000$. In fact as the value of K is increased, the complete depletion approximation becomes a better and better approximation. For reverse biases K becomes very large and the complete depletion approximation is therefore a very good approximation. However for small values of K i.e. large forward biases the approximation is not good. It results in much higher values of peak field in the junction for such cases and the potential distribution is also very much different from the actual potential distribution obtained by taking into account the mobile charge carriers. The extent of space charge region is much larger than that given by the approximation. This can be seen from Fig. 11 in the slow approach of the exact potential towards the neutral potential for large values of z .

Similar conclusions about the validity of complete depletion approximation can be derived from the comparison of capacitances. From Table 5.16 a comparison of total capacitance C_t calculated by taking into account mobile charge



FIG. 12

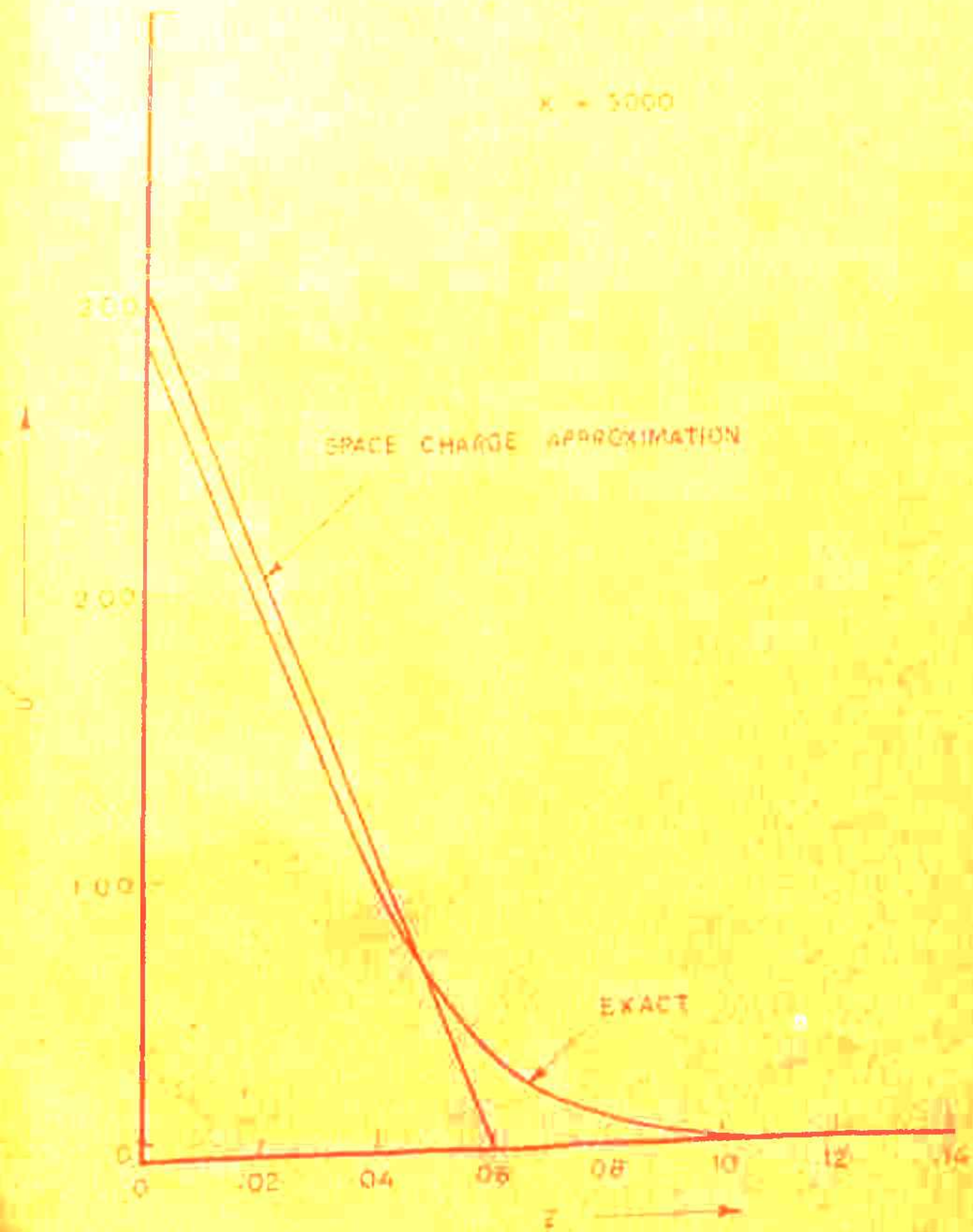


FIG. 14

carriers and the complete depletion approximation capacitance C_{cd} shows that the latter is erroneous for small values of K . From $K = 20$ onwards the agreement is good. Also it can be seen from the table that neutral capacitance C_n is very large for low values of K and dominates over the space charge capacitance C_p . But it rapidly decreases with K till at about $K = 5$ it becomes equal to the space charge capacitance. Henceforth C_p dominates while C_n keeps falling rapidly till at $K = 5000$ it is three orders of magnitude less than C_p . A comparison of C_p and C_{cd} shows that C_p is less than C_{cd} for values of K less than about 2. For values of K higher than 2, C_p is greater than C_{cd} and approaches C_{cd} for higher values of K . But the agreement between C_p and C_{cd} is good for all values of K .

Chapter-VI.

Conclusion	146
Appendix A	151
Appendix B	157

CHAPTER- VI._C_O_N_C_L_U_S_I_O_N_

We have carried out a study of the effect of various scattering mechanisms on electron transport in GaAs using displaced Maxwellian approach. We find that at lower energies the polar optical phonon scattering is the dominant scattering mechanism in both the central and satellite valleys and the velocity field ($v - E$) characteristic upto the threshold field is primarily governed by the polar mode scattering in the central valley. Other scattering mechanisms in the central and satellite valleys have only very small effect on this part of the characteristic. Beyond the threshold field, upto the valley field, the $v-E$ characteristic is mainly governed by the non-equivalent intervalley scattering. The greater the strength of this mechanism the slower the transfer of electrons to the satellite valleys, consequently, lesser the magnitude of the post threshold negative slope and higher the valley field. Beyond the valley field, the characteristic is dominated by the equivalent intervalley scattering among the satellite valleys and to a lesser extent by acoustic and polar mode scatterings.

The study of effect of lattice temperature on electron transport shows that the threshold field decreases with increasing lattice temperature. A decrease in the energy separation between central and satellite valleys with the increase of lattice temperature has been identified as the cause for this effect.

However, we have not considered the non-parabolicity of the central valley and the wave vector dependence of the cell periodic part of Bloch functions. For a more complete study these factors must be taken into account. Since the inclusion of these factors means a great deal of complication in the formulation, the semi analytical techniques (the displaced Maxwellian and Relaxation time approaches) appear to be inadequate to deal with the problem. Only the Monte Carlo approach seems to be the promising approach for theoretical study of electron transport.

In the study of impact ionization, we have tried to provide a more rigorous theoretical basis for the calculation of ionization coefficient for electrons in GaAs. In the conventional theories of Wolff, Shockley and Baraff, the threshold energy for impact ionization is usually taken as $3/2 E_g$ or as an adjustable parameter. A constant ratio is assumed between the transition probabilities for impact ionization and optical phonon emission. Besides, there is no theoretical treatment of impact ionization in the literature that takes into account the presence of non-equivalent central and satellite valleys in GaAs. We have attempted to incorporate this feature in our calculation. Various processes have been considered by which the electrons (in the central and satellite valleys) and holes in GaAs impact ionize. An analytical approach has been

developed to determine the threshold energy for impact ionization for each process. Since the processes with low threshold energies become operative first, we have carried out a time dependent perturbation calculation of the transition probability for impact ionization for such processes to estimate their relative effectiveness for impact ionization. We have found that the ratio between the transition probabilities for impact ionization and optical phonon scattering is strongly energy dependent. The ratio functions are vastly different in the two valleys. A central valley electron of a certain energy has a much higher transition probability for impact ionization than a satellite valley electron of the same energy. Also the transition probability for impact ionization for an electron, in general, may depend upon not only its energy but also on the direction of its wave vector.

Monte Carlo calculation of ionization coefficient for electrons has been carried out. The results show good agreement with the experimental results. The Monte Carlo calculation also shows that about 25 to 30% of the ionizing collisions take place in the central valley and that this percentage increases at lower fields. Despite the fact that there are only about 5% of the total electrons in the central valley at these high fields, the large transition probability for impact ionization in this valley makes this valley important for impact ionization.

However, once again, the non parabolicity of the central valley had to be left out for the sake of simplicity and for retaining the closed forms for various expressions. At higher energies that are of interest in impact ionization, the non parabolicity of the central valley may well play an important role. Besides in the absence of more accurate estimates for the various overlap integrals we have had to make rather crude estimates for them. More accurate values for these integrals are desirable for better calculations. The transition probabilities for impact ionization have been calculated only for the electrons having their wave vector in (100) direction. Their use in other directions particularly for the satellite valley is not justified at least at lower fields. At higher fields where the electron motion is stream lined in the field direction (maximum anisotropy condition) is their use justifiable but an increase in the mean free distance travelled by an electron in the field direction before encountering an optical phonon collision with the field shows that the electron distribution is not quite anisotropic even at 1500 kV/cm. When more information about the relevant quantities becomes available a more accurate calculation using the various threshold energies and exact energy dependence of transition probabilities for impact ionization for various processes may be attempted. We have also neglected the higher valleys in the conduction band, partly on the grounds that since these valleys are much above the valence band, the threshold energies for electrons in these

valleys will be very large and partly because not much information is yet available about them. When more details about the band structure of GaAs away from the band minima becomes available it would be desirable to incorporate them in the calculation.

Lastly, the study of effect of mobile charge carriers on junction potential -field distributions and capacitance shows that the space charge approximation is an excellent approximation at reverse biases but not at forward biases. At forward biases, the actual space charge region is much larger and the peak field in the junction is smaller than that given by the space charge approximation.

APPENDIX-A.EVALUATION OF INTEGRALS INVOLVED IN THE CONSERVATION EQUATIONS:

We shall evaluate here the net rate of change of momentum due to equivalent intervalley scattering in one of the satellite valleys. The procedure for evaluating the net rate of change of electron number, momentum and energy for a valley by other scattering mechanisms is similar and only the final results are given for them.

We want to evaluate

$$\int \left[\frac{\partial}{\partial t} f_2(\vec{k}) \right]_e (\vec{k} - \vec{k}_2) d\vec{k}$$

where \vec{k}_2 is the wave vector corresponding to the minimum of the satellite valley. We have

$$\int \left[\frac{\partial}{\partial t} f_2(\vec{k}) \right]_e (\vec{k} - \vec{k}_2) d\vec{k} = \frac{2\pi}{k} (2e-1) \frac{k}{2\rho\omega_e V} \frac{V}{8\pi^3} \Xi e^2 \left[- \int f_2(\vec{k}') (\vec{k} - \vec{k}_2) \left[N_c \delta \{ E(\vec{k}) - E(\vec{k}') - k\omega_e \} \right. \right. \\ \left. \left. + (N_c+1) \delta \{ E(\vec{k}') - E(\vec{k}) + k\omega_e \} \right] d\vec{k}' d\vec{k} \right. \\ \left. + (\vec{k} - \vec{k}_2) \int f_2(\vec{k}') \left[N_c \delta \{ E(\vec{k}) - E(\vec{k}') - k\omega_e \} + (N_c+1) \delta \{ E(\vec{k}') - E(\vec{k}) + k\omega_e \} \right] d\vec{k}' d\vec{k} \right] \quad (A1)$$

where the first term in (A1) gives the rate of change of momentum of the valley due to electrons scattering out from the valley to other equivalent valleys by absorption or emission of intervalley phonons. The second term gives the rate of change of momentum due to electrons being scattered into the valley from other equivalent valleys by absorption or emission of intervalley phonons. After interchanging the

variables of integration \bar{k} and \bar{k}' in the second term we can rearrange (A1) as

$$\int \left[\frac{\partial}{\partial t} f_2(\bar{k}) \right]_{\bar{e}} (\bar{k} - \bar{K}_2) d\bar{k} = \frac{2\pi}{h} (Z_0 - 1) \frac{hV}{2\mu\omega_0 V} \frac{\Xi_e^2}{8\pi^3} \left[\right. \quad (A2)$$

$$\left. (N_e + 1) \int f_2(\bar{k}) (\bar{k}' - \bar{k}) \delta \{ E(\bar{k}') - E(\bar{k}) + h\omega_0 \} d\bar{k}' d\bar{k} + N_e \int f_2(\bar{k}) (\bar{k}' - \bar{k}) \delta \{ E(\bar{k}') - E(\bar{k}) - h\omega_0 \} d\bar{k}' d\bar{k} \right]$$

We adopt following transformation:

$$\bar{k}' - \bar{k} = \bar{r} \quad (A3a)$$

$$d\bar{k}' = d\bar{r} \quad (A3b)$$

and take the polar axis along $\bar{k} - \bar{K}_2$. The first of the two integrals in (A2) then becomes

$$\int_{r=0}^{\infty} \int_{\theta=0}^{\pi} \int_{\phi=0}^{2\pi} f_2(\bar{k}) \bar{r} \delta \left\{ h\omega_0 + \frac{h^2 r^2}{2m_2} + \frac{h^2}{m_2} r |\bar{k} - \bar{K}_2| \cos\theta \right\} r^2 dr \sin\theta d\theta d\phi d\bar{k} \quad (A4)$$

Since the argument of delta function is independent of ϕ , integration over ϕ is straight forward. The only non zero contribution to the integral comes from the component of \bar{r} along polar axis and (A4) becomes.

$$2\pi \frac{(\bar{k} - \bar{K}_2)}{|\bar{k} - \bar{K}_2|} \int_{r=0}^{\infty} \int_{\theta=0}^{\pi} f_2(\bar{k}) r \cos\theta \delta \left\{ h\omega_0 + \frac{h^2 r^2}{2m_2} + \frac{h^2}{m_2} r |\bar{k} - \bar{K}_2| \cos\theta \right\} r^2 dr \sin\theta d\theta d\bar{k} \quad (A5)$$

We make following substitution:

$$h\omega_0 + \frac{h^2 r^2}{2m_2} + \frac{h^2}{m_2} r |\bar{k} - \bar{K}_2| \cos\theta = Z \quad (A6)$$

Then (A5) becomes

$$2\pi \frac{(\bar{k} - \bar{K}_2)}{|\bar{k} - \bar{K}_2|} \int_{r=0}^{\infty} \int_{\theta=0}^{Z_0} f_2(\bar{k}) r \frac{(Z - h\omega_0 - \frac{h^2 r^2}{2m_2})}{\left(\frac{h^2}{m_2} r |\bar{k} - \bar{K}_2| \right)^2} \delta(Z) r^2 dr dZ d\bar{k} \quad (A7)$$

where
$$Z_l = \hbar\omega_c + \frac{\hbar^2 r^2}{2m_2} - \frac{\hbar^2}{m_2} r |\vec{k} - \vec{k}_2|$$

$$Z_u = \hbar\omega_c + \frac{\hbar^2 r^2}{2m_2} + \frac{\hbar^2}{m_2} r |\vec{k} - \vec{k}_2|$$

For the integral over z to be non vanishing the signs of the lower and upper limits for z in (A7) must be opposite. This means r must lie between r_l and r_u where

$$r_l = |\vec{k} - \vec{k}_2| - \sqrt{|\vec{k} - \vec{k}_2|^2 - \frac{2m_2}{\hbar^2} \hbar\omega_c} \text{ and } r_u = |\vec{k} - \vec{k}_2| + \sqrt{|\vec{k} - \vec{k}_2|^2 - \frac{2m_2}{\hbar^2} \hbar\omega_c} \quad (\text{A8})$$

Hence the integral (A7) becomes

$$2\pi \int_{|\vec{k} - \vec{k}_2|}^{|\vec{k} - \vec{k}_2|} \frac{f_2(\vec{k})}{|\vec{k} - \vec{k}_2|} \int_{r_l}^{r_u} \frac{r \left(-\hbar\omega_c - \frac{\hbar^2 r^2}{2m_2} \right) r^2 dr d\vec{k}}{\left(\frac{\hbar^2 r}{m_2} |\vec{k} - \vec{k}_2| \right)^2} \quad (\text{A9})$$

The integration over r can now be carried out and (A9)

gives

$$-\frac{8\pi m_2}{\hbar^2} \frac{m_2}{\hbar^2} \int \frac{(\vec{k} - \vec{k}_2)}{|\vec{k} - \vec{k}_2|} f_2(\vec{k}) (E_2(\vec{k}) - \Delta_2)^{\frac{1}{2}} (E_2(\vec{k}) - \Delta_2 - \hbar\omega_c)^{\frac{1}{2}} d\vec{k} \quad (\text{A10})$$

Similarly integration over \vec{k}' can be carried out

in the second term of (A2). (A2) can then be written as

$$-\frac{2\pi}{\hbar} (2e-1) \frac{\hbar}{2p\omega_c V} \frac{2\pi m_2}{\hbar^2} \frac{m_2}{\hbar^2} \int \frac{(\vec{k} - \vec{k}_2)}{|\vec{k} - \vec{k}_2|} f_2(\vec{k}) \left[(N_e+1) (E_2(\vec{k}) - \Delta_2)^{\frac{1}{2}} \times \right. \\ \left. (E_2(\vec{k}) - \Delta_2 - \hbar\omega_c)^{\frac{1}{2}} + N_e (E_2(\vec{k}) - \Delta_2)^{\frac{1}{2}} (E_2(\vec{k}) - \Delta_2 + \hbar\omega_c)^{\frac{1}{2}} \right] d\vec{k} \quad (\text{A11})$$

One can substitute the explicit form of $f_2(\vec{k})$ from equn(1.20) in (A11) and carry out the straight forward integration over angular variables using \vec{d}_2 as polar axis. Finally the integration over k can be changed over to integration over E where E is defined as follows

$$E = E_2(\vec{k}) - \Delta_2$$

The evaluation of the integral over E can not be carried out analytically and one has to resort to numerical solution. The various terms in the conservation equations (1.22) reduced to a single integral over E are given below.

INTEGRALS INVOLVING FIELD :

$$\int_i \left[\frac{\partial f_i(\vec{k})}{\partial t} \right]_F d\vec{k} = 0 \quad (A12)$$

$$\int_i \left[\frac{\partial f_i(\vec{k})}{\partial t} \right]_F (\vec{k} - \vec{k}_i) d\vec{k} = -\frac{e}{\hbar} n_i \vec{F} \quad (A13)$$

$$\int_i \left[\frac{\partial f_i(\vec{k})}{\partial t} \right]_F [E_i(\vec{k}) - \Delta_i] d\vec{k} = -\frac{e\hbar}{m_i} n_i \vec{F} \cdot \vec{d}_i \quad (A14)$$

INTEGRALS INVOLVING POLAR OPTICAL PHONON SCATTERING:

$$\int_i \left[\frac{\partial f_i(\vec{k})}{\partial t} \right]_{p_0} d\vec{k} = 0 \quad (A15)$$

$$\int_i \left[\frac{\partial f_i(\vec{k})}{\partial t} \right]_{p_0} (\vec{k} - \vec{k}_i) d\vec{k} = -\vec{d}_i \frac{2}{3} \frac{n_i \Omega_{ii}^{(p_0)}}{(k_B T_i)^2} \int_0^\infty \exp\left(\frac{-E}{k_B T_i}\right) U \left\{ \left(\frac{3E}{m_i}\right)^{1/2} \frac{\hbar d_i}{k_B T_i} \right\} Q(E) E dE \quad (A16)$$

$$\int_i \left[\frac{\partial f_i(\vec{k})}{\partial t} \right]_{p_0} [E_i(\vec{k}) - \Delta_i] d\vec{k} = -\frac{\hbar \omega_0}{k_B T_i} n_i \Omega_{ii}^{(p_0)} \int_0^\infty \exp\left(\frac{-E}{k_B T_i}\right) \times \quad (A17)$$

$$V \left\{ \left(\frac{3E}{m_i}\right)^{1/2} \frac{\hbar d_i}{k_B T_i} \right\} \left\{ (N_0 + 1) \phi(E - \hbar \omega_0) - N_0 \phi(E) \right\} dE$$

where

$$\Omega_{ii}^{(p_0)} = \frac{2m_i e^2 \omega_0}{\hbar} \left(\frac{1}{\epsilon_\infty} - \frac{1}{\epsilon_0} \right) \frac{1}{(2\pi m_i k_B T_i)^{3/2}} \exp\left(\frac{-\hbar^2 d_i^2}{2m_i k_B T_i}\right) \quad (A18)$$

$$d_i = |\bar{d}_i|$$

(A19)

The functions U and V are defined by

$$U(x) = 3x^{-3} (x \cosh x - \sinh x)$$

(A20)

$$V(x) = x^{-1} \sinh x$$

(A21)

and the functions ϕ and Q are given by

$$\phi(E) = \text{Log} \left\{ \frac{(E + \hbar\omega_0)^{1/2} + E^{1/2}}{(E + \hbar\omega_0)^{1/2} - E^{1/2}} \right\}$$

(A22)

$$Q(E) = E^{-1} \left[(N_0 + 1) \left\{ E^{1/2} (E - \hbar\omega_0)^{1/2} + \frac{1}{2} \hbar\omega_0 \phi(E - \hbar\omega_0) \right\} \right. \\ \left. + N_0 \left\{ E^{1/2} (E + \hbar\omega_0)^{1/2} - \frac{1}{2} \hbar\omega_0 \phi(E) \right\} \right]$$

(A23)

We adopt here and here after the convention that the square roots of negative quantities are to be set zero in order to omit the terms having imaginary values of $(E - \hbar\omega_0)^{1/2}$ which correspond to emission of optical phonons by electrons with energy less than the optical phonon energy.

INTEGRALS INVOLVING ACOUSTIC PHONON SCATTERING:

$$\int_i \left[\frac{\partial f_i(\vec{k})}{\partial t} \right]_{ac} d\vec{k} = 0$$

(A24)

$$\int_i \left[\frac{\partial f_i(\vec{k})}{\partial t} \right]_{ac} (\vec{k} - \vec{k}_i) d\vec{k} = -\bar{d}_i \left(\frac{k_B T_0}{3m_i S^2} \right) \frac{n_i - \Omega_{ii}}{(k_B T_i)^3} \times$$

(A25)

$$\int_0^\infty \exp\left(\frac{-E}{k_B T_i}\right) U \left\{ \left(\frac{2E}{m_i}\right)^{1/2} \frac{\hbar d_i}{k_B T_i} \right\} E^2 dE$$

$$\int_i \left[\frac{\partial f_i(\vec{k})}{\partial t} \right]_{sc} [E_i(\vec{k}) - \Delta_i] = 0$$

(Since we have assumed the acoustic scattering to be elastic) (A26)

where

$$\Omega_{ii}^{sc} = \frac{16 m_i^4 \Xi_a^2 (k_B T_i)^2}{\hbar^4 \rho (\pi m_i k_B T_i)^{3/2}} \exp\left(-\frac{\hbar^2 d_i^2}{2 m_i k_B T_i}\right) \quad (A27)$$

INTEGRALS INVOLVING NON-EQUIVALENT INTERVALLEY SCATTERING:

$$\int_i \left[\frac{\partial f_i(\vec{k})}{\partial t} \right]_{ij} d\vec{k} = -\frac{n_i \Omega_{ij}^{(ij)}}{(k_B T_i)^2} \int_0^\infty \left\{ \left(\frac{2E}{m_i} \right)^{1/2} \frac{\hbar d_i}{k_B T_i} \right\} H_{ij}^{(1)}(E) dE + \frac{n_j \Omega_{ji}^{(ij)}}{(k_B T_j)^2} \int_0^\infty \left\{ \left(\frac{2E}{m_j} \right)^{1/2} \frac{\hbar d_j}{k_B T_j} \right\} H_{ji}^{(1)}(E) dE \quad (A28)$$

$$\int_i \left[\frac{\partial f_i(\vec{k})}{\partial t} \right]_{ij} (\vec{k} - \vec{k}_i) d\vec{k} = -\vec{d}_i \frac{3}{2} \frac{\Omega_{ij}^{(ij)} n_i}{(k_B T_i)^3} \int_0^\infty \left\{ \left(\frac{2E}{m_i} \right)^{1/2} \frac{\hbar d_i}{k_B T_i} \right\} H_{ij}^{(3)}(E) dE \quad (A29)$$

$$\int_i \left[\frac{\partial f_i(\vec{k})}{\partial t} \right]_{ij} [E_i(\vec{k}) - \Delta_i] d\vec{k} = -\frac{n_i \Omega_{ij}^{(ij)}}{(k_B T_i)^2} \int_0^\infty \left\{ \left(\frac{2E}{m_i} \right)^{1/2} \frac{\hbar d_i}{k_B T_i} \right\} H_{ij}^{(3)}(E) dE + \frac{n_j \Omega_{ji}^{(ij)}}{(k_B T_j)^2} \int_0^\infty \left\{ \left(\frac{2E}{m_j} \right)^{1/2} \frac{\hbar d_j}{k_B T_j} \right\} H_{ji}^{(3)}(E) dE \quad (A30)$$

$$\frac{n_j \Omega_{ji}^{(ij)}}{(k_B T_j)^2} \int_0^\infty \left\{ \left(\frac{2E}{m_j} \right)^{1/2} \frac{\hbar d_j}{k_B T_j} \right\} H_{ji}^{(3)}(E) dE$$

where

$$-n_{ij}^{(ij)} = \frac{2 \Xi_{ij}^2 m_j^2 k_B (T_i T_j)^{1/2}}{\pi \hbar^2 \rho \hbar \omega_{ij}} \frac{1}{(2\pi m_j k_B T_j)^{3/2}} \exp\left(-\frac{\hbar^2 d_i^2}{2 m_i k_B T_i}\right) \quad (A31)$$

$$\text{and } H_{ij}^{(mm)} = \exp\left(-\frac{E}{k_B T_i}\right) \left[(N_{ij} + 1) \left\{ E^m (E + \Delta_i - \Delta_j - \hbar \omega_{ij}) \right\}^{n-1/2} + N_{ij} \left\{ E^m (E + \Delta_i - \Delta_j + \hbar \omega_{ij}) \right\}^{n-1/2} \right] \quad (A32)$$

The integrals involving equivalent intervalley scattering can be obtained by setting $i = 2$ and $j = 2$ in equns. (A28) through (A32) and noting $N_{22} = N_e$; $\Xi_{22} = \Xi_e$; $\omega_{22} = \omega_e$

APPENDIX-B.

DETERMINATION OF THE REGION OF INTEGRATION IN \bar{k}_2 SPACE

For a given \bar{k}_1 , only those values of \bar{k}_2 can participate in impact ionization for which the energy and momentum conservation equations can be solved to obtain real values of \bar{k}_1' and \bar{k}_2' .

The energy and momentum conservation equations are

$$\hbar\omega_0 = [\epsilon(\bar{k}_1') + \epsilon(\bar{k}_2') - \epsilon(\bar{k}_1) - \epsilon(\bar{k}_2)] = 0 \quad (B1)$$

$$\bar{k}_1 + \bar{k}_2 = \bar{k}_1' + \bar{k}_2' \quad (B2)$$

If we define

$$\bar{k}_1 + \bar{k}_2 = 2\bar{k} \quad (B3)$$

and

$$\bar{k}_1' - \bar{k}_2' = 2\bar{k}$$

then the momentum conservation equation (B2) becomes the set of equations

$$\bar{k}_1' = \bar{k}_0 + \bar{k} \quad (B4)$$

and

$$\bar{k}_2' = \bar{k}_0 - \bar{k} \quad (B5)$$

Using (B4) and (B5) (momentum conservation equation) in equn. (B1) (energy conservation equation) we can obtain the magnitude of \bar{k} i.e.

$$k^2 = \frac{m_1}{\hbar^2} \left[\epsilon(\bar{k}_1) - E_g - \frac{\hbar^2 k_2^2}{2m_k} - \frac{\hbar^2}{m_1} k_0^2 \right] \quad (B6)$$

$$k^2 = \frac{m_1}{\hbar^2} \left[\epsilon(\bar{k}_1) - E_j - \frac{\hbar^2 k_2^2}{2m_k} - \frac{\hbar^2}{m_1} \frac{(k_1^2 + k_2^2 + 2\bar{k}_1 \cdot \bar{k}_2)}{4} \right] \quad (B7)$$

Only that region of \bar{k}_2 space participates in ionization for which k is real i.e. the RHS of (B7) is greater than zero. The RHS of (B7) can be rearranged to give

$$k^2 = \frac{m_1}{\hbar^2} \left[\epsilon(\bar{k}_1) - E_j - a(\bar{k}_2 + \gamma\bar{k}_1)^2 - b/a k_1^2 \right] \quad (B8)$$

where

$$a = \frac{\hbar^2}{2m_k} + \frac{\hbar^2}{4m_1} \quad (B9)$$

$$\text{and} \quad b = \frac{\hbar^2}{2m_k} \cdot \frac{\hbar^2}{4m_1} \quad (B10)$$

$$\text{If we define} \quad (B11)$$

$$\bar{r} = \bar{k}_2 + \gamma\bar{k}_1$$

then

$$k^2 = \frac{m_1}{\hbar^2} \left[\epsilon(\bar{k}_1) - E_j - ar^2 - b/a k_1^2 \right] \quad (B12)$$

For RHS of (B12) to be greater than zero, $|\bar{r}|$ must lie between 0 and r_{\max} where

$$r_{\max} = \sqrt{\frac{1}{a} (\epsilon(\bar{k}_1) - E_j - b/a k_1^2)} \quad (B13)$$

Thus the region of \bar{k}_2 space that participates in ionization is that for which \bar{r} has its magnitude less than r_{\max} . If we transform the variable of integration from \bar{k}_2 to \bar{r} with the help of eqn. (B11), then the region of integration in \bar{k}_2 space (the region that participates in impact ionization) is transformed into a spherical region of radius r_{\max} in the \bar{r} space.

REFERENCES

1. J. B. Gunn, Solid State Commun. 1, 88 (1963).
2. A. G. Foyt and A. L. McWhorter, Trans. IEEE, ED-13, 79 (1966).
3. J. A. Allen, M. Shyam, Y. S. Chen and G. L. Pearson, Appl. Phys. Letters, 7, 78 (1965).
4. J. A. Allen, M. Shyam and G. L. Pearson, Phys. Rev. Letters, 9, 39 (1966).
5. J. B. Gunn, Proc. Int. Conf. on the Physics of Semiconductors, Paris, 1964 (Paris Dunod), pp. 199.
6. J. S. Heeks, A. D. Coode and C. P. Sandbank, Proc. IEEE, 53, 554 (1965).
7. A. R. Huston, A. Jayraman, A. G. Chynoweth, A. S. Corriell and M. L. Feldman, Phys. Rev. Letters, 14, 639 (1965).
A. R. Huston, A. Jayraman, A. S. Corriell, Phys. Rev., 155, 786 (1967).
8. B. K. Ridley and T. B. Watkins, Proc. Phys. Soc. 78, 293 (1961).
B. K. Ridley and T. B. Watkins, Proc. Phys. Soc., 78, 710 (1961).
9. C. Hilsum, Proc. IRE, N. Y., 50, 185 (1962).
10. H. Ehrenreich, J. Phys. Chem. Solids, 2, 131 (1957).
H. Ehrenreich, Phys. Rev., 120, 1951 (1960).
11. E. M. Conwell, M. O. Vassel, Phys. Rev., 166, 797 (1968).
12. L. W. James, R. C. Eden, J. L. Moll and W. B. Spicer, Phys. Rev., 174, 909 (1963).

13. W. E. Spicer and R. C. Eden, Proc. Int. Conf. Phys. Semiconds. Moscow (1968) pp 65.
14. M. L. Cohen and T. K. Bergstrasser, Phys. Rev., **141**, 789 (1966).
15. E. H. Pollak, J. W. Higginbotham and M. Cardona, J. Phys. Soc., Japan. Suppl. **21**, 20 (1966).
16. D. Jones and A. H. Lettington, Solid St. Commun. **7**, 1319 (1969).
17. J. A. Van Vochten, Phys. Rev. **31**, 3351 (1970).
18. T. C. Collins, D. J. Stuckel and R. N. Euwema, Phys. Rev., **31**, 724 (1970).
19. F. Herman and W. E. Spicer, Phys. Rev., **175**, 906 (1968).
20. N. Fawcett, A. D. Boardman and S. Swain, J. Phys. Chem. Solids. **31**, 1963 (1970).
- 21.^a J. Callaway, J. Electronics, **2**, 330 (1957).
- 21.^b R. Braunsstein, J. Phys. Chem. Solids, **8**, 288 (1957)
22. H. Welker and H. Weiss, Solid State Physics, Edited by F. Seitz and D. Turnbull (Academic Press, N. Y.) 1956, Vol. 3.
23. L. G. Spitzer and J. H. Whelan, Phys. Rev., **114**, 59 (1959).
24. E. O. Kane, J. Phys. Chem. Solids, **1**, 249 (1957).
25. H. Ehrenreich, J. Phys. Chem. Solids, **9**, 129 (1959).
26. G. S. Paigee, Prog. Semicond. **8**, 62 (1964).
27. J. L. Birman, M. Lax and R. Loudon, Phys. Rev. **145**, 620 (1966).
28. P. N. Butcher and N. Fawcett, Proc. Phys. Soc., **86**, 1205 (1965).
29. A. H. Wilson, The Theory of Metals, Cambridge University Press, London and New York, 1953.

- .. Shockley, *Electrons and holes in semiconductors*,
in Ser. Phys., Princeton, New Jersey, 1950, Chapter 11.
29. T. Kurosawa, Proc. Int. Conf., Phys. Semiconds., Kyoto, 1966.
 T. Kurosawa, J. Phys. Soc., Japan, Suppl. 21, 424 (1966).
 31. A. D. Boardman, W. Fawcett, and H. D. Rees, Solid State Commun. 6, 305 (1968).
 32. J. G. Ruch, and G. S. Kino, Phys. Rev. 174, 921 (1968).
 J. G. Ruch, and G. S. Kino, Appl. Phys. Lett. 10, 40 (1967).
 33. R. Stratton, Proc. Roy Soc., A246, 406 (1958).
 34. R. Stratton, Proc. Roy. Soc., A242, 355 (1957).
 35. P. A. Wolff, Phys. Rev., 95, 1415 (1954).
 36. W. Shockley, Solid State Electronics, 2, 35 (1961).
 37. J. L. Moll and R. Van Overstraeten, Solidstate Electronics, 6, 147 (1963).
 38. G. A. Baraff, Phys. Rev., 128, 2507 (1962).
 39. G. A. Baraff, Phys. Rev., 133, A26 (1964).
 40. J. L. Moll and N. Meyer, Solid State Electronics, 3, 155 (1961).
 41. H. Frolich and B. V. Paranjape, Proc. Phys. Soc. (London), B69, 21 (1956).
 42. R. Stratton, J. Phys. Soc., Japan, 17, 590 (1962).
 43. G. H. Wannier, Bell Syst. Tech. Journal, 32, 170 (1953).
 44. D. J. Bartelink, J. L. Moll and N. Meyer, Phys. Rev., 130, 972 (1963).
 45. References to earlier experimental work cited in ref. 32.

46. S. Antoncik and P. T. Lands-Berg , Proc. Phys. Soc.,
(London) 32, 337 (1963).
47. A. . . Deattie and P. T. Landsberg, Proc. Roy. Soc. (London)
A249, 16 (1959).
48. S. Antoncik and J. Tauc, Semiconductors and Semimetals,
Vol. 2, Academic Press, N. Y. and London (1966).
49. L. W. James and J. L. Moll, Phys. Rev., 183, 740 (1969).
50. J. G. Ruch and W. Fawcett, J. Appl. Phys. 41, 3843 (1970).
51. I. . . Bott and H. R. Holliday, IEEE Trans. Electron Devices,
ED-14, 522 (1967).
52. H. D. Rees, Phys. Lett. 26A, 416 (1968).
53. H. D. Rees , J. Phys. Chem. Solids, 30, 643 (1969).
54. Joe. H. Mize and J. Grady Cox, Essentials of Simulation,
Englewood Cliffs, N. J., Prentice Hall, (1968).
55. Monte Carlo Methods, Hammersley, J.M., and D.C.
Handstcomb., John Wiley & Sons, Inc, New York, 1964
56. V. Franz, Hand Buch Der Physik, Springer Verlag, Berlin,
(1956) pp. 190.
57. S. P. Morgan and F. M. Smits, Bell. Syst. Tech. Journal,
39, 1573 (1960).
58. P. N. Butcher and W. Fawcett, Phys. Letters, 21, 489 (1966).
59. Chandra Shekhar and S. K. Sharma, Phys. Letts. 50A,120 (1974)
60. R. A. Logan, A. G. Chynoweth and B. G. Cohen, Phys. Rev.,
128, 2518 (1962).

LIST OF PUBLICATIONS.

1. Threshold energy for impact ionization in GaAs, Chandra Shekhar and S. K. Sharma, Indian Journal of Pure and Applied Physics, Vol. 12, 179 (1974).
2. Threshold energy for impact ionization by holes in GaAs, Chandra Shekhar and S. K. Sharma, Phys. Lett. 50A, 120 (1974).
3. Threshold energy for impact ionization by electrons in GaAs considering the non parabolicity of the central valley, Chandra Shekhar and S. K. Sharma, to be published in Physics Letters A.
4. Effect of mobile charge carriers on junction potential distribution, field distribution and capacitance, Chandra Shekhar, S. K. Sharma and Suman Kumar, to be published in IETE (India).
5. Temperature dependence of transport properties in GaAs, Chandra Shekhar and S. K. Sharma, to be published in Ind. J. Pure. Appl. Phys.
6. Transition probability for impact ionization in GaAs, Chandra Shekhar and S. K. Sharma, Communicated to Journal of Physics C.
7. A Monte Carlo calculation of ionization coefficient in GaAs, Chandra Shekhar and S. K. Sharma, Communicated to Journal of Physics C.